PARTITION OF UNITY ISOGEOMETRIC ANALYSIS FOR SINGULARLY PERTURBED PROBLEMS AND FOURTH ORDER DIFFERENTIAL EQUATIONS CONTAINING SINGULARITIES

by

Sinae Kim

A dissertation submitted to the faculty of
The University of North Carolina at Charlotte
in partial fulfillment of the requirements
for the degree of Doctor of Philosophy in
Applied Mathematics

Charlotte

2016

Approved by:

_____

Dr. Hae-soo Oh

_____

Dr. Joel Avrin

_____

Dr. Shaozhong Deng

_____

Dr. Churlzu Lim

ABSTRACT

SINAE KIM. Partition of unity isogeometric analysis for singularly perturbed problems and fourth order differential equations containing singularities. (Under the direction of DR. HAE-SOO OH)

The design basis functions in IGA are refined and enhanced by extra enrichment functions and various local refinements with the use of partition of unity (PU) functions with flat-top. These reconditioned and modified basis functions are pushed forward to the physical domain by the original design mapping for analysis. With this method (PU-IGA), the corresponding stiffness matrix has a smaller bandwidth, and local refinements become simpler. We apply PU-IGA to various singularly perturbed problems incorporating boundary layer enrichment functions developed by boundary layer analysis. Here, we construct the PU functions on the reference domain and push-forward them to a physical domain through geometric mapping for the construction of enriched global basis functions on a physical domain. Therefore, we have advantages in calculating stiffness matrices and load vectors with integrals over rectangular areas. Next, we apply PU-IGA, which is enriched with singular functions that resemble singularities, to fourth order differential equations containing singularities. This direct enrichment method yields an accurate numerical solution; however, it yields large matrix condition numbers and integrals of singular functions. To alleviate these limitations, we propose a mapping method by constructing a singular mapping from the reference domain onto the singular zone of the physical domain. This singular mapping transforms polynomials on the reference domain to singular basis functions on the physical domain. This mapping method has the same effect

as the directly enriched PU-IGA but yields small condition numbers and no singular integrals.

ACKNOWLEDGMENTS

Thank God for everything. I know You walk with me in every step of my life. Nothing is impossible with You. Deep appreciation goes out to those who have believed in me and have supported me with prayers. In particular: Dr. Hae-soo Oh, thank you for being my mentor and teacher, I respect for your gentle character, hard work, controlled life style, and patient understanding. Mom, my role model in faith, character, and sacrifice of your life for others. You would believe in me and be proud of me no matter what I would do. Dad, my role model in passion for life and calling. I know I am always in your prayers and in your cares. Parents-in-law, thank you for supporting me with your prayers and deep understanding. Chun, my beloved husband. You are the God's given rock in my life. Samuel, my best son, who has the favorite Bible verses in heart. Your hope to spend more time with mommy and your confidence in me expedite this work done. Abigail, my proud daughter, who has packed lunch for mommy, has fed your brother and sister, and has a caring heart for others. Elizabeth, my sweetest daughter, who feels sympathy for others, especially for mommy, comforts me, and prays for me in the morning and evening. You guys are truly my joy and happiness that God has given me. Your encouraging letters made me cry and laugh for defenses, conferences and every event. You are mighty on the land. You will reach far beyond what I can imagine. Eunae and Jinhwan, thank you for being my sister and my brother and believing in me, whom I would always stand by and pray for. Dr. Hyunjoo Kim, thank you for your timely advice and all of your help. Dr. Bongsoo Jang, thank you for the life lesson and advice. Birce Palta, thank

you for your friendship first, and for all of your help second.

TABLE OF CONTENTS

LIST OF FIGURES

LIST OF TABLES

CHAPTER 1: INTRODUCTION

Isogeometric Analysis (IGA) is a new approach that combines Computer Aided Design (CAD) and Finite Element Analysis (FEA), in which the same basis functions used to represent the geometry are used to approximate the solution of differential equations. IGA provides advantages in the construction of basis functions with any order of regularity and the use of the exact geometry for analysis within the framework of the Galerkin method. However, the standard Galerkin method does not give an accurate numerical solution to such problems as singularly perturbed problems or elliptic boundary value problems with singularities. Thus, in order to obtain accurate numerical solutions, we enrich the approximate space by adding boundary layer functions or singular functions using Partition of Unity (PU) with flat-top, referred to as Partition of Unity Isogeometric Analysis (PU-IGA). Oh et al. in [35] and [36] use PU with flat-top to solve singularity problems.

Most of the numerical methods used to solve the singularly perturbed problems are based on domain decomposition or refined meshes near the boundary layer. ([23], [37], [38], and [50]) In [15], Hong et al. approximated the solution of the singularly perturbed convection-diffusion problem using piecewise linear finite element space enriched with boundary layer correctors in a rectangle and in a circle. In this dissertation, using a similar approach, we derive the boundary layer approximation through boundary layer analysis, shown in [27], and use that approximation as an enrich-

ment function into the approximation space. Instead of using mesh refinement, we can obtain fairly accurate numerical solutions of convection-diffusion equations with boundary layer on the circular and rectangular domains. We also apply boundary layer analysis to singularly perturbed problems on a different domain, an ellipse.

Enriched PU-IGA is extended to solve a singularly perturbed parabolic problem. In [3], [5], [21], [26] , and [51], the authors find numerical solutions of parabolic perturbed problems in a rectangular domain by using the Finite Difference method. Hong [17] approximates the singularly perturbed parabolic problem on circular domain using a quasi-uniform triangulation and piecewise linear finite element approximation space, which are enriched with boundary layer correctors constructed near the circular boundary. Mesh refinements around the boundary layer is costly because we need to solve the linear system at each time step in parabolic problems. Instead of using mesh refinements on the boundary layer zone, we introduce the boundary layer functions into approximation spaces with use of PU with flat-top.

Babuska and Oh [29] introduced the mapping technique, called the Method of Auxiliary Mapping (MAM), to solve second order elliptic PDEs containing corner singularities in the framework of conventional FEM. Using similar techniques, we introduce a Mapping Method to solve the fourth order differential equations containing singularities, which generate singular basis functions on a physical domain by a singular geometric mapping.

In a similar manner to singular perturbed problems, we can also obtain accurate numerical solutions for this singularity problem by using enriched PU-IGA, where singular functions that resemble the singular behavior are directly added into the

approximation space. However, enriched PU-IGA for fourth order equations yields large condition numbers and singular integrals. These limitations are overcome by the Mapping Method.

This dissertation is organized as follows. In Chapter 2, we review definitions, terminologies and properties of Isogeometric Analysis, B-splines and Partition of Unity. We also briefly review Boundary Layer Analysis. In Chapter 3, we prove error estimates of PU-IGA, with respect to PU with flat-top, and construct basis functions of enriched PU-IGA in general. In Chapter 4, we apply enriched PU-IGA to perturbed convection-diffusion problems in circular and in rectangular domains. We define an enriched approximation space that incorporates the boundary layer functions and present numerical results. In Chapter 5, we apply enriched PU-IGA to a perturbed parabolic problem by enriching the approximation space with boundary layer functions. We calculate convergence rates of numerical solutions obtained by enriched FEM in which the backward Euler method is used for time discretization, and piecewise linear basis functions are used for the space approximation. In Chapter 6, we solve fourth-order equations containing singularities with two approaches: enriched PU-IGA and PU-IGA with Mapping Method. We present numerical results of these two approaches, comparing them to those of IGA without enrichment. The conclusion follows in Chapter 7.

CHAPTER 2: PRELIMINARIES

We introduce definitions and terminologies that are used throughout this dissertation.

2.1 Weak Solution in Sobolev Space and Galerkin Method

For an integer $k \geq 0$, the *Sobolev space* $H^k(\Omega)$ is defined by

$$H^k(\Omega) = \{v \in L_2(\Omega) \mid D^\alpha v \in L_2(\Omega),\ \forall |\alpha| \leq k\}.$$

Suppose we are concerned with an elliptic boundary value problem on a domain Ω with Dirichlet boundary condition $g(x, y)$ along the boundary $\partial\Omega$. Let

$$\mathcal{W} = \{w \in H^1(\Omega) : w|_{\partial\Omega} = g\} \text{ and } \mathcal{V} = \{w \in H^1(\Omega) : w|_{\partial\Omega} = 0\}.$$

The variational formulation of the Dirichlet boundary value problem can be written as: Find $u \in \mathcal{W}$ such that

$$\mathcal{B}(u, v) = \mathcal{L}(v), \text{ for all } v \in \mathcal{V}, \tag{1}$$

where $\mathcal{B}$ is a continuous bilinear form that is $\mathcal{V}$-elliptic [39], and $\mathcal{L}$ is a continuous linear functional. The solution to (1) is called a *weak solution*, which is equivalent to the strong (classical) solution to an elliptic PDE, whenever u is smooth enough. The

energy norm of the trial function u is defined by

$$\|u\|_{\text{eng}} = \left[\frac{1}{2}\mathcal{B}(u,u)\right]^{1/2}.$$

Let $\mathcal{W}^h \subset \mathcal{W}$ and $\mathcal{V}^h \subset \mathcal{V}$ be finite dimensional subspaces. We can write the Galerkin form (a discrete variational equation) of (1) as follows: Given g^h, find $u^h = w^h + g^h$, where $w^h \in \mathcal{V}^h$, such that

$$\mathcal{B}(u^h, v^h) = \mathcal{L}(v^h), \text{ for all } v^h \in \mathcal{V}^h,$$

which can be rewritten as: Find the trial function $w^h \in \mathcal{V}^h$ such that

$$\mathcal{B}(w^h, v^h) = \mathcal{L}(v^h) - \mathcal{B}(g^h, v^h), \text{ for all test functions } v^h \in \mathcal{V}^h. \tag{2}$$

2.2 Partition of Unity

Let $\bar{\Omega}$ be the closure of $\Omega \subset R^d$. We define the vector space $\mathcal{C}(\bar{\Omega})$ to consist of all those functions $\phi \in C^m(\Omega)$ for which $D^\alpha\phi$ is bounded and uniformly continuous on Ω for $|\alpha| = \alpha_1 + ... + \alpha_d \leq m$. A function $\phi \in C^m(\Omega)$ is said to be a C^m-continuous function. If Ψ is a function defined on Ω, the *support* of Ψ is defined as

$$\text{supp}\Psi = \overline{\{x \in \Omega \mid \Psi(x) \neq 0\}}$$

The *norm* and *semi-norm* are defined for $u \in H^k(\Omega)$ as follows:

$$\|u\|_{k,\Omega} = (\sum_{|\alpha|\leq k}\int_\Omega |\partial^\alpha u|^2 dx)^{1/2}, \quad \|u\|_{k,\infty,\Omega} = \max_{|\alpha|\leq k}\{\text{ess.sup}|\partial^\alpha u(x)| : x \in \Omega\},$$
$$|u|_{k,\Omega} = (\sum_{|\alpha|=k}\int_\Omega |\partial^\alpha u|^2 dx)^{1/2}, \quad |u|_{k,\infty,\Omega} = \max_{|\alpha|=k}\{\text{ess.sup}|\partial^\alpha u(x)| : x \in \Omega\}.$$

A family $\{U_k \mid k \in \mathcal{D}\}$ of open subsets of R^d is said to be *a point finite open covering* of $\Omega \subset R^d$, if there is M such that any $x \in \Omega$ lies in at most M of the open sets U_k and $\Omega \subseteq \bigcup_{k \in \mathcal{D}} U_k$.

For a point finite open covering $\{U_k \mid k \in \mathcal{D}\}$ of a domain Ω, suppose there is a family of Lipschitz functions $\{\phi_k \mid k \in \mathcal{D}\}$ on Ω satisfying the following conditions:

1. For $k \in \mathcal{D}$, $0 \leq \phi_k(x) \leq 1, \quad x \in R^d$

2. The support of ϕ_k is contained in $\overline{U}_k$, for each $k \in \mathcal{D}$

3. $\sum_{k \in \mathcal{D}} \phi_k(x) = 1$ for each $x \in \Omega$

Then, $\{\phi_k \mid k \in \mathcal{D}\}$ is called *a partition of unity (PU)* subordinate to the covering $\{U_k \mid k \in \mathcal{D}\}$. The covering sets $\{U_k\}$ are called *patches*.

A weight function (or window function) is a non-negative continuous function with compact support and is denoted by $w(x)$. Consider the following conical window function: For $x \in R$,

$$w(x) = \begin{cases} (1-x^2)^l, & |x| \leq 1 \\ 0, & |x| > 1, \end{cases}$$

where l is an integer. Then, $w(x)$ is a C^{l-1}-continuous function. In R^d, the weight function $w(x)$ can be constructed from a one dimensional weight function as $w(x) = \prod_{i=1}^{d} w(x_i)$, where $x = (x_1, ..., x_d)$. We use the normalized window function defined by

$$w_\delta^l(x) = Aw(\frac{x}{\delta}), \qquad A = \frac{(2l+1)!}{2^{2l+1}(l!)^2\delta}, \tag{3}$$

where A is the constant such that $\int_R w_\delta^l(x)dx = 1$ in [11]. Here a normalizing factor δ is a positive real number less than 1, which is specified in section 2.6.

2.3 Isogeometric Analysis

Isogeometric Analysis combines Computer-Aided Design (CAD) and Finite Element Analysis (FEA), where geometry model for analysis should be modified and meshed from the original geometry from CAD. Isogeometric Analysis focuses on only one geometric model(CAD representation), which can be utilized directly for analysis. We follow notations and definitions in [7], [41] and [42]. There are many computational geometry basis functions that could serve as a basis for Isogeometric Analysis. Non-Uniform Rational B-Splines (NURBS) is the most widely used computational geometry basis function, the industry standard, in engineering design. NURBS can exactly represent all conic sections; for example, circles, cylinders, spheres, and ellipsoids. They have useful properties for analysis, such as variation diminishing, convex hull properties, higher order continuity, and refinements.

Isogeometric Analyis Structure

In Isogeometric Analysis, we consider one mesh on the physical domain, *physical mesh*, which is a decomposition of the actual geometry. Physical mesh has two elements: the patch and the knot span. Several geometry mappings might define an actual geometry. One geometry mapping defines a *patch*, which might be a whole geometry or a part of the geometry. Each patch has two representations: one in a reference domain and one in a physical domain.

Each patch can be decomposed into knot spans, which are bounded by knots. Basis

functions are smooth within a knot span and C^{p-m}-continuous across knots, where p is the degree of the polynomial and m is the multiplicity of the knot. They also have representations in both reference and physical domains.

2.4 B-splines and NURBS

NURBS are built from B-splines, which are defined by a knot vector.

Knot Vectors

A *Knot vector* is a non-decreasing set of coordinates in the reference domain, written as

$$\Xi = \{\xi_1, \xi_2, ..., \xi_{n+p+1}\}, \quad \xi_i \in R,$$

where ξ_i is i^{th} knot, p is the polynomial degree, and n is the number of basis functions used to construct a B-spline curve. The knots divide the reference domain into elements. B-spline functions constructed by a knot vector are piecewise polynomials joined together along knot lines. The functions are smooth within a knot span.

If the knots are equally spaced, a knot vector is said to be *uniform*. Otherwise, the knot vector is said to be *non-uniform*. The *multiplicities* of a knot value, or how many times the knot value is repeated, decides the continuity of the basis function across the knot.

If a knot vector has the first and the last knot value with multiplicity $p + 1$, it is said to be *open*. Open knot vectors are the standard in the CAD literature. Basis functions formed from open knot vectors are interpolatory at the ends of the reference domain.

B-splines

With a knot vector, the B-spline basis functions are defined recursively starting with piecewise constants ($p = 0$):

$$N_{i,1} = \begin{cases} 1 & \text{if } \xi_i \leq \xi < \xi_{i+1} \\ 0 & \text{otherwise.} \end{cases} \tag{4}$$

For $p = 1, 2, 3, ...$, they are defined by

$$N_{i,p+1}(\xi) = \frac{\xi - \xi_i}{\xi_{i+p} - \xi_i} N_{i,p}(\xi) + \frac{\xi_{i+p+1} - \xi}{\xi_{i+p+1} - \xi_{i+1}} N_{i+1,p}(\xi), \tag{5}$$

where p is degree of B-spline basis function. This is referred to as the *Cox-de Boor recursion formula*.

There are several important features of B-spline basis functions.

1. Partition of unity

$$\sum_{i=1}^{n} N_{i,p+1}(\xi) = 1, \qquad \forall \xi \in [\xi_1, \xi_{n+p+1}]$$

2. Nonnegativity

$$N_{i,p+1} \geq 0, \qquad \forall \xi \in [\xi_1, \xi_{n+p+1}]$$

3. C^{p-m}-continuous across the knot, where m is the multiplicity of the knot value and p is the degree of B-spline functions

4. Any given function with degree p has $p + 1$ knot span of support.

5. Any given function shares support with $2p + 1$ functions, including itself.

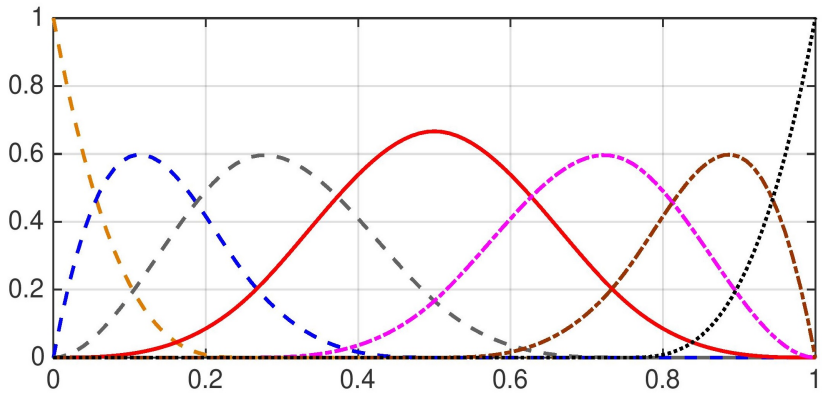

Figure 1: B-spline functions $N_{i,4}(\xi)$, $i = 1, 2, \cdots, 7$ of degree $p = 3$ corresponding to the knot vector $\Xi = \{0, 0, 0, 0, 0.25, 0.5, 0.75, 1, 1, 1, 1\}$. The supports of $N_{k,4}(\xi), k = 1, \ldots, 7$, respectively, are $[0, 0.25], [0, 0.5], [0, 0.75], [0, 1], [0.25, 1], [0.5, 1], [0.75, 1]$.

C^2-continuous B-spline functions with degree 3 by an open knot vector are presented in Figure 1. From the figure, one can see the support of any given function and how many functions intersect with the given function.

Given n basis functions, $N_{i,p+1}, i = 1, 2, ..., n$ and corresponding control points $B_i \in \mathbb{R}^d, i = 1, 2, ..., n$ (vector-valued coefficients), a piecewise-polynomial *B-spline curve* is given by

$$C(\xi) = \sum_{i=1}^{n} N_{i,p+1}(\xi) B_i.$$

Given a *control net* $B_{i,j}, i = 1, 2, ..., n, j = 1, 2, ..., m$, polynomial degree p and q, and knot vectors $\Xi = \{\xi_1, \xi_2, ..., \xi_{n+p+1}\}$, and $\Im = \{\eta_1, \eta_2, ..., \eta_{m+q+1}\}$, a tensor product *B-spline surface* is defined by

$$S(\xi, \eta) = \sum_{i=1}^{n} \sum_{j=1}^{m} N_{i,p+1}(\xi) M_{j,q+1}(\eta) B_{i,j},$$

where $N_{i,p+1}(\xi)$ and $M_{j,q+1}(\eta)$ are univariate B-spline basis functions of degree p and q, corresponding to knot vectors Ξ and $\Im$, respectively.

Given a *control lattice* $\{B_{i,j,k}\}, i = 1, 2, ..., n, j = 1, 2, ..., m, k = 1, 2, ..., l,$ polynomial degree $p, q,$ and $r,$ and knot vectors $\Xi = \{\xi_1, \xi_2, ..., \xi_{n+p+1}\}$, $\Im = \{\eta_1, \eta_2, ..., \eta_{m+q+1}\}$, and $\Re = \{\zeta_1, \zeta_2, ..., \zeta_{l+r+1}\}$, a B-spline solid is defined by

$$S(\xi, \eta, \zeta) = \sum_{i=1}^{n} \sum_{j=1}^{m} \sum_{k=1}^{l} N_{i,p+1}(\xi) M_{j,q+1}(\eta) L_{k,r+1}(\zeta) B_{i,j,k}.$$

Non-Uniform Rational B-Splines

NURBS can exactly represent various geometries that cannot be represented by B-splines, such as conic sections.

Define *weighting function*

$$W(\xi) = \sum_{i=1}^{n} N_{i,p+1}(\xi) w_i,$$

where w_i is the i^{th} *weight*. NURBS basis is given by

$$R_i^p(\xi) = \frac{N_{i,p+1}(\xi) w_i}{W(\xi)} = \frac{N_{i,p+1}(\xi) w_i}{\sum_{\hat{i}=1}^{n} N_{\hat{i},p+1}(\xi) w_{\hat{i}}},$$

which is clearly a piecewise rational function. A NURBS curve is defined by

$$C(\xi) = \sum_{i=1}^{n} R_i^p(\xi) B_i.$$

This formulation is similar to that of a B-spline curve.

NURBS surfaces and solids are defined analogously in terms of the rational basis functions:

$$R_{i,j}^{p,q}(\xi, \eta) = \frac{N_{i,p+1}(\xi) M_{j,q+1}(\eta) w_{i,j}}{\sum_{\hat{i}=1}^{n} \sum_{\hat{j}=1}^{m} N_{\hat{i},p+1}(\xi) M_{\hat{j},q+1}(\eta) w_{\hat{i},\hat{j}}},$$

$$R_{i,j,k}^{p,q,r}(\xi, \eta, \zeta) = \frac{N_{i,p+1}(\xi) M_{j,q+1}(\eta) L_{k,r+1}(\zeta) w_{i,j,k}}{\sum_{\hat{i}=1}^{n} \sum_{\hat{j}=1}^{m} \sum_{\hat{k}=1}^{l} N_{\hat{i},p+1}(\xi) M_{\hat{j},q+1}(\eta) L_{\hat{k},r+1}(\zeta) w_{\hat{i},\hat{j},\hat{k}}}.$$

NURBS, rational basis functions, have many properties in common with piecewise polynomial B-splines, such as continuity of the functions, support, partition of unity, nonnegativity, and convex hull property.

2.5 Refinements

The basis functions can be refined in many ways, leaving the geometry unchanged. We can control element size, degree of the basis, and continuity of the basis for refinement.

Knot Insertion

We can refine the basis through *knot insertion*. New knots can be inserted into the original knot vector without changing the geometry. Given a knot vector $\Xi = \{\xi_i, \xi_2, ..., \xi_{n+p+1}\}$, we have an *extended* knot vector $\bar{\Xi} = \{\bar{\xi}_1 = \xi_1, \bar{\xi}_2, ..., \bar{\xi}_{n+m+p+1} = \xi_{n+p+1}\}$, such that $\Xi \subset \bar{\Xi}$. With the extended knot vector, new $n+m$ basis functions are constructed by Cox-de Boor formula, and new $n+m$ control points are defined from the linear combination of the original control points by

$$\begin{bmatrix} \bar{B}_1 \\ \vdots \\ \bar{B}_{n+m} \end{bmatrix} = \begin{bmatrix} \\ T^p \\ \\ \end{bmatrix} \begin{bmatrix} B_1 \\ \vdots \\ B_n \end{bmatrix}$$

where

$$T_{ij}^0 = \begin{cases} 1 & \bar{\xi}_i \in [\xi_j, \xi_{j+1}) \\ 0 & \text{otherwise} \end{cases}$$

$$T_{ij}^{q+1} = \frac{\bar{\xi}_{i+q} - \xi_j}{\xi_{j+q} - \xi_j} T_{ij}^q + \frac{\xi_{j+q+1} - \bar{\xi}_{i+q}}{\xi_{j+q+1} - \xi_{j+1}} T_{ij+1}^q \qquad \text{for } q = 0, 1, 2, ..., p-1$$

The solution space is refined by adding more basis functions through knot insertion. Knot insertion is similar to the h-version of classical FEM because it divides the original element into new elements. However, they are different in the continuity of basis functions. If we insert new knot value p times and the functions are C^0-continuous, then this knot insertion is exactly same as the h-version in FEM.

Order Elevation

Next, we can refine the basis by *order elevation* in which the degree of basis functions are increased without changing the original geometry. When the degree p is increased, multiplicities of each knot is also increased, but a new knot is not added. The process is as follows:

1. Repeat every knot in the original knot vector up to p, which is the degree of basis functions.

2. Increase the degree of the basis functions on each element.

3. Remove unnecessary knots to combine the segments into one B-spline curve.

Order elevation is similar to the p-version in classical FEM as it increases the degree of the basis functions. However, they are different in continuity of basis functions; FEM p-version always starts with C^0-continuous basis functions, while order elevation can start with the basis functions with any regularity.

k-Refinements

We increase the degree of the original basis function up to q degree and then insert a new knot value $\bar{\xi}$. The new basis functions are C^{q-1}-continuous at $\bar{\xi}$. This is called

k-refinement. There is no analogue in classical FEM. In summary, pure k-refinement keeps the element size h fixed but increases the continuity at newly inserted knots along with the polynomial order. Pure p-refinement increases the polynomial order while the basis remains C^0. Pure h-refinement inserts new knot values p times so the basis functions are C^0-continuous.

By knot insertion and order elevation, one can refine the basis functions in various ways beyond simple h, p, and k-refinements.

2.6 Partition of Unity Functions with Flat-top

We briefly review one-dimensional PU with flat-top. For details of this construction, we refer to [30], in which Oh et al. showed that PU functions with flat-top lead to a small matrix condition number. Throughout this dissertation, we choose the small real number δ, usually, $0.01 \leq \delta \leq 0.1$, for the width of non flat-top part of the PU functions. However, δ can be as small as 0.001 if there is a patch containing singularities.

For any positive integer n, C^{n-1}-continuous piecewise polynomial basic PU functions are constructed as follows: For integers $n \geq 1$, we define a piecewise polynomial function $\phi_{g_n}^{(pp)}$ by

$$\phi_{g_n}^{(pp)}(x) = \begin{cases} \phi_{g_n}^{L}(x) = (1+x)^n g_n(x), & x \in [-1, 0] \\ \phi_{g_n}^{R}(x) = (1-x)^n g_n(-x), & x \in [0, 1] \\ 0, & |x| \geq 1, \end{cases} \tag{6}$$

where $g_n(x) = a_0^{(n)} + a_1^{(n)}(-x) + a_2^{(n)}(-x)^2 + ..., +a_{n-1}^{(n)}(-x)^{n-1}$, whose coefficients are

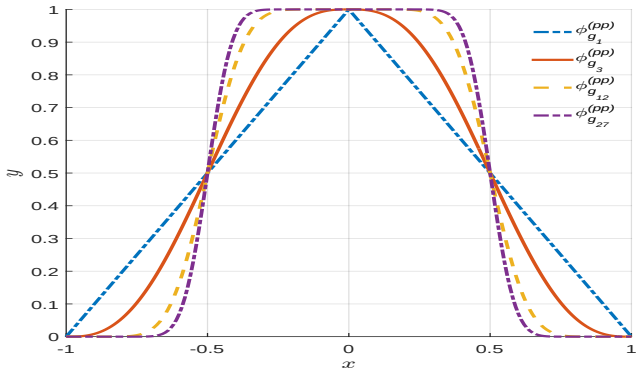

Figure 2: Reference PU functions $\phi_{g_n}^{(pp)}$ with respect to various regularities

inductively constructed by the following recursion formula:

$$a_k^{(n)} = \begin{cases} 1, & k = 0 \\ \sum_{j=0}^{k} a_j^{(n-1)}, & 0 < k \leq n-2 \\ 2(a_{n-2}^{(n)}), & k = n-1. \end{cases}$$

The $\phi_{g_n}^{(pp)}$ is depicted in Figure 2 for various regularities.

The $\phi_{g_n}^{(pp)}$ has the following properties [11]:

- $\phi_{g_n}^{(pp)}(x) + \phi_{g_n}^{(pp)}(x-1) = 1, \quad \forall x \in [0,1]$. Hence, $\{\phi_{g_n}^{(pp)}(x-j) \mid j \in Z\}$ is PU on R.

- The $\phi_{g_n}^{(pp)}$ is a C^{n-1}-continuous piecewise polynomial of degree $2n-1$.

We can construct C^{n-1}-continuous PU function with flat-top whose support is $[a -$

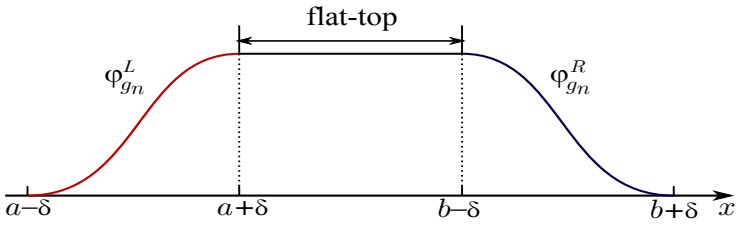

Figure 3: PU with flat-top $\psi^{(\delta,n-1)}_{[a,b]}(x)$

$\delta, b+\delta]$ with $a+\delta < b-\delta$ by the basic PU function $\phi^{(pp)}_{g_n}$.

$$\psi^{(\delta,n-1)}_{[a,b]}(x) = \begin{cases} \phi^L_{g_n}(\dfrac{x-(a+\delta)}{2\delta}), & x \in [a-\delta, a+\delta] \\ 1, & x \in [a+\delta, b-\delta] \\ \phi^R_{g_n}(\dfrac{x-(b-\delta)}{2\delta}), & x \in [b-\delta, b+\delta] \\ 0, & x \notin [a-\delta, b+\delta]. \end{cases} \tag{7}$$

In order to make a PU function a flat-top, we assume $\delta \leq \dfrac{b-a}{3}$. The $\psi^{(\delta,n-1)}_{[a,b]}$ is depicted in Figure 3. If $\varphi : [-\delta, \delta] \to [0,1]$ is defined by

$$\varphi(x) = \frac{x+\delta}{2\delta},$$

then we have

$$\phi^R_{g_n}(\varphi(x)) + \phi^L_{g_n}(\varphi(x)-1) = 1, \quad \xi \in [-\delta, \delta]$$

by the first property of PU function $\phi^{(pp)}_{g_n}$, $\phi^R_{g_n}(\xi) + \phi^L_{g_n}(\xi - 1) = 1, \quad \xi \in [0,1]$. Therefore, the collection of $\psi^{(\delta,n-1)}_{[a,b]}$ is PU.

The gradient of the PU function with flat-top $\psi^{(\delta,n-1)}_{[a,b]}$ is bounded as follows:

$$\left| \frac{d}{dx} \left[\psi^{(\delta,n-1)}_{[a,b]}(x) \right] \right| \leq \frac{C_1}{2\delta}, \tag{8}$$

Table 1: The upper bound of the gradient of reference PU function $\phi_{g_n}^{(pp)}$ of (6) for various degrees

degree	$n=2$	$n=3$	$n=5$	$n=7$	$n=10$	$n=15$	$n=20$	$n=30$
upper bound	1.5	1.88	2.46	2.93	3.52	4.33	5.01	6.15

where C_1 is an upper bound of the gradient of $\phi_{g_n}^{(pp)}$ defined by (6). The upper bounds of the gradient of $\phi_{g_n}^{(pp)}$ for various degree are shown in Table 1 [30].

The second derivative of the PU function with flat-top $\psi_{[a,b]}^{(\delta,n-1)}$ is bounded as follows:

$$\left| \frac{d^2}{dx^2} \left[\psi_{[a,b]}^{(\delta,n-1)}(x) \right] \right| \leq \frac{C_2}{4\delta^2}. \tag{9}$$

Here, C_2 is an upper bound of the second derivative of $\phi_{g_n}^{(pp)}$ defined by (6).

2.7 Boundary Layer Analysis

We follow the definitions and terminologies of [27]. Usually, we cannot solve the equations from mathematical models analytically. Then, we approximate the solution of the equation through approximation and/or numerical methods. The perturbation method is one of approximation techniques used for the equations that have small terms.

Consider a differential equation

$$F(x, y, y', y'', \varepsilon) = 0, \tag{10}$$

where x is the independent variable and y is the dependent variable. In the equation, the parameter ε is shown explicitly, $\varepsilon \ll 1$. (10) is called the *perturbed problem*. A

perturbation series is a power series in ε of the form

$$y_0(x) + \varepsilon y_1(x) + \varepsilon^2 y_2(x).... \tag{11}$$

Regular perturbation method is as follows:

- Assume the perturbation series (11) as a solution of the differential equation (10).
- Substitute the series (11) into the differential equation (10).
- Find $y_0, y_1, y_2...$

Usually, the first two or three terms of the series form an approximate solution, called *perturbation solution*. If the approximation is uniform, the regular perturbation method is generally successful. The term y_0 is called the *leading order term*; the terms $\varepsilon y_1, \varepsilon^2 y_2, ...$ are called *higher-order correction terms* that are expected to be small. If the method is successful, y_0 will be the solution of the *unperturbed problem*

$$F(x, y, y', y'', 0) = 0,$$

in which ε is set to zero. However, There are many situations where a regular perturbation method does not give an approximate solution.

- When the small parameter multiplies the highest derivative in the problem.
- When setting the small parameter equal to zero changes the character of the problem, as in the case of a partial differential equation changing type or an algebraic equation changing degree. In other words, the solution for $\varepsilon = 0$ is fundamentally different in character from the solutions for ε close to zero.

- When problems occur on infinite domains, giving secular terms (correction term that is not small).
- When singular points are present in the interval of interest.
- When the equations that model physical processes have multiple time or spatial scales.

These problems are called *singular perturbation problems*. The singular perturbation method applied to the problems that have boundary layers is called the *boundary layer theory* or *matched asymptotic expansions*. The boundary layer theory is as follows.

- Determine whether there is a *boundary layer*, where the solution is changing very rapidly in a narrow interval
- Determine where the boundary layer is located.
- Find the leading-order perturbation term by setting $\varepsilon = 0$. This is a valid approximation in a large outer region (*outer layer*) away from the boundary layer.
- Rescale the independent variable x in the boundary layer by selecting a small spatial scale that will reflect rapid and abrupt changes and will force each term in the equation into its proper form in the rescaled variables. The inner approximation in the boundary layer is found by rescaling.
- The *inner* and *outer* approximations can be matched to obtain a uniformly valid approximation over the entire interval of interest.

To illustrate the boundary layer theory, we approximate a solution of a singularly perturbed problem, following the example in [27]. Consider a model boundary value problem

$$\varepsilon y'' + (1+\varepsilon)y' + y = 0, \quad 0 < x < 1,$$

$$y(0) = 0, \quad y(1) = 1,$$

where $0 < \varepsilon \ll 1$. We present the numerical result of this problem in Chapter 4.

Outer Approximation

In the region where $x = \mathcal{O}(1)$, the solution could be approximated by setting $\varepsilon = 0$ in the equation to obtain

$$y' + y = 0$$

and selecting the boundary condition $y(1) = 1$. This gives the outer approximation

$$y_o(x) = e^{1-x}.$$

Inner Approximation

In the boundary layer, there are significant changes in y that take place on a very short interval, which suggests a length scale on the order of a function of ε, say $\delta(\varepsilon)$. If we change the variable via

$$\xi = \frac{x}{\delta(\varepsilon)}, \qquad y(x) = y(\delta(\varepsilon)\xi) \equiv Y(\xi) \tag{12}$$

and use the chain rule, the differential equation (12) becomes

$$\frac{\varepsilon}{\delta(\varepsilon)^2} Y''(\xi) + \frac{(1+\varepsilon)}{\delta(\varepsilon)} Y'(\xi) + Y(\xi) = 0,$$

Table 2: Three cases to consider for dominant balancing

	Same Order	Small in comparison
i.	$\varepsilon/\delta(\varepsilon)^2 \sim 1/\delta(\varepsilon)$	$\varepsilon/\delta(\varepsilon),\ 1$
ii.	$\varepsilon/\delta(\varepsilon)^2 \sim 1$	$1/\delta(\varepsilon),\ \varepsilon/\delta(\varepsilon)$
iii.	$\varepsilon/\delta(\varepsilon)^2 \sim \varepsilon/\delta(\varepsilon)$	$1/\delta(\varepsilon),\ 1$

where prime denotes derivatives with respect to ξ. By this scale transformation, we examine the boundary layer close up.

The coefficients of the four terms in the differential equation are:

$$\frac{\varepsilon}{\delta(\varepsilon)^2}, \quad \frac{1}{\delta(\varepsilon)}, \quad \frac{\varepsilon}{\delta(\varepsilon)}, \quad 1. \tag{13}$$

If the scaling is correct, each will reflect the order of magnitude of the term in which it appears. To determine the scale factor $\delta(\varepsilon)$, we estimate the magnitudes by considering all possible dominant balances between pairs of terms in (13) (*dominant balancing*). In the pairs, we include the first term because it was ignored in the outer layer, and it is known that it plays a significant role in the boundary layer. Because the goal is to make a simplification in the problem we do not consider dominant balancing of three terms. If all four terms are equally important, no simplification can be made. Therefore, there are three cases to consider in Table 2.

In case i of Table 2, $\varepsilon/\delta(\varepsilon)^2 \sim 1/\delta(\varepsilon)$ forces $\delta(\varepsilon) = O(\varepsilon)$, then $\varepsilon/\delta(\varepsilon)^2$ and $1/\delta(\varepsilon)$ are both order $1/\varepsilon$, which is large compared to $\varepsilon/\delta(\varepsilon)$ and 1. Therefore, a consistent scaling is possible if we select $\delta(\varepsilon) = O(\varepsilon)$; hence, we take

$$\delta(\varepsilon) = \varepsilon.$$

Therefore, the scaled differential equation (12) becomes

$$Y'' + Y' + \varepsilon Y' + \varepsilon Y = 0. \tag{14}$$

Now, we can apply the regular perturbation method to (14). Because we are interested only in the leading-order approximation, which we denote by Y_i, we set $\varepsilon = 0$ in (14) to obtain

$$Y_i'' + Y_i' = 0.$$

The general solution is

$$Y_i(\xi) = C_1 + C_2 e^{-\xi}.$$

Because the boundary layer is located near $x = 0$, we apply the boundary condition $y(0) = 0$, or $Y_i(0) = 0$. This yields $C_2 = -C_1$, and so

$$Y_i(\xi) = C_1(1 - e^{-\xi}).$$

In terms of y and x,

$$y_i(x) = C_1(1 - e^{-x/\varepsilon}). \tag{15}$$

This is the inner approximation for $x = O(\epsilon)$.

In summary, we have the approximate solution

$$y_o(x) = e^{1-x}, \quad x = O(1)$$

$$y_i(x) = C_1(1 - e^{-x/\varepsilon}), \quad x = O(\varepsilon),$$

each valid for an appropriate rage of x. There remains to determine the constant C_1, which is accomplished by the process of matching. We are mainly interested in

the inner approximation in the boundary layer analysis to approximate the boundary layer behavior.

CHAPTER 3: PARTITION OF UNITY ISOGEOMETRIC ANALYSIS

In the framework of Isogeometric Galerkin method, we partition the domain into patches using Partition of Unity (PU) with flat-top to place the necessary basis functions on each patch, which is referred to as Partition of Unity Isogeometric Analysis (PU-IGA).

3.1 Construction of Partition of Unity Functions with Flat-top

First, we show how to construct partition of unity with flat-top.

- **PU functions constructed by convolutions:** The PU function with flat-top (7) can be constructed by the convolution,

$$\psi_{[a,b]}^{(\delta,n-1)}(x) = \chi_{[a,b]}(x) * w_\delta^n(x), \tag{16}$$

  where the scaled window function w_δ^n is defined by (3), and the characteristic function is defined by

$$\chi_{[a,b]}(x) = \begin{cases} 1 & \text{if } x \in [a,b], \\ 0 & \text{if } x \notin [a,b]. \end{cases}$$

- **PU functions constructed by B-splines:** Using the PU property of the B-splines, the PU function with flat-top (7) can also be constructed by B-spline functions.

  1. For $\mathcal{C}^1$-continuous piecewise polynomial PU functions with flat-top, let

$N_{i,4}(x), i = 1, \ldots, 12$ be B-splines of degree 3 that correspond to the open knot vector:

$$\Big\{ \underbrace{0,..,0}_{4}, \underbrace{a-\delta, a-\delta}_{2}, \underbrace{a+\delta, a+\delta}_{2}, \underbrace{b-\delta, b-\delta}_{2}, \underbrace{b+\delta, b+\delta}_{2}, \underbrace{1,..,1}_{4} \Big\}$$

A polynomial $P_3(x)$ of degree 3 defined on $[a-\delta, a+\delta]$ is uniquely determined by four constraints:

$$P_3(a-\delta) = 0, \quad P_3(a+\delta) = 1$$
$$\frac{d}{dx}P_3(a-\delta) = \frac{d}{dx}P_3(a+\delta) = 0$$

$\phi^L_{g_2}(\frac{x-(a+\delta)}{2\delta})$ satisfies the four constraints, and $N_{5,4}(x) + N_{6,4}(x)$ satisfies the four constraints. Therefore, we have

$$\phi^L_{g_2}(\frac{x-(a+\delta)}{2\delta}) = N_{5,4}(x) + N_{6,4}(x), \text{ for } x \in [a-\delta, a+\delta].$$

Similarly, we have

$$\phi^R_{g_2}(\frac{x-(b-\delta)}{2\delta}) = N_{7,4}(x) + N_{8,4}(x), \text{ for } x \in [b-\delta, b+\delta].$$

Using the partition of unity property of B-splines, we have

$$N_{5,4}(x) + N_{6,4}(x) + N_{7,4}(x) + N_{8,4}(x) = 1, \text{ for } x \in [a+\delta, b-\delta].$$

2. For $\mathcal{C}^2$-continuous piecewise polynomial PU functions with flat-top, let $N_{i,6}(x), i = 1, \ldots, 18$, be B-splines of degree 5 corresponding to the open

knot vector,

$$\Big\{\underbrace{0,..,0}_{6},\underbrace{a-\delta,..,a-\delta}_{3},\underbrace{a+\delta,..,a+\delta}_{3},\underbrace{b-\delta,..,b-\delta}_{3},\underbrace{b+\delta,..,b+\delta}_{3},\underbrace{1,..,1}_{6}\Big\}.$$

A polynomial $P_5(x)$ of degree 5 defined on $[a-\delta, a+\delta]$ is uniquely determined by six constraints: three at $a-\delta$ and three at $a+\delta$,

$$\begin{aligned} P_5(a-\delta) = 0, \quad P_5(a+\delta) = 1 \\ \frac{d}{dx}P_5(a-\delta) = \frac{d}{dx}P_5(a+\delta) = 0 \\ \frac{d^2}{dx^2}P_5(a-\delta) = \frac{d^2}{dx^2}P_5(a+\delta) = 0 \end{aligned}$$

$\phi^L_{g_3}(\frac{x-(a+\delta)}{2\delta})$ satisfies the six constraints, and $N_{7,6}(x)+N_{8,6}(x)+N_{9,6}(x)$ satisfies the six constraints. Therefore, we have

$$\phi^L_{g_3}(\frac{x-(a+\delta)}{2\delta}) \;=\; N_{7,6}(x)+N_{8,6}(x)+N_{9,6}(x), \text{ for } x\in[a-\delta,a+\delta].$$

Similarly, we have

$$\phi^R_{g_3}(\frac{x-(b-\delta)}{2\delta}) \;=\; N_{10,6}(x)+N_{11,6}(x)+N_{12,6}, \text{ for } x\in[b-\delta,b+\delta].$$

Moreover, we have

$$N_{7,6}(x)+N_{8,6}(x)+N_{9,6}(x)+N_{10,6}(x)+N_{11,6}(x)+N_{12,6}=1, \text{ for } x\in[a+\delta,b-\delta].$$

3. In general, for each n, the $\mathcal{C}^{n-1}$-continuous piecewise polynomial PU function with flat-top can be constructed by the B-splines of degree $2n-1$,

$N_{i,2n}(x), i = 1, \ldots, 6n$, corresponding to the open knot vector:

$$\Big\{ \underbrace{0,..,0}_{2n}, \underbrace{a-\delta,..,a-\delta}_{n}, \underbrace{a+\delta,..,a+\delta}_{n}, \underbrace{b-\delta,..,b-\delta}_{n}, \underbrace{b+\delta,..,b+\delta}_{n}, \underbrace{1,..,1}_{2n} \Big\}.$$

We have

$$\psi_{[a,b]}^{(\delta,n-1)}(x) = \begin{cases} \sum_{k=1}^{n} N_{2n+k,2n}(x) & \text{if} \quad x \in [a-\delta, a+\delta] \\ \sum_{k=1}^{2n} N_{2n+k,2n}(x) = 1 & \text{if} \quad x \in [a+\delta, b-\delta] \\ \sum_{k=1}^{n} N_{3n+k,2n}(x) & \text{if} \quad x \in [b-\delta, b+\delta] \\ 0 & \text{if} \quad x \notin [a-\delta, b+\delta]. \end{cases} \tag{17}$$

3.2 Two Dimensional PU with Flat-top

Let $\hat{\Omega} = [0,1] \times [0,1]$ be the parameter space. Partition $\hat{\Omega}$ into rectangular subdomains $\hat{\Omega}_{ij}$ as follows:

- $[0,1]$ is a disjoint union of subintervals $[\xi_i, \xi_{i+1}), i = 1, 2, \ldots, N-1$ and $[\xi_N, \xi_{N+1}]$.

  $\delta_\xi = \min\{\xi_{i+1} - \xi_i : i = 1, \ldots, N\}$.

- $[0,1]$ is a disjoint union of subintervals $[\eta_j, \eta_{j+1}), i = 1, 2, \ldots, M-1$ and $[\eta_M, \eta_{M+1}]$.

  $\delta_\eta = \min\{\eta_{j+1} - \eta_j : j = 1, \ldots, M\}$.

- $\hat{\Omega}_{ij} = [\xi_i, \xi_{i+1}) \times [\eta_j, \eta_{j+1})$. Assume $0 < \delta \leq \min\{\delta_\xi/3, \delta_\eta/3\}$.

Let w_δ^η be the scaled window function defined by (3). Since the sum of characteristic functions of partitioned subintervals is one on $[0,1]$ ($\sum_{i=1}^{N} \chi_{[\xi_i, \xi_{i+1})} = 1$), the

convolutions of w_δ^n with the characteristic functions become a PU.

$$\Big(\sum_{i=1}^{N}\chi_{[\xi_i,\xi_{i+1})}\Big) * w_\delta^n = \sum_{i=1}^{N}(\chi_{[\xi_i,\xi_{i+1})} * w_\delta^n) = \sum_{i=1}^{N}\hat{\Psi}_i(\xi) = 1, \text{ for each } \xi \in [0,1],$$
$$\Big(\sum_{j=1}^{M}\chi_{[\eta_j,\eta_{j+1})}\Big) * w_\delta^n = \sum_{j=1}^{M}(\chi_{[\eta_j,\eta_{j+1})} * w_\delta^n) = \sum_{i=1}^{N}\hat{\Psi}_j(\eta) = 1, \text{ for each } \eta \in [0,1].$$

Let two dimensional PU with flat-top be a tensor product of one dimensional PUs as follows:

$$\hat{\Psi}_{i,j}(\xi,\eta) = \Big(\chi_{[\xi_i,\xi_{i+1})} * w_\delta^n\Big) \times \Big(\chi_{[\eta_j,\eta_{j+1})} * w_\delta^n\Big), \text{ for } i = 1,\dots,N; j = 1,\dots,M. \quad (18)$$

Then, we have the following:

1. $\sum_{i=1}^{N}\sum_{j=1}^{M}\hat{\Psi}_{i,j}(\xi,\eta) = 1, \text{ for each } (\xi,\eta) \in \hat{\Omega}.$

2. $\text{supp}\hat{\Psi}_{i,j} = \Big([\xi_i - \delta, \xi_{i+1} + \delta] \cap [0,1]\Big) \times \Big([\eta_j - \delta, \eta_{j+1} + \delta] \cap [0,1]\Big).$

3. $\hat{\Psi}_{i,j}(\xi,\eta)$ are $\mathcal{C}^{n-1}$-continuous PU functions with flat-top.

4. $\chi_{[\xi_i,\xi_{i+1})} * w_\delta^n$ and $\chi_{[\eta_j,\eta_{j+1})} * w_\delta^n$ are given by (16). Hence, for example, if $1 \le i,j \le 3$, $\hat{\Omega}_{ij}$, $\text{supp}\hat{\Psi}_{i,j}$, and $\hat{\Psi}_{i,j}(\xi,\eta)$ are as follows:

$$\hat{\Omega}_{11} = [0,a]\times[0,c], \quad \hat{\Omega}_{21} = [a,b]\times[0,c], \quad \hat{\Omega}_{31} = [b,1]\times[0,c],$$
$$\hat{\Omega}_{12} = [0,a]\times[c,d], \quad \hat{\Omega}_{22} = [a,b]\times[c,d], \quad \hat{\Omega}_{32} = [b,1]\times[c,d],$$
$$\text{supp}(\hat{\Psi}_{11}) = [0,a+\delta]\times[0,c+\delta], \quad \text{supp}(\hat{\Psi}_{21}) = [a-\delta,b+\delta]\times[0,c+\delta],$$
$$\text{supp}(\hat{\Psi}_{31}) = [b-\delta,1]\times[0,c+\delta], \quad \text{supp}(\hat{\Psi}_{12}) = [0,a+\delta]\times[c-\delta,d+\delta],$$
$$\text{supp}(\hat{\Psi}_{22}) = [a-\delta,b+\delta]\times[c-\delta,d+\delta], \quad \text{supp}(\hat{\Psi}_{32}) = [b-\delta,1]\times[c-\delta,d+\delta],$$

$$\hat{\Psi}_{11}(\xi,\eta)=\psi^{\delta}_{[0,a]}(\xi)\cdot\psi^{\delta}_{[0,c]}(\eta),\ \hat{\Psi}_{21}(\xi,\eta)=\psi^{\delta}_{[a,b]}(\xi)\cdot\psi^{\delta}_{[0,c]}(\eta),\ \hat{\Psi}_{31}(\xi,\eta)=\psi^{\delta}_{[b,1]}(\xi)\cdot\psi^{\delta}_{[0,c]}(\eta),$$

$$\hat{\Psi}_{12}(\xi,\eta)=\psi^{\delta}_{[0,a]}(\xi)\cdot\psi^{\delta}_{[c,d]}(\eta),\ \hat{\Psi}_{22}(\xi,\eta)=\psi^{\delta}_{[a,b]}(\xi)\cdot\psi^{\delta}_{[c,d]}(\eta),\ \hat{\Psi}_{32}(\xi,\eta)=\psi^{\delta}_{[b,1]}(\xi)\cdot\psi^{\delta}_{[c,d]}(\eta),$$

where $\psi^{(\delta,n-1)}_{[\alpha,\beta]}$ is defined by (7), and $\hat{\Omega}_{ij}, 1\le i,j\le 3$, are the rectangles, shown in Figure 4.

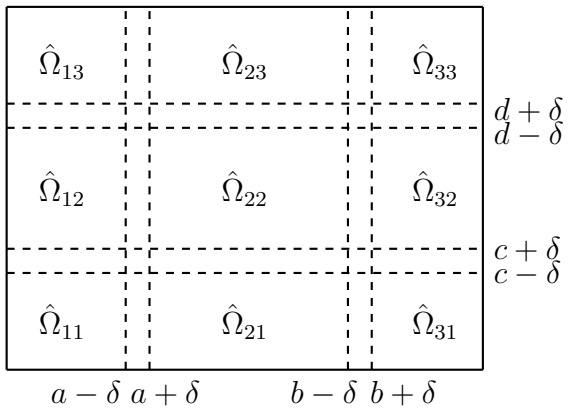

Figure 4: Supports of 2D PU with Flat-top $\hat{\Psi}_{ij}$ and subdomains $\hat{\Omega}_{ij}, 1\le i,j\le 3$

3.3 Error Analysis for PU-IGA

We estimate the error bound of the PU-Galerkin method with respect to PU with flat-top, modifying the proofs [1, 30]. The proof of the higher dimensional case is similar to that of the one-dimensional case. First, we prove one-dimensional error bound.

Let $\Omega=[\alpha,\beta]$ and $x_0=\alpha<x_1<,\ldots,x_N=\beta$ be a partition of Ω. Let $\{\psi^{\delta}_i\}_{i=1}^N$ be PU with flat-top and 2δ be the size of a non flat-top zone. For each $i=1,\ldots,N$, let $Q_i=[x_{i-1}-\delta,x_i+\delta]$, $\mathrm{supp}(\psi^{\delta}_i)=Q_i$ and $\sum_{i=1}^N\psi^{\delta}_i(x)=1$ for all $x\in\Omega$. Let $\mathcal{V}_i=\mathrm{span}\{f^i_k(x),k=1,\ldots,n_i\}$ be the local approximation space on patch Q_i, and $\mathcal{V}=\mathrm{span}\{\psi^{\delta}_i(x)f^i_k(x):k=1,\ldots,n_i,i=1,\ldots,N\}$ be the global approxima-

tion space on Ω. Let U^i be a local approximation of u on the patch Q_i. Then, Galerkin approximation of the true solution $u(x)$ on the patch Q_i can be expressed as $\sum_{k=1}^{n_i} \xi_k^i f_k^i(x), \xi_k^i \in R$. The PU Galerkin approximation with respect to PU functions with flat-top $\psi_i^\delta(x)$ for the true solution $u(x)$ on the whole domain can be expressed as

$$u(x) \approx U(x) = \sum_{i=1}^{N} \psi_i^\delta(x) \Big(\sum_{k=1}^{n_i} \xi_k^i f_k^i(x) \Big),$$

for some constants $\xi_k^i, k = 1, \ldots, n_i, i = 1, \ldots, N$. The total number of global basis functions is $\sum_{i=1}^{N} n_i$.

Suppose for each i, there is $U^i \in \mathcal{V}_i$ such that

$$\begin{aligned}
\|u - U^i\|_{L^2(Q_i \cap \Omega)} &\le \varepsilon_0(i), \qquad \|\frac{d}{dx}(u - U^i)\|_{L^2(Q_i \cap \Omega)} \le \varepsilon_1(i) \\
\|\frac{d^2}{dx^2}(u - U^i)\|_{L^2(Q_i \cap \Omega)} &\le \varepsilon_2(i), \qquad \|u - U^i\|_{L^2(Q_i^\delta \cap \Omega)} \le \varepsilon_0^\delta(i) \\
\|\frac{d}{dx}(u - U^i)\|_{L^2(Q_i^\delta \cap \Omega)} &\le \varepsilon_1^\delta(i), \qquad \|\frac{d^2}{dx^2}(u - U^i)\|_{L^2(Q_i^\delta \cap \Omega)} \le \varepsilon_2^\delta(i)
\end{aligned} \tag{19}$$

where $Q_i^\delta = [x_{i-1} - \delta, x_{i-1} + \delta] \cup [x_i - \delta, x_i + \delta] \subset Q_i = [x_{i-1} - \delta, x_i + \delta]$ and $\text{meas}(Q_i^\delta \cap \Omega) \le 4\delta$. The first three are local errors on the patch Q_i. The last three are local errors on the non flat-top zone, Q_i^δ.

Theorem 1. Under the assumptions (19), we have the following error estimates:

$$\begin{aligned}
(i) \quad \|u - U\|_{L^2(\Omega)} &\le \sqrt{2} \Big\{ \sum_{i=1}^{N} [\varepsilon_0(i)]^2 \Big\}^{1/2} \\
(ii) \quad \|\frac{d}{dx}(u - U)\|_{L^2(\Omega)} &\le 2 \Big\{ \sum_{i=1}^{N} \Big[[\frac{C_1}{2\delta}]^2 [\varepsilon_0^\delta(i)]^2 + [\varepsilon_1(i)]^2 \Big] \Big\}^{1/2} \\
(iii) \quad \|\frac{d^2}{dx^2}(u - U)\|_{L^2(\Omega)} &\le \Big\{ 6 \sum_{i=1}^{N} \Big([\frac{C_2}{4\delta^2}]^2 [\varepsilon_0^\delta(i)]^2 + 4 [\frac{C_1}{2\delta}]^2 [\varepsilon_1^\delta(i)]^2 + [\varepsilon_2(i)]^2 \Big) \Big\}^{1/2},
\end{aligned}$$

where $C_1 = \|\frac{d\phi_{g_n}^{(pp)}(x)}{dx}\|_\infty$ and $C_2 = \|\frac{d^2\phi_{g_n}^{(pp)}(x)}{dx^2}\|_\infty$, and $\phi_{g_n}^{(pp)}(x)$ is the unscaled reference PU function defined by (6), and the size of δ is

$$\min\{0.05, 0.05 \cdot (h/3)\} \le \delta \le \min\{0.1, h/3\} \quad \text{in [30].}$$

Proof. (i) Consider the following new partition of Ω:

$$x_1^* = x_0, \quad x_k^* = (x_{k-1} + x_k)/2, \text{ for } k = 2, \ldots, N-1, \quad x_N^* = x_N.$$

Then, these two PU functions ψ_k^δ, ψ_{k+1}^δ are non zero on the subinterval $[x_k^*, x_{k+1}^*]$, for $k = 1, \ldots, N-1$. Thus, we have

$$\begin{aligned}
\int_\Omega (u-U)^2 &= \int_\Omega \Big[(\sum_{i=1}^N \psi_i^\delta)u - \sum_{i=1}^N (\psi_i^\delta \sum_{k=1}^{n_i} \xi_k^i f_k^i)\Big]^2, \quad \text{by } \sum_{i=1}^N \psi_i^\delta = 1 \\
&= \sum_{k=1}^{N-1} \int_{[x_k^*, x_{k+1}^*]} \Big[\sum_{i=1}^N \psi_i^\delta \Big(u - U^i\Big)\Big]^2, \quad \text{by } U^i(x) = \sum_{k=1}^{n_i} \xi_k^i f_k^i(x) \\
&= \sum_{k=1}^{N-1} \int_{[x_k^*, x_{k+1}^*]} \Big[\psi_k^\delta \Big(u - U^k\Big) + \psi_{k+1}^\delta \Big(u - U^{k+1}\Big)\Big]^2 \\
&\le \sum_{k=1}^{N-1} \int_{[x_k^*, x_{k+1}^*]} 2\Big[[\psi_k^\delta \Big(u - U^k\Big)]^2 + [\psi_{k+1}^\delta \Big(u - U^{k+1}\Big)]^2\Big] \\
&= 2\sum_{k=1}^{N-1} \int_{[x_k^*, x_{k+1}^*]} \sum_{i=1}^N \big[\psi_i^\delta \Big(u - U^i\Big)\big]^2 \\
&= 2\int_\Omega \sum_{i=1}^N \big[\psi_i^\delta \Big(u - U^i\Big)\big]^2 \\
&\le 2\sum_{i=1}^N \int_{Q_i \cap \Omega} \Big[u - U^i\Big]^2, \quad \text{by } 0 \le \psi_i^\delta \le 1 \\
&= 2\sum_{i=1}^N [\varepsilon_0(i)]^2, \quad \text{by } \|u - U^i\|_{L^2(Q_i \cap \Omega)} = \varepsilon_0(i)
\end{aligned}$$

□

Proof. (ii) Using a similar argument adopted in (i), we have

$$
\begin{aligned}
\int_\Omega [\frac{d}{dx}(u-U)]^2 &= \int_\Omega \Big[\frac{d}{dx}\{(\sum_{i=1}^N \psi_i^\delta)u - \sum_{i=1}^N (\psi_i^\delta \sum_{k=1}^{n_i} \xi_k^i f_k^i)\}\Big]^2 \\
&= \int_\Omega \Big[\sum_{i=1}^N \frac{d}{dx}\big[\psi_i^\delta\Big(u-U^i\Big)\big]\Big]^2, \quad \text{by } U^i = \sum_{k=1}^{n_i} \xi_k^i f_k^i \\
&= \int_\Omega \Big[\sum_{i=1}^N [\frac{d}{dx}\psi_i^\delta](u-U^i) + \sum_{i=1}^N \psi_i^\delta [\frac{d}{dx}(u-U^i)]\Big]^2 \\
&\le 2\int_\Omega \Big(\sum_{i=1}^N [\frac{d}{dx}\psi_i^\delta](u-U^i)\Big)^2 + 2\int_\Omega \Big(\sum_{i=1}^N \psi_i^\delta [\frac{d}{dx}(u-U^i)]\Big)^2 \\
&\le 4\int_\Omega \sum_{i=1}^N \Big([\frac{d}{dx}\psi_i^\delta](u-U^i)\Big)^2 + 4\int_\Omega \sum_{i=1}^N \Big(\psi_i^\delta [\frac{d}{dx}(u-U^i)]\Big)^2 \\
&\le 4\sum_{i=1}^N \int_{Q_i\cap\Omega} \Big([\frac{d}{dx}\psi_i^\delta]^2(u-U^i)^2 + [\psi_i^\delta]^2[\frac{d}{dx}(u-U^i)]^2\Big) \\
&\le 4\sum_{i=1}^N \Big(\int_{Q_i\cap\Omega} [\frac{d}{dx}\psi_i^\delta]^2(u-U^i)^2 + \int_{Q_i\cap\Omega} [\frac{d}{dx}(u-U^i)]^2\Big), \quad \text{by } 0\le\psi_i^\delta\le 1 \\
&\le 4\sum_{i=1}^N \Big([\frac{C_1}{2\delta}]^2 \int_{Q_i^\delta\cap\Omega} (u-U^i)^2 + \int_{Q_i\cap\Omega} [\frac{d}{dx}(u-U^i)]^2\Big) \quad \text{by (8)} \\
&\le 4\sum_{i=1}^N \Big([\frac{C_1}{2\delta}]^2 [\varepsilon_0^\delta(i)]^2 + [\varepsilon_1(i)]^2\Big)
\end{aligned}
$$

□

Proof. (iii) Using a similar argument adopted in (i) and (ii), we have

$$
\begin{aligned}
&\int_\Omega [\frac{d^2}{dx^2}(u-U)]^2 = \int_\Omega \Big[\frac{d^2}{dx^2}\{\sum_{i=1}^N \psi_i^\delta u - \sum_{i=1}^N \psi_i^\delta U^i\}\Big]^2 = \int_\Omega \Big[\sum_{i=1}^N \frac{d^2}{dx^2}\big[\psi_i^\delta\Big(u-U^i\Big)\big]\Big]^2 \\
= &\sum_{k=1}^{N-1} \int_{[x_k^*, x_{k+1}^*]} \Big[\sum_{i=1}^N [\frac{d^2}{dx^2}\psi_i^\delta](u-U^i) + \sum_{i=1}^N 2\frac{d}{dx}\psi_i^\delta \frac{d}{dx}(u-U^i) + \sum_{i=1}^N \psi_i^\delta [\frac{d^2}{dx^2}(u-U^i)]\Big]^2 \\
\le\ & 3\sum_{k=1}^{N-1} \int_{[x_k^*, x_{k+1}^*]} \Big\{\Big[\sum_{i=1}^N [\frac{d^2}{dx^2}\psi_i^\delta](u-U^i)\Big]^2 + \Big[2\sum_{i=1}^N \frac{d}{dx}\psi_i^\delta \frac{d}{dx}(u-U^i)\Big]^2 + \Big[\sum_{i=1}^N \psi_i^\delta [\frac{d^2}{dx^2}(u-U^i)]\Big]^2
\end{aligned}
$$

$$
\begin{aligned}
&\leq 6\int_{\Omega}\sum_{i=1}^{N}\Big\{\Big[[\frac{d^2}{dx^2}\psi_i^{\delta}](u-U^i)\Big]^2+4\Big[\frac{d}{dx}\psi_i^{\delta}\frac{d}{dx}(u-U^i)\Big]^2+\Big[\psi_i^{\delta}[\frac{d^2}{dx^2}(u-U^i)]\Big]^2\Big\}\\
&\leq 6\sum_{i=1}^{N}\int_{Q_i\cap\Omega}\Big\{\Big[[\frac{d^2}{dx^2}\psi_i^{\delta}](u-U^i)\Big]^2+4\Big[\frac{d}{dx}\psi_i^{\delta}\frac{d}{dx}(u-U^i)\Big]^2+\Big[\psi_i^{\delta}[\frac{d^2}{dx^2}(u-U^i)]\Big]^2\Big\}\\
&\leq 6\sum_{i=1}^{N}\Big([\frac{C_2}{4\delta^2}]^2[\varepsilon_0^{\delta}(i)]^2+4[\frac{C_1}{2\delta}]^2[\varepsilon_1^{\delta}(i)]^2+[\varepsilon_2(i)]^2\Big),\quad \text{by (9)}.
\end{aligned}
$$

□

In Theorem 1, (ii) and (iii) shows that the error bound in the energy norm depends on the selection of δ, which is the size of a non flat-top zone. With small δ size, we might have small local errors, ε_0^{δ}, ε_1^{δ}, and ε_2^{δ}, but we could have large constant $C/2\delta$. (i) shows that the error bound in the L^2-norm does not depend on the selection of δ. We choose δ between 0.001 and 0.1. An optimal choice of δ was discussed in [19].

Next, we prove the error bound in the energy norm for the two dimensional case.

Theorem 2. Let $x=(x_1,x_2)\in\mathbb{R}^2$, $\{\psi_i(x)\}_{i=1}^N$ be the two-dimensional PU with flat-top. Let the support of $\psi_i(x)$ be Ω_i, and the non flat-top part of the support of $\psi_i(x)$ be Ω_i^{δ}. Suppose $u\in H^2(\Omega)$ is the true solution, U^i is the local approximation on the patch Ω_i, and U is the Galerkin approximation with respect to PU with flat-top $\{\psi_i(x)\}_{i=1}^N$ on the whole domain Ω. Then, $U^i(x)=\sum_{k=1}^{n_i}\xi_k^i f_k^i(x)$ and $U(x)=\sum_{i=1}^{N}\psi_i(\sum_{k=1}^{n_i}\xi_k^i f_k^i(x))$. Suppose the local errors on Ω_i and Ω_i^{δ} are as follows:

$$
\|u-U^i\|_{L^2(\Omega_i)}\leq\varepsilon_0(i),\qquad \|\bigtriangledown(u-U^i)\|_{L^2(\Omega_i)}\leq\varepsilon_1(i),\qquad \|\triangle(u-U^i)\|_{L^2(\Omega_i)}\leq\varepsilon_2(i),
$$

$$
\|u-U^i\|_{L^2(\Omega_i^{\delta})}\leq\varepsilon_0^{\delta}(i),\qquad \|\bigtriangledown(u-U^i)\|_{L^2(\Omega_i^{\delta})}\leq\varepsilon_1^{\delta}(i),\qquad \|\triangle(u-U^i)\|_{L^2(\Omega_i^{\delta})}\leq\varepsilon_2^{\delta}(i).
$$

Then, we have the following error estimate:

$$\|\triangle(u-U)\|^2_{L^2(\Omega)} \leq 27\Big\{\sum_{k=1}^{N}\Big[[\frac{C_2}{2\delta^2}]^2[\varepsilon_0^\delta(k)]^2 + 4[\frac{C_1}{\delta}]^2[\varepsilon_1^\delta(k)]^2 + [\varepsilon_2(k)]^2\Big]\Big\},$$

where $C_1 = \|\frac{d\phi_{g_n}^{(pp)}(x_1)}{dx_1}\|_\infty$ and $C_2 = \|\frac{d^2\phi_{g_n}^{(pp)}(x_1)}{dx_1^2}\|_\infty$, and $\phi_{g_n}^{(pp)}(x_1)$ is the unscaled reference PU function defined by (6).

Proof.

$$\begin{aligned}
&\|\triangle(u-U)\|^2_{L^2(\Omega)} = \|\triangle\Big(\sum_{i=1}^{N}\psi_i u - \sum_{i=1}^{N}\psi_i U^i\Big)\|^2_{L^2(\Omega)} = \|\triangle\Big(\sum_{i=1}^{N}\psi_i(u-U^i)\Big)\|^2_{L^2(\Omega)}\\
&= \|\Big(\sum_{i=1}^{N}\triangle\psi_i(u-U^i) + 2\sum_{i=1}^{N}\bigtriangledown\psi_i \bigtriangledown (u-U^i) + \sum_{i=1}^{N}\psi_i\triangle(u-U^i)\Big)\|^2_{L^2(\Omega)}\\
&\leq 3\Big[\|\sum_{i=1}^{N}\triangle\psi_i(u-U^i)\|^2_{L^2(\Omega)} + \|2\sum_{i=1}^{N}\bigtriangledown\psi_i \bigtriangledown (u-U^i)\|^2_{L^2(\Omega)} + \|\sum_{i=1}^{N}\psi_i\triangle(u-U^i)\|^2_{L^2(\Omega)}\Big]
\end{aligned}$$

By Lemma 3, each ψ_i has non void intersections with, at most, nine PU functions in its support. By Lemma 4, $\|\triangle\psi_i\|$ and $\|\bigtriangledown\psi_i\|$ are bounded by constants. Hence, we have

$$\begin{aligned}
&\|\triangle(u-U^i)\|^2_{L^2(\Omega)}\\
&\leq 3\cdot 9\Big[\sum_{i=1}^{N}\|\triangle\psi_i(u-U^i)\|^2_{L^2(\Omega)} + 4\sum_{i=1}^{N}\|\bigtriangledown\psi_i \bigtriangledown (u-U^i)\|^2_{L^2(\Omega)} + \sum_{i=1}^{N}\|\psi_i\triangle(u-U^i)\|^2_{L^2(\Omega)}\Big]\\
&\leq 27\Big\{\sum_{i=1}^{N}\Big(\frac{C_2}{2\delta^2}\Big)^2\|(u-U^i)\|^2_{L^2(\Omega_i^\delta)} + 4\sum_{i=1}^{N}\Big(\frac{C_1}{\delta}\Big)^2\|\bigtriangledown(u-U^i)\|^2_{L^2(\Omega_i^\delta)} + \sum_{i=1}^{N}\|\triangle(u-U^i)\|^2_{L^2(\Omega_i)}\Big\}\\
&\leq 27\Big\{\sum_{k=1}^{N}\Big[(\frac{C_2}{2\delta^2})^2[\varepsilon_0^\delta(k)]^2 + 4(\frac{C_1}{\delta})^2[\varepsilon_1^\delta(k)]^2 + [\varepsilon_2(k)]^2\Big]\Big\}.
\end{aligned}$$

□

Lemma 3. Two dimensional ψ_i is defined by (18). The support of ψ_i is rectangular.

$$\begin{aligned}
\|\sum_{i=1}^{N} \triangle\psi_i(u-U^i)\|^2_{L^2(\Omega)} &\leq 9\sum_{i=1}^{N} \|\Big(\triangle\psi_i(u-U^i)\Big)\|^2_{L^2(\Omega)} \\
\|\sum_{i=1}^{N} \bigtriangledown\psi_i \bigtriangledown (u-U^i)\|^2_{L^2(\Omega)} &\leq 9\sum_{i=1}^{N} \| \bigtriangledown \psi_i \bigtriangledown (u-U^i)\|^2_{L^2(\Omega)} \\
\|\sum_{i=1}^{N} \psi_i\triangle(u-U^i)\|^2_{L^2(\Omega)} &\leq 9\sum_{i=1}^{N} \|\psi_i\triangle(u-U^i)\|^2_{L^2(\Omega)}.
\end{aligned}$$

Proof.

$$\|\sum_{i=1}^{N} \triangle\psi_i(u-U^i)\|^2_{L^2(\Omega)} = \int_\Omega \Big[\sum_{i=1}^{N} \triangle\psi_i(u-U^i)\Big]^2 = \sum_{k=1}^{N}\int_{\Omega_k} \Big[\sum_{i=1}^{N} \triangle\psi_i(u-U^i)\Big]^2$$

Only nine PU functions do not vanish on each patch, Ω_k. Three one-dimensional PU functions in the one direction and the other three one-dimensional PU functions in the other direction do not vanish in each interval, respectively.

$$\begin{aligned}
&= \sum_{k=1}^{N}\int_{\Omega_k} \Big(\triangle\psi_{i1}(u-U^{i1}) + \triangle\psi_{i2}(u-U^{i2}) + ... + \triangle\psi_{i9}(u-U^{i9})\Big)^2 \\
&\leq \sum_{k=1}^{N}\int_{\Omega_k} 9\Big[\Big(\triangle\psi_{i_1}(u-U^{i_1})\Big)^2 + \Big(\triangle\psi_{i_2}(u-U^{i_2})\Big)^2 + ... + \Big(\triangle\psi_{i_9}(u-U^{i_9})\Big)^2\Big] \\
&= \sum_{k=1}^{N}\int_{\Omega_k} 9\sum_{i=1}^{N}\Big[\Big(\triangle\psi_i(u-U^i)\Big)\Big]^2 = 9\int_\Omega \sum_{i=1}^{N}\Big[\Big(\triangle\psi_i(u-U^i)\Big)\Big]^2 \\
&= 9\sum_{i=1}^{N}\int_\Omega \Big[\Big(\triangle\psi_i(u-U^i)\Big)\Big]^2 = 9\sum_{i=1}^{N} \|\Big(\triangle\psi_i(u-U^i)\Big)\|^2
\end{aligned}$$

Similarly, we can prove the other two inequalities. □

Lemma 4. Let $x = (x_1, x_2) \in R^2$ and $\psi_i(x)$ be a two-dimensional PU, $\psi_i(x) = \phi_{i_1}(x_1)\phi_{i_2}(x_2)$, which is a tensor product of one-dimensional PUs $\phi_{i_1}(x_1)$ and $\phi_{i_2}(x_2)$. Assume that the one-dimensional PUs have the same size non-flat top part, 2δ. Then,

we have

$$\| \bigtriangledown \psi_i\| \leq \frac{C_1}{\delta}, \qquad \|\triangle\psi_i\| \leq \frac{C_2}{2\delta^2}$$

where $C_1 = \|\frac{d\phi_{g_n}^{(pp)}(x_1)}{dx_1}\|_\infty$ and $C_2 = \|\frac{d^2\phi_{g_n}^{(pp)}(x_1)}{dx_1^2}\|_\infty$, and $\phi_{g_n}^{(pp)}(x_1)$ is the unscaled reference PU function defined by (6).

Proof.

$$\begin{aligned}
\| \bigtriangledown \psi_i\| &= \| \bigtriangledown \phi_{i_1}(x_1)\phi_{i_2}(x_2)\| = \sqrt{(\frac{d\phi_{i_1}(x_1)\phi_{i_2}(x_2)}{dx_1})^2 + (\frac{d\phi_{i_1}(x_1)\phi_{i_2}(x_2)}{dx_2})^2} \\
&\leq \|\frac{d\phi_{i_1}(x_1)\phi_{i_2}(x_2)}{dx_1}\| + \|\frac{d\phi_{i_1}(x_1)\phi_{i_2}(x_2)}{dx_2}\| \leq \|\frac{d\phi_{i_1}(x_1)}{dx_1}\| + \|\frac{d\phi_{i_2}(x_2)}{dx_2}\| \\
&\leq \frac{C_1}{2\delta} + \frac{C_1}{2\delta} = \frac{C_1}{\delta}
\end{aligned}$$

$$\begin{aligned}
\|\triangle\psi_i\| &= \|\triangle\phi_{i_1}(x_1)\phi_{i_2}(x_2)\| = \|\frac{d^2\phi_{i_1}(x_1)\phi_{i_2}(x_2)}{{dx_1}^2} + \frac{d^2\phi_{i_1}(x_1)\phi_{i_2}(x_2)}{{dx_2}^2}\| \\
&\leq \|\frac{d^2\phi_{i_1}(x_1)\phi_{i_2}(x_2)}{{dx_1}^2}\| + \|\frac{d^2\phi_{i_1}(x_1)\phi_{i_2}(x_2)}{{dx_2}^2}\| \leq \|\frac{d^2\phi_{i_1}(x_1)}{{dx_1}^2}\| + \|\frac{d^2\phi_{i_2}(x_2)}{{dx_2}^2}\| \\
&\leq \frac{C_2}{4\delta^2} + \frac{C_2}{4\delta^2} = \frac{C_2}{2\delta^2}
\end{aligned}$$

□

Theorem 2 shows that the error in the energy norm depends on δ, size of the non flat-top part as we observe in the error estimate of one dimension.

3.4 Total Cost Comparison of PU-IGA with IGA

The total cost for a numerical method is determined by the number of quadrature points, the polynomial degrees of the basis functions, the regularity of enrichment functions, the number of elements, the spatial dimension, etc. Extensive cost comparisons of IGA-Collocation and IGA-Galerkin with FEA-Galerkin were shown in

[45]. We compare the computational cost of PU-IGA with that of IGA in bandwidth, operation counts, and number of Gauss points.

Let $N_{i,p+1}(x), i = 1, \ldots, m_k^p$, be $\mathcal{C}^{p-k}$-continuous B-spline functions of degree p corresponding to the open knot vector:

$$\Xi = \{\underbrace{0, \ldots, 0}_{p+1}, \underbrace{\xi_1, \ldots, \xi_1}_{k}, \underbrace{\xi_2, \ldots, \xi_2}_{k}, \ldots, \underbrace{\xi_{n-1}, \ldots, \xi_{n-1}}_{k}, \underbrace{\xi_n, \ldots, \xi_n}_{k}, \underbrace{1, \ldots, 1}_{p+1}\} \tag{20}$$

where $1 \leq k \leq p$ and $m_k^p = nk + p + 1$.

Suppose $AX = B$ is the algebraic system of the discrete variational equation of $-u'' = f$ with respect to B-spline basis functions, corresponding to (20).

- **Bandwidth** For a sparse matrix $A = [a_{ij}]_{1 \leq i,j \leq m_k^p}$, the smallest integers l_1 and l_2, such that $a_{ij} = 0$ for $i - j > l_1$ and $a_{ij} = 0$ for $j - i > l_2$, are called the lower and the upper bandwidth, respectively. The bandwidth of A is defined by $l_1 + l_2$.

  The bandwidth of the matrix A is $2p$ if $k = 1$ or $k = p$; $2p-1$ otherwise. As for IGA, we use B-spline basis functions of high orders, $p \geq 10$ in Table 5, of the numerical example in Chapter 4. While, the author in [15] uses the piecewise linear basis functions for the conventional FEM for the results, shown in Table 5. In this example, the bandwidth of A by IGA is orders of magnitude larger than that of A corresponding to piecewise linear basis functions because IGA uses higher degrees of basis functions. If they use the same degree, the bandwidth would be the same. In PU-IGA, we choose the degree of B-splines in patch-wise manner without sacrificing the regularity of local approximation functions. For

example, we could choose $\mathcal{C}^9$-continuous B-spline basis functions of degree 10 on a patch, Q_1, where we need higher order basis functions. Whereas, we could select $\mathcal{C}^1$-continuous B-spline basis functions of degree 2 on another patch, Q_2, where higher degree of basis functions are not required. If we use IGA, then we should use the basis functions of degree 10 for the whole domain. Then, the bandwidth of A would be 20. However, if we use PU-IGA, which divides patches and puts different degrees of basis functions into each patch, we could have block matrices A_1 and A_2 of A with A_1 of bandwidth 4 and A_2 of bandwidth 20.

- **Operation Counts**

  Let k, multiplicity of (20) be 1 or p. Since the stiffness matrix A is symmetric, then operation counts for LU factorization and forward/backward substitution is $p^2 \cdot m_p^k/2 + 2p \cdot m_p^k$, where m_p^k is the number of basis functions and p is the degree of B-splines.

  Instead of using one degree and one family of B-spline basis functions for the whole domain, if we choose selectively the degree and a family of B-splines in a patch-wise manner, then the number of operations can be reduced because of less basis functions and smaller degrees on each patch.

- **Number of quadrature points**

  Suppose $f_l^i(x), l = 1, \ldots, n_i$, are local approximation polynomials of degree p on a patch, $Q_i = [x_{i-1} - \delta, x_i + \delta]$, and $\psi_{Q_i}^{\delta}(x)$ is a $\mathcal{C}^1$-continuous PU function with flat-top of degree 3. Then, $\psi_{Q_i}^{\delta}(x) f_l^i(x), l = 1, \ldots, n_i$, are polynomials of degree $p+3$ on the non flat-top parts, $Q_i^{\delta} = [x_{i-1} - \delta, x_{i-1} + \delta] \cup [x_i - \delta, x_i + \delta]$, and are

polynomials of degree p on the flat-top part $[x_i + \delta, x_{i+1} - \delta]$. The number of quadrature points for the integral on the non flat-top part is $(p+4)/2$, while the number of quadrature points for the integral on the flat-top part is $(p+1)/2$. Hence, the total number of quadrature points for the integral of $\mathcal{C}^1$-continuous three piece-polynomial $\psi^{\delta}_{Q_i}(x) f^i_l(x)$ on Q_i is

$$\frac{p+1}{2} + (p+4)$$

because we have two parts of non flat-top parts. While IGA needs the number of quadrature points, $(p+1)/2$. In PU-IGA, a few extra quadrature points are required for the integrals of polynomial local approximation functions defined on non flat-top zones.

3.5 Basis Functions of Enriched PU-IGA

In this section, we describe how to construct basis functions in enriched PU-IGA. Let

$$\hat{\Psi}_{ij}, \quad \text{for } i = 1, \ldots, N; j = 1, \ldots, M. \tag{21}$$

be PU functions with flat-top defined on the reference domain $\hat{\Omega} = [0,1] \times [0,1]$. Note that we construct PU functions on the reference domain rather than a physical domain.

We use the following notations for enriched PU-IGA:

1. Subdomains of Ω, $\hat{\Omega}_{ij} = [\xi_i, \xi_{i+1}] \times [\eta_j, \eta_{j+1}]$

2. $\text{supp}(\hat{\Psi}_{ij}) = [\xi_i - \delta, \xi_{i+1} + \delta] \times [\eta_j - \delta, \eta_{j+1} + \delta] \equiv \hat{\Omega}^*_{ij}$

3. $\varphi_{ij} : \hat{\Omega} = [0,1] \times [0,1] \longrightarrow \text{supp}(\hat{\Psi}_{ij})$ is the linear mapping from the parameter domain onto a patch $\text{supp}(\hat{\Psi}_{ij}) \supset \hat{\Omega}_{ij}$.

4. $\hat{B}_{st}(\xi,\eta) = N_s(\xi) \times M_t(\eta)$, $1 \le s \le n_p$ and $1 \le t \le m_q$ are two-dimensional B-spline functions defined on $[0,1] \times [0,1]$ parameter domain.

5. $\tilde{B}_{st}^{(ij)} = \hat{B}_{st} \circ \varphi_{ij}^{-1}$, for $1 \le i \le N, 1 \le j \le M$, $1 \le s \le n_p, 1 \le t \le m_q$, are two-dimensional B-spline functions defined on the patch, Ω_{ij}^{*}.

Let $G : \hat{\Omega} \longrightarrow \Omega$ be a design mapping. Suppose we know an enrichment function $h(x,y)$ that resembles either a boundary layer function or a singular function on a subdomain $\Omega_{i_0,j_0} = G(\hat{\Omega}_{i_0 j_0})$ of physical domain Ω.

We call $\hat{h} = (h \circ G)$ the *pullback* of the enrichment function h into the reference domain, and $h = \hat{h} \circ G^{-1}$ the *push-forward* of $\hat{h}$ into the physical domain.

The basis functions on the parameter domain are those in $\hat{\mathcal{V}}_1 \cup \hat{\mathcal{V}}_0$ that consist of B-spline functions and an enrichment function modified by PU functions, where

$$\hat{\mathcal{V}}_1 = \left\{ \begin{array}{ll} \left(\hat{\Psi}_{ij} \cdot \tilde{B}_{st}^{(ij)}\right) & : \ 1 \le s \le n_i; 1 \le t \le n_j, \text{ and} \\ & \qquad i = 1, \ldots, N; j = 1, \ldots, M, \ ij \ne i_0 j_0 \end{array} \right\},$$

$$\hat{\mathcal{V}}_0 = \left\{ \hat{h}(\xi,\eta) \cdot \hat{\Psi}_{i_0 j_0}(\xi,\eta), \quad \left(\hat{\Psi}_{i_0 j_0} \cdot \tilde{B}_{st}^{(i_0 j_0)}\right) \ : \ 1 \le s \le n_{i_0}; 1 \le t \le n_{j_0} \right\}.$$

Now the approximation space $\mathcal{V}^h$ in the physical domain Ω enriched by $h(x,y)$ is the vector space spanned by linearly independent basis functions in $(\hat{\mathcal{V}}_1 \circ G^{-1}) \cup (\hat{\mathcal{V}}_0 \circ G^{-1})$:

$$\mathcal{V}^h = \text{span}\Big(\hat{\mathcal{V}}_1 \circ G^{-1} \cup \hat{\mathcal{V}}_0 \circ G^{-1}\Big).$$

Then, we calculate the stiffness matrix by the reference element approach. Let

$$\nabla_x = (\frac{\partial}{\partial x}, \frac{\partial}{\partial y})^T, \quad \nabla_\xi = (\frac{\partial}{\partial \xi}, \frac{\partial}{\partial \eta})^T, \quad \mathbf{G} : \hat{\Omega} = [0,1] \times [0,1] \longrightarrow \Omega$$

Suppose $\mathcal{B}(u,v) = \int_\Omega (\nabla_x v)^T \cdot (\nabla_x u)$. Then for two basis functions in $\mathcal{V}^h$ we have

$$\begin{aligned}
&\mathcal{B}(\Big(\hat{\Psi}_{ij} \cdot \tilde{B}^{(ij)}_{s't'}\Big) \circ G^{-1}, \Big(\hat{\Psi}_{lm} \cdot \tilde{B}^{(lm)}_{st}\Big) \circ G^{-1}) \\
&= \int_\Omega (\nabla_x \Big(\hat{\Psi}_{lm} \cdot \tilde{B}^{(lm)}_{s't'}\Big) \circ G^{-1})^T \cdot (\nabla_x \Big(\hat{\Psi}_{ij} \cdot \tilde{B}^{(ij)}_{st}\Big) \circ G^{-1}) dxdy \\
&= \int_{\hat{\Omega}^*_{ij;lm}} (\nabla_\xi \Big(\hat{\Psi}_{lm} \cdot \tilde{B}^{(lm)}_{s't'}\Big))^T \cdot \Big[(J(\mathbf{G})^{-1})^T \cdot J(\mathbf{G})^{-1} |J(\mathbf{G})|\Big] (\nabla_\xi \Big(\hat{\Psi}_{ij} \cdot \tilde{B}^{(ij)}_{st}\Big)) d\xi d\eta
\end{aligned}$$

where $\hat{\Omega}^*_{ij;lm} = \text{supp}\hat{\Psi}_{ij} \cap \text{supp}\hat{\Psi}_{lm}$, $\hat{\Omega}^*_{ij;lm}$ is a slim rectangle with δ width or length if $ij \neq lm$, and $\hat{\Omega}^*_{ij;lm}$ is a rectangle which is the support of $\hat{\Psi}_{ij}$, if $ij = lm$.

Unlike PU-FEM and enriched IGA in [35, 36], since PU functions are constructed in the reference domain, the intersection of supports of any two basis functions modified by the PU function is always a rectangle on the reference domain that we could integrate easily. Note that we could have this feature, integration over rectangular area, since PU functions are constructed in the reference domain.

CHAPTER 4: SINGULARLY PERTURBED CONVECTION DIFFUSION EQUATIONS IN A CIRCLE

4.1 Introduction

We consider a singularly perturbed problem that is a stationary convection-diffusion equation

$$\begin{cases} -\varepsilon \triangle u - u_y = f(x,y) & \text{in } \Omega \\ u = 0 & \text{on } \partial\Omega \end{cases} \tag{22}$$

where $0 < \varepsilon \ll 1$, Ω is the unit circle centered at $(0,0)$, and the function f is as smooth as needed.

The variational formulation of (22) reads: Find $u^\varepsilon \in H_0^1(\Omega)$ such that

$$a(u,v) := \varepsilon(\nabla u, \nabla v) - (u_y, v) = (f,v), \quad \forall v \in H_0^1(\Omega). \tag{23}$$

In [13, 14], the authors discussed the problem (22) analytically. It was shown that a boundary layer occurs around the lower half circle, $x^2 + y^2 = 1, y < 0$, and singular behaviors can occur at the characteristic points $(\pm 1, 0)$ if f does not satisfy compatibility conditions.

In [23], [37], [38] and [50], finer meshes around the boundary layer and domain decomposition are used to solve singularly perturbed problems. In [13, 14], the authors studied convection-diffusion equations in rectangular and circular domains using uni-

form rectangular meshes that incorporate boundary layer correctors. [15] showed the numerical solutions to the problem using a piecewise linear classical finite element space enriched by the boundary layer correctors. Similarly, we develop the boundary layer functions through boundary layer analysis and approximate the solution of (22) in PU-IGA finite element space enriched by the boundary layer functions that are scaled by a PU function. We apply enriched PU-IGA to the same problem as [15] tested and compare the results. We have better numerical results with less degree of freedom than that of [15]. We extend this to a singular perturbation problem on ellipse in which we similarly develop the boundary layer approximation through boundary layer analysis.

4.2 Geometric Mapping

We define the geometric mapping G from the parameter to physical domains. The mapping $G : \hat{\Omega} \longrightarrow \Omega$ is defined by

$$G(\xi, \eta) = (x(\xi, \eta), y(\xi, \eta) = ((1 - \eta)\cos 2\pi\xi, (1 - \eta)\sin 2\pi\xi) \tag{24}$$

where $\eta = 1 - r, r$ is the distance to the origin and $2\pi\xi$ is the polar angle from origin of the circle. We define the reference domain as $\hat{\Omega} = [0, 1] \times [0, 1]$ and the physical domain as $\Omega = \{(x, y)|x^2+y^2 \leq 1\}$. Note that Isogeometric analysis makes it possible to use the exact geometric representation of CAD objects for analysis, a circle in this example. For our convenience, we express mapping G by parametrization rather than the linear combination of NURBS basis functions since we use parametric mapping G when we analyze the boundary layer approximation.

4.3 Boundary Layer Analysis

We analyze the boundary layer approximation on the reference domain using the geometric mapping, $G(\xi, \eta)$ defined by (24). Let

$$\hat{u}(\xi, \eta) = u \circ G(\xi, \eta).$$

By the chain rule,

$$\frac{\partial \hat{u}}{\partial \xi} = \frac{\partial u}{\partial x}(G(\xi,\eta)\frac{\partial x}{\partial \xi} + \frac{\partial u}{\partial y}(G(\xi,\eta))\frac{\partial y}{\partial \xi}, \qquad \frac{\partial \hat{u}}{\partial \eta} = \frac{\partial u}{\partial x}(G(\xi,\eta)\frac{\partial x}{\partial \eta} + \frac{\partial u}{\partial y}(G(\xi,\eta))\frac{\partial y}{\partial \eta}.$$

We have

$$\frac{\partial u}{\partial x} = -\frac{\sin 2\pi\xi}{2\pi(1-\eta)}\frac{\partial \hat{u}}{\partial \xi} - \cos 2\pi\xi \frac{\partial \hat{u}}{\partial \eta}, \qquad \frac{\partial u}{\partial y} = -\frac{\cos 2\pi\xi}{2\pi(1-\eta)}\frac{\partial \hat{u}}{\partial \xi} - \sin 2\pi\xi \frac{\partial \hat{u}}{\partial \eta},$$

$$\triangle u = \frac{\partial^2 u}{\partial x^2} + \frac{\partial^2 u}{\partial y^2} = \frac{\partial^2 \hat{u}}{\partial \eta^2} - \frac{1}{1-\eta}\frac{\partial \hat{u}}{\partial \eta} + \frac{1}{(1-\eta)^2}\frac{\partial^2 \hat{u}}{\partial \xi^2}.$$

By this change of variables, the equation (22) becomes

$$\begin{aligned} -\varepsilon \triangle u - u_y &= -\varepsilon \frac{\partial^2 \hat{u}}{\partial \eta^2} - \frac{\varepsilon}{4\pi^2(1-\eta)^2}\frac{\partial^2 \hat{u}}{\partial \xi^2} + \frac{\varepsilon}{1-\eta}\frac{\partial \hat{u}}{\partial \eta} - \frac{\cos 2\pi\xi}{2\pi(1-\eta)}\frac{\partial \hat{u}}{\partial \xi} + \sin 2\pi\xi \frac{\partial \hat{u}}{\partial \eta} \\ &= f((1-\eta)\cos 2\pi\xi, (1-\eta)\sin 2\pi\xi). \end{aligned} \tag{25}$$

We analyze the behavior in the boundary layer around $\eta = 0, 0 \leq \xi \leq 1/2$ in the reference domain. There are significant changes in $\hat{u}$ taking place on a very short η interval, which suggest a length scale on the order of a function of ε, say ε^α. We introduce the stretched variable

$$\bar{\eta} = \frac{\eta}{\varepsilon^\alpha}.$$

The equation (25) is transformed to

$$-\varepsilon^{1-2\alpha}\frac{\partial^2\hat{u}}{\partial\bar{\eta}^2}-\frac{\varepsilon}{4\pi^2(1-\varepsilon^{\alpha}\bar{\eta})^2}\frac{\partial^2\hat{u}}{\partial\xi^2}+\frac{\varepsilon^{1-\alpha}}{1-\varepsilon^{\alpha}\bar{\eta}}\frac{\partial\hat{u}}{\partial\bar{\eta}}-\frac{\cos 2\pi\xi}{2\pi(1-\varepsilon^{\alpha}\bar{\eta})}\frac{\partial\hat{u}}{\partial\xi}+\sin 2\pi\xi\varepsilon^{-\alpha}\frac{\partial\hat{u}}{\partial\bar{\eta}}=f(G^{-1}(\xi,\eta)).$$

The coefficients of the terms in the differential equation are

$$\varepsilon^{1-2\alpha},\quad \varepsilon,\quad \varepsilon^{1-\alpha},\quad \varepsilon^{-\alpha}, \tag{26}$$

To determine α, we estimate these magnitudes by considering all possible dominant balances between pairs of terms in (26). If $\varepsilon^{1-2\alpha}$ and $\varepsilon^{-\alpha}$ are the same order, both of them are order $1/\varepsilon$, which is large compared to ε and $\varepsilon^{1-\alpha}$. Therefore, a consistent scaling is possible if we select $\alpha = 1$. In other words, a reasonable boundary layer equation is determined by setting $\alpha = 1$ by dominant balancing. Hence, we have

$$-\varepsilon^{-1}\frac{\partial^2\hat{u}}{\partial\bar{\eta}^2}-\frac{\varepsilon}{4\pi^2(1-\varepsilon\bar{\eta})^2}\frac{\partial^2\hat{u}}{\partial\xi^2}+\frac{1}{1-\varepsilon\bar{\eta}}\frac{\partial\hat{u}}{\partial\bar{\eta}}-\frac{\cos 2\pi\xi}{2\pi(1-\varepsilon\bar{\eta})}\frac{\partial\hat{u}}{\partial\xi}+\sin 2\pi\xi\varepsilon^{-1}\frac{\partial\hat{u}}{\partial\bar{\eta}}=f(G),$$

$$-\frac{\partial^2\hat{u}}{\partial\bar{\eta}^2}-\frac{\varepsilon^2}{4\pi^2(1-\varepsilon\bar{\eta})^2}\frac{\partial^2\hat{u}}{\partial\xi^2}+\frac{\varepsilon}{1-\varepsilon\bar{\eta}}\frac{\partial\hat{u}}{\partial\bar{\eta}}-\frac{\varepsilon\cos 2\pi\xi}{2\pi(1-\varepsilon\bar{\eta})}\frac{\partial\hat{u}}{\partial\xi}+\sin 2\pi\xi\frac{\partial\hat{u}}{\partial\bar{\eta}}=\varepsilon f(G). \tag{27}$$

Now, we can apply the regular perturbation to (27). Because we are interested only in the leading-order approximation, we set $\varepsilon = 0$ in (27) to obtain

$$-\frac{\partial^2\hat{u}}{\partial\bar{\eta}^2}\frac{\partial\hat{u}}{\partial\xi}+\sin 2\pi\xi\frac{\partial\hat{u}}{\partial\bar{\eta}}=0.$$

The general solution is

$$\hat{u}(\xi,\bar{\eta})=C_1+C_2\exp(\sin 2\pi\xi)\bar{\eta}.$$

Because the boundary layer is located around the lower half circle on the physical domain, hence near $\eta = 0$ and $1/2 < \xi < 1$ on the reference domain, we apply the boundary condition $\hat{u} = 0$ at $\eta = 0$. Thus, we have

$$C_2 = -C_1,$$

$$\hat{u}(\xi, \bar{\eta}) = C_1(1 - \exp(\sin 2\pi\xi)\bar{\eta}), \quad 1/2 < \xi < 1.$$

In terms of ξ and η

$$\hat{u}(\xi, \eta) = C_1(1 - \exp(\sin 2\pi\xi)\frac{\eta}{\varepsilon}), \quad 1/2 < \xi < 1.$$

The boundary layer approximation can be written as

$$\hat{u}(\xi, \eta) = C_1(1 - \exp(\sin 2\pi\xi)\frac{\eta}{\varepsilon})\ \chi_{[1/2,1]}(\xi),$$

where $\chi_A(\xi)$ is the characteristic function of A.

4.4 PU-IGA Approximation Space

We define IGA approximation space, $\tilde{\mathcal{V}}$, and the enriched PU-IGA approximation space, $\mathcal{V}$, which includes the boundary layer element, φ_0:

$$\begin{aligned}
\tilde{\mathcal{V}} &= \{\sum_{i=1}^{N} c_i R_i(x, y)\} \subset H_0^1(\Omega) \\
\mathcal{V} &= \{\sum_{i=1}^{N} c_i R_i(x, y) + \sum_{i=1}^{M} d_i(\varphi_0(\xi, \eta) \circ G^{-1})(N_i(\xi) \circ G^{-1})\} \subset H_0^1(\Omega),
\end{aligned}$$

where c_i and d_i are amplitude constants, N is the number of B-splines corresponding to the knot vectors in ξ and η directions, M is the number of basis functions along Γ_l, where $\Gamma_l = \{(x, y) =\mid x^2 + y^2 = 1, y < 0\}$, $R_i(x, y)$ is push-forwards of tensor product

of univariate B-splines $1 \leq i \leq N$, $N_i(\xi)$ is B-spline basis functions in ξ direction $1 \leq i \leq M$, and $\varphi_0(\xi, \eta)$ is the boundary layer function defined by

$$\varphi_0(\xi, \eta) = (1 - \exp(\frac{\sin 2\pi\xi}{\varepsilon}\eta))\psi(\eta)\chi_{[0.5,1]}(\xi). \tag{28}$$

(28) is the boundary layer approximation multiplied by PU with flat-top, $\psi(\eta)$ defined by

$$\psi(\eta) = \begin{cases} 0, & \text{if } \eta \in [b+\delta, 1] \\ \phi^R_{g_2}(\frac{\eta-(b-\delta)}{2\delta}, & \text{if } \eta \in [b-\delta, b+\delta] \\ 1, & \text{if } \eta \in [0, b-\delta] \end{cases} \tag{29}$$

We can now formulate the following discrete analogues of the problem (23). Find a $\tilde{u}_h \in \tilde{\mathcal{V}}$ and $u_h \in \mathcal{V}$, respectively, such that

$$\begin{aligned} a(\tilde{u}_h, v) &= (f, v), \quad \forall v \in \tilde{\mathcal{V}} \\ a(u_h, v) &= (f, v), \quad \forall v \in \mathcal{V}, \end{aligned}$$

where $a(\cdot, \cdot)$ is the bilinear form defined by (23).

To treat the boundary layers, we add the boundary layer functions in $\mathcal{V}$. There are several ways to augment the basis of $\tilde{\mathcal{V}}$ by adding different boundary layer functions.

1. $\{\varphi_0(\xi_1, \eta)N_1(\xi), \varphi_0(\xi_2, \eta)N_2(\xi), ..., \varphi_0(\xi_M, \eta)N_M(\xi)\}$,

2. $\{\varphi_0(0.75, \eta)N_1(\xi), \varphi_0(0.75, \eta)N_2(\xi), ..., \varphi_0(0.75, \eta)N_M(\xi)\}$,

3. $\{\varphi_0(\xi, \eta)N_1(\xi), \varphi_0(\xi, \eta)N_2(\xi), ..., \varphi_0(\xi, \eta)N_M(\xi)\}$,

where M is the number of B-splines in ξ direction on the lower semicircle. Here, φ_0 is

the boundary layer function defined by (28). First, we obtain M different enrichment functions by plugging in different values in ξ direction. Second, we obtain only one enrichment function by plugging in one value in ξ direction. In the first and second one, we consider the boundary layer function as a function of η. Lastly, we obtain a boundary layer function as a function of ξ and η. For convenience of implementation, we are going to use the second choice of a boundary layer function, which is plugging a specific value in ξ direction into the boundary layer function, namely

$$\hat{\varphi}_0(\eta) = (1 - \exp(\frac{-\eta}{\varepsilon}))\psi(\eta). \tag{30}$$

Incorporating the boundary layer functions that absorb the singularity behavior in the finite space, we expect accurate numerical results in the PU-IGA framework without using fine meshes around the boundary layer.

4.5 Construction of Basis Functions

We divide the physical domain into three patches to apply different basis functions on each patch. In the outer region (away from the boundary layer), we could obtain an optimal solution by the standard Galerkin method. The boundary layer zone requires more sophisticated basis functions;therfore, we add boundary layer functions on the patch where the boundary layer is.

Partition of the Domain Ω

We consider that a covering of the physical domain consists of three patches: one

disk and two annular regions, shown in Fig. 5, that are defined as follows:

$$\begin{aligned}\Omega_1^* &= \{(x,y) : 0 \le x^2+y^2 \le (1-(b-\delta))^2\},\\ \Omega_2^* &= \{(x,y) : (1-(b+\delta))^2 \le x^2+y^2 \le (1-(a-\delta))^2\},\\ \Omega_3^* &= \{(x,y) : (1-(a+\delta))^2 \le x^2+y^2 \le 1\}. \end{aligned} \tag{31}$$

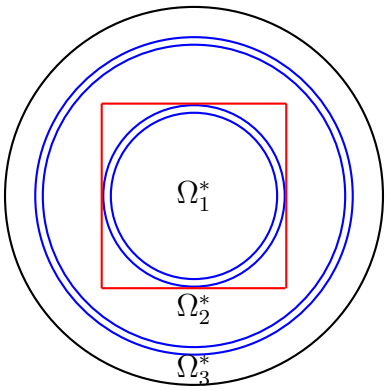

Figure 5: Supports of circular PU functions in the physical domain.

To construct basis functions on these three patches, we need to construct PU functions with flat-top, Ψ_1, Ψ_2, Ψ_3, defined on three patches $\Omega_1^*, \Omega_2^*, \Omega_3^*$, respectively. For this end, we consider a covering of the parameter domain $\hat{\Omega}$, consisting of the following three patches:

$$\hat{\Omega}_1^* = [0,1]\times[b-\delta,1], \quad \hat{\Omega}_2^* = [0,1]\times[a-\delta,b+\delta], \quad \hat{\Omega}_3^* = [0,1]\times[0,a+\delta].$$

Construction of PU function on the reference domain

For constructions of circular PU functions with flat-top, we define PU functions

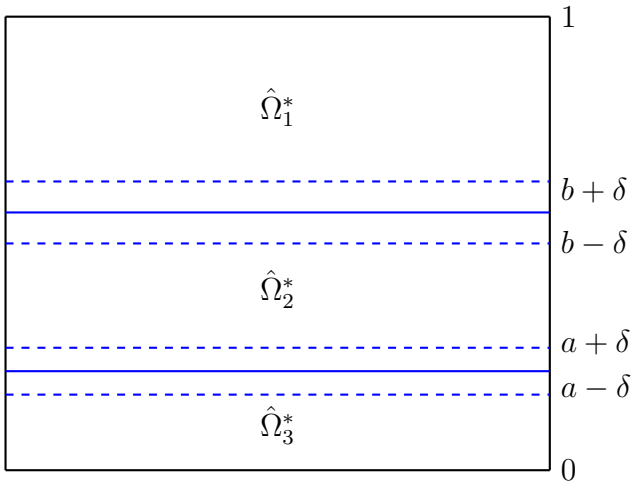

Figure 6: Supports of PU function with flat-top in the reference Domain, $\hat{\Omega}_1^* = [1,0]\times[b-\delta,1], \hat{\Omega}_2^* = [1,0]\times[a-\delta,b+\delta], \hat{\Omega}_3^* = [1,0]\times[0,a+\delta]$.

$\hat{\Psi}_i, i=1,2,3$, on rectangular patches $\hat{\Omega}_i^*, i=1,2,3$, respectively, as follows:

$$\hat{\Psi}_1(\xi,\eta) = \begin{cases} \phi_{g_2}^L(\frac{\eta-(b+\delta)}{2\delta}) & \text{if } \eta\in[b-\delta,b+\delta] \\ 1 & \text{if } \eta\in[b+\delta,1] \\ 0 & \text{if } \eta\notin[b-\delta,1], \end{cases} \tag{32}$$

$$\hat{\Psi}_2(\xi,\eta) = \begin{cases} \phi_{g_2}^L(\frac{\eta-(a+\delta)}{2\delta}) & \text{if } \eta\in[a-\delta,a+\delta] \\ 1 & \text{if } \eta\in[a+\delta,b-\delta] \\ \phi_{g_2}^R(\frac{\eta-(b-\delta)}{2\delta}) & \text{if } \eta\in[b-\delta,b+\delta] \\ 0 & \text{if } \eta\notin[a-\delta,b+\delta], \end{cases} \tag{33}$$

$$\hat{\Psi}_3(\xi,\eta) = \begin{cases} \phi_{g_2}^R(\frac{\eta-(a-\delta)}{2\delta}) & \text{if } \eta\in[a-\delta,a+\delta] \\ 1 & \text{if } \eta\in[0,a-\delta] \\ 0 & \text{if } \eta\notin[0,a+\delta], \end{cases} \tag{34}$$

where $\phi_{g_2}^R(x)$ and $\phi_{g_2}^L(x)$ are $\mathcal{C}^1$-continuous functions defined by (6) as follows:

$$\phi_{g_2}^R(x) = (1-x)^2(1+2x), \text{ and } \quad \phi_{g_2}^L(x) = (1+x)^2(1-2x).$$

Note that we construct PU functions on the reference domain so that we could integrate over the rectangular area. If we construct the PU on the physical domain, we might have irregular shapes to integrate over.

Now, we have the following parameters, PU functions, and patches that are used in this section:

1. $\Omega_1^* = G(\hat{\Omega}_1^*), \quad \Omega_2^* = G(\hat{\Omega}_2^*), \quad \Omega_3^* = G(\hat{\Omega}_3^*)$.

2. $\hat{\Psi}_1(\xi,\eta) + \hat{\Psi}_2(\xi,\eta) + \hat{\Psi}_3(\xi,\eta) = 1$ for each $(\xi,\eta) \in [0,1] \times [0,1]$.

3. Let $\Psi_k \equiv \hat{\Psi}_k \circ G^{-1}, k = 1,2,3$. Then, their supports are three patches defined by (31): that is, $\text{supp}(\Psi_k) = \Omega_k^*$, $k = 1,2,3$, shown in Figure 5. In this figure, two narrow annuli are non flat-top parts of the PU functions Ψ_k.

4. We choose different parameters a, b, and δ for different diffusion coefficients ε:

$$a = 0.05(0.005), \quad b = 1/2, \quad \delta = 0.01(0.001), \text{ when } \varepsilon = 10^{-3}(10^{-4}).$$

Basis functions whose supports are Ω_1^* (Disk)

Since $G : \hat{\Omega}_1^* \longrightarrow \Omega_1^*$, defined by (24), is not one to one, unlike the constructions of basis functions on Ω_2^* and Ω_3^*, we directly construct the basis functions on the patch $\Omega_1^* \subset \Omega$. That is, they are not the push-forwards of basis functions on $\hat{\Omega}_1^*$ (Fig. 6) by the geometric mapping G.

Let

$$\hat{N}_k(t) = {}_qC_k(1-t)^{q-k}t^k, \quad k = 0,1,2,\ldots,q$$

be the Bernstein polynomials (Bézier functions) of degree q defined on $[0,1]$. Consider

a linear transformation $T_1 : [-(1-(b+\delta)), 1-(b+\delta)] \longrightarrow [0,1]$. Then, the transformed Bernstein polynomials by the linear transformation T_1 are

$$\widetilde{N}_{k+1}(x) = \hat{N}_k(T_1(x)) = {}_qC_k(1-T_1(x))^{q-k}(T_1(x))^k, \quad k = 0,1,2,\ldots,q. \tag{35}$$

Since the inverse of the geometric mapping G defined by (24) is

$$G^{-1}(x,y) = \Big(\xi(x,y), \eta(x,y)\Big) = \Big(\frac{1}{2\pi}\tan^{-1}\frac{y}{x}, 1-\sqrt{x^2+y^2}\Big),$$

a circular PU function on Ω_1^* is defined by

$$\Psi_1(x,y) = (\hat{\Psi}_1 \circ G^{-1})(x,y) \;\; = \;\; \begin{cases} 1 & \text{if } (x,y) \in \Omega_1^{*1}, \\ \phi_{g_2}^L(\frac{\eta(x,y)-(b+\delta)}{2\delta}) & \text{if } (x,y) \in \Omega_1^{*2}, \\ 0 & \text{if } x^2+y^2 \geq [1-(b-\delta)]^2, \end{cases} \tag{36}$$

where

$$\Omega_1^{*1} = \{(x,y) : x^2+y^2 \leq [1-(b+\delta)]^2\},$$

$$\Omega_1^{*2} = \{(x,y) : [1-(b+\delta)]^2 \leq x^2+y^2 \leq [1-(b-\delta)]^2\},$$

which are the inner most disk and the smaller narrow annulus, respectively, inside the square of Fig. 5. Multiplying the circular PU function (36) to the tensor product of (35), we obtain basis functions on Ω_1^* in the following set

$$\mathcal{V}^A = \{B_{ij}(x,y) = \Psi_1(x,y)\cdot\widetilde{N}_i(x)\cdot\widetilde{N}_j(y) : \text{ for } 1 \leq i,j \leq q+1\}. \tag{37}$$

The bilinear form for the basis functions can be calculated as follows:

$$\begin{aligned}
&\iint_{\Omega_1^*} \nabla_x B_{ij} \cdot \nabla_x B_{i'j'} \\
= &\iint_{\Omega_1^{*1}} \nabla_x B_{ij} \cdot \nabla_x B_{i'j'} + \iint_{\Omega_1^{*2}} \nabla_x B_{ij} \cdot \nabla_x B_{i'j'} \\
= &\int_0^{2\pi} \int_0^{1-(b+\delta)} \Big(\nabla_x B_{ij} \cdot \nabla_x B_{i'j'}\Big)(r\cos\theta, r\sin\theta) r dr d\theta \\
&+ \int_0^1 \int_{b-\delta}^{b+\delta} \Big((J(G)^{-1})\nabla_\xi (B_{ij} \circ G)\Big)^T \cdot \Big(J(G)^{-1}\nabla_\xi (B_{i'j'} \circ G)\Big) |J(G)| d\xi d\eta.
\end{aligned}$$

Since the geometric mapping G is bijective on $[0,1] \times [b-\delta, b+\delta]$, we can integrate pull-backs of the basis functions over $[0,1] \times [b-\delta, b+\delta]$ in the reference domain.

Basis functions whose supports are Ω_2^* (Annular Region)

Let $T_2 : [a-\delta, b+\delta] \longrightarrow [0,1]$ be the bijective linear mapping. Then, the transformed Berstein polynomials by the linear transformation T_2 are

$$\widetilde{M}_{k+1}^B(\eta) = {}_qC_k(1-T_2(\eta))^{q-k} T_2(\eta)^k, \quad k = 0,1,2,\ldots,q (q \geq 3). \tag{38}$$

Let $\hat{N}_k(\xi), k = 1,2,\ldots,4p-2$, be B-splines corresponding to an open knot vector with $p \geq 3$,

$$\{\underbrace{0\ldots0}_{p+1}, \underbrace{1/4\ldots1/4}_{p-1}, \underbrace{1/2\ldots1/2}_{p-1}, \underbrace{3/4\ldots3/4}_{p-1}, \underbrace{1\cdots1}_{p+1}\}. \tag{39}$$

Next, $\hat{N}_1$ and $\hat{N}_{4p-2}$, the first and the last B-spline functions, respectively, are joined to form one blending function, denoted by $\hat{N}_1^B(\xi)$, so that they can be periodic after

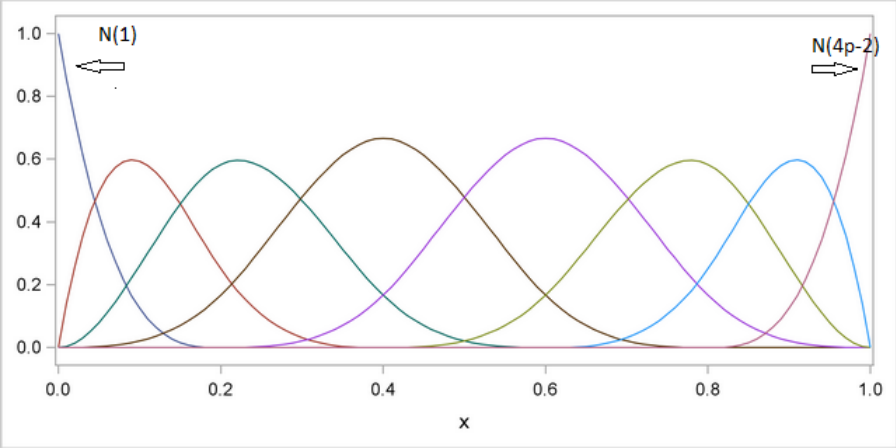

Figure 7: Periodic basis function joining the first and the last B-splines

push-forwarded to the annular region $\Omega_2^* \cup \Omega_3^*$ through the mapping G:

$$\hat{N}_1^B(\xi) = \begin{cases} (1-4\xi)^p & \text{if } \xi \in [0,1/4] \quad (\text{that is } \hat{N}_1(\xi)) \\ 0 & \text{if } \xi \in [1/4,3/4] \\ (4\xi-3)^p & \text{if } \xi \in [3/4,1] \quad (\text{that is } \hat{N}_{4p-2}(\xi)). \end{cases} \tag{40}$$

$$\hat{N}_k^B(\xi) = \hat{N}_k(\xi), k = 2, \ldots, 4p-3. \tag{41}$$

Now, the push-forward of the PU function $\hat{\Psi}_2$ of (33) onto the physical domain Ω is denoted by

$$\Psi_2(x,y) = (\hat{\Psi}_2 \circ G^{-1})(x,y) = \hat{\Psi}_2(\xi(x,y), \eta(x,y)).$$

Then, basis functions on the annular region Ω_2^* are the following $\mathcal{C}^0$-continuous function with the cardinality $(4p-3)(q+1)$:

$$\mathcal{V}^B = \left\{ \Psi_2(x,y) \cdot \left[\left(\hat{N}_k^B \times \widetilde{M}_l^B \right) \circ G^{-1} \right](x,y) : 1 \le k \le 4p-3, 1 \le l \le q+1 \right\}.$$

Remark 1. For applications of Collocation IGA and numerical methods for higher order equations, it is possible to modify the members of $\mathcal{V}^B$ to be $\mathcal{C}^1$-continuous

functions. Now, the basis functions in $\mathcal{V}^B$ are $\mathcal{C}^1$-continuous except at points in $\{(x,0) : x \in (1-(b+\delta), 1-(a-\delta))\}$, where $\left(\hat{N}_k^B \times \widetilde{M}_l^B\right) \circ G^{-1}(x,y)$ have discontinous derivatives if $k = 1$. However, if $(1-4\xi)^p$ and $(4\xi-3)^p$, respectively, are modified to $(1-4\xi)^{p-1}(1+(p-1)\xi)$ and $(4\xi)^{p-1}(p+1-4p\xi)$ in the construction of $\hat{N}_1^B(\xi)$, all basis functions become $\mathcal{C}^1$-continuous functions.

Enriched basis functions whose supports are Ω_3^* (Boundary Layer)

Since the boundary layer occurs along the lower half of the unit circle, we enrich this region with the boundary layer function $\hat{\phi}_0$, defined by (30).

Let $T_3 : [0, a+\delta] \longrightarrow [0,1]$ be the bijective linear mapping. Then Berstein polynomials transformed by T_3 are

$$\widetilde{M}_{k+1}^C(\eta) = {}_qC_k(1-T_3(\eta))^{q-k}T_2(\eta)^k, \quad k = 0,1,2,\ldots,q.$$

Suppose $\hat{N}_k^B(\xi)$ are same periodic B-spline functions for Ω_2^* corresponding to the knot vector (39). Then we have this augmented basis functions:

$$\begin{aligned}
\hat{\mathcal{V}}_1^S &= \left\{\hat{N}_k^B(\xi)\cdot\hat{\varphi}_0(\eta) : k = 2p+1,\ldots,4p-3\right\},\\
\hat{\mathcal{V}}_2^S &= \left\{\hat{\Psi}_3(\xi,\eta)\cdot\left(\hat{N}_k^B(\xi)\cdot\widetilde{M}_l^C(\eta)\right) : 1 \le k \le 4p-3, \quad 2 \le l \le q+1\right\},
\end{aligned}$$

where $\hat{\Psi}_3$ is defined by (34).

Since $\widetilde{M}_1^C(\eta) = 1$ for $\eta = 0$ and the boundary layer problem has the homogeneous boundary condition along $\partial\Omega$, $\hat{\Psi}_3(\xi,\eta)\cdot\hat{N}_k^B(\xi)\cdot\widetilde{M}_1^C(\eta)$ are excluded in $\hat{\mathcal{V}}_2^S$. We augment the enrichment function $\hat{\phi}_0(\eta)$ along the lower half circle for $k = 2p+1,\ldots,4p-3$ in $\hat{\mathcal{V}}_1^S$.

Now a family of enriched basis functions on the boundary layer region Ω_3^* is

$$\mathcal{V}^C = \left(\hat{\mathcal{V}}_1^S \circ G^{-1}\right) \cup \left(\hat{\mathcal{V}}_2^S \circ G^{-1}\right). \tag{42}$$

Note that the number of functions in $\mathcal{V}^C$ is $(2p-3)+(4p-3)q$. Then, combining three sets $\mathcal{V}^A, \mathcal{V}^B, \mathcal{V}^C$ of basis functions constructed above, we finally construct an enriched approximation space $\mathcal{V}$ to deal with the boundary layer effects, that is

$$\mathcal{V} = \text{span}\left(\mathcal{V}^A \cup \mathcal{V}^B \cup \mathcal{V}^C\right). \tag{43}$$

Note that $\mathcal{V}$ contains a special boundary layer function modified by PU functions with flat-top.

Galerkin method

The enriched Galerkin method for the boundary layer problem (22) is as follows: Find $u_h \in \mathcal{V}$ such that

$$\varepsilon(\nabla u_h, \nabla v) - ((u_h)_y, v) = (f, v), \quad \forall v \in \mathcal{V}$$

where $\mathcal{V} = \{\underbrace{\varphi_1, ..., \varphi_N}_{\text{B-splines}}, \underbrace{\varphi_{N+1}, ..., \varphi_{N+M}}_{\text{enrichment functions}}\}$. Since $u_h(x,y) = \sum_{i=1}^{N+M} c_i \varphi_i(x)$, We can write

$$\sum_{i=1}^{N+M} c_i[\varepsilon(\nabla\varphi_i, \nabla\varphi_j) - (\frac{\partial\varphi_i}{\partial y}, \varphi_j)] = (f, \varphi_j), \quad j = 1, ..., N+M. \tag{44}$$

In matrix form, the linear system (44) can be written as

$$Ac = b,$$

where

$$A = \begin{bmatrix} a_{11} & \dots & a_{1L} \\ \vdots & \vdots & \vdots \\ a_{L1} & \dots & a_{LL} \end{bmatrix}, c = \begin{bmatrix} c_1 \\ \vdots \\ c_L \end{bmatrix}, b = \begin{bmatrix} b_1 \\ \vdots \\ b_L \end{bmatrix}$$

where $L = M + N$, $a_{ij} = \varepsilon(\nabla\varphi_i, \nabla\varphi_j) - (\frac{\partial\varphi_i}{\partial y}, \varphi_j)$, and $b_i = (f, \varphi_i)$. The stiffness matrix consists of four block matrices, A_1, A_2, A_3, A_4,

$$A = \begin{bmatrix} A_1 & A_2 \\ A_3 & A_4 \end{bmatrix}$$

The submatrix A_1 is composed of the terms involving only the B-splines whereas the submatrices A_2, A_3 and A_4 involve the boundary layer functions. For $N + 1 \leq i, j \leq N + M$, the bilinear form in A_4 can be calculated as follows

$$\begin{aligned} a(\nabla\varphi_i, \nabla\varphi_j) &= \varepsilon \iint_\Omega \nabla\varphi_i \nabla\varphi_j - \frac{\partial\varphi_i}{\partial y}\varphi_j dxdy \\ &= \varepsilon \iint_{\hat{\Omega}} (J(G)^{-1}\nabla(\hat{N}_i(\xi)\hat{\varphi}_0(\eta))^T (J(G)^{-1}\nabla(\hat{N}_j(\xi)\hat{\varphi}_0(\eta))|J(G)|d\xi d\eta \\ &- \varepsilon \iint_{\hat{\Omega}} (J(G)_2^{-1}\nabla(\hat{N}_i(\xi)\hat{\varphi}_0(\eta))(\hat{N}_j(\xi)\hat{\varphi}_0(\eta))|J(G)|d\xi d\eta, \end{aligned}$$

where

$$J(G) = \begin{bmatrix} \frac{\partial x}{\partial \xi} & \frac{\partial y}{\partial \xi} \\ \frac{\partial x}{\partial \eta} & \frac{\partial y}{\partial \eta} \end{bmatrix} = \begin{bmatrix} -2\pi(1-\eta)\sin 2\pi\xi & 2\pi(1-\eta)\cos 2\pi\eta \\ -\cos 2\pi\xi & -\sin 2\pi\xi \end{bmatrix},$$

and $|J(G)| = 2\pi(1-\eta)$ is the determinant of Jacobian of $G(\xi, \eta)$, geometry mapping and $J(G)_2^{-1}$ is the second row of $J(G)^{-1}$.

For $1 \leq i \leq N, N + 1 \leq j \leq N + M$, the bilinear form in A_2 can be calculated as

follows:

$$\begin{aligned} a(\nabla\varphi_i, \nabla\varphi_j) &= \varepsilon \iint_{\Omega} \nabla\varphi_i \nabla\varphi_j - \frac{\partial\varphi_i}{\partial y}\varphi_j dxdy \\ &= \varepsilon \iint_{\hat{\Omega}} (J(G)^{-1}\nabla(\hat{N}_i(\xi)\hat{M}_i(\eta)))^T (J(G)^{-1}\nabla(\hat{N}_j(\xi)\hat{\varphi}_0(\eta)))|J(G)|d\xi d\eta \\ &- \varepsilon \iint_{\hat{\Omega}} (J(G)_2^{-1}\nabla(\hat{N}_i(\xi)\hat{M}_i(\eta)))(\hat{N}_j(\xi)\hat{\varphi}_0(\eta))|J(G)|d\xi d\eta \end{aligned}$$

4.6 Numerical Results

We present numerical solutions of (22) obtained by standard IGA and enriched PU-IGA, which is enriched by the boundary layer function estimated by boundary layer analysis.

One dimensional singularly perturbed convection-diffusion problem

We consider one dimensional convection-diffusion problem.

$$\begin{cases} \varepsilon u'' + (1+\varepsilon)u' + u = 0, \quad 0 < x < 1, \\ u(0) = 0, \quad u(1) = 1. \end{cases} \tag{45}$$

Equation (45) can be solved exactly

$$u(x) = \frac{1}{e^{-1} - e^{-1/\varepsilon}}(e^{-x} - e^{-x/\varepsilon}).$$

By the boundary layer analysis, we obtain the boundary layer approximation, u_i developed by (15),

$$u_i = C(1 - e^{-x/\varepsilon}), \quad \text{for } x = O(\varepsilon).$$

Then, we modify the boundary layer approximation by a PU function $\psi(x)$ and obtain

Table 3: Maximum error of 1D convection-diffusion problem obtained by standard IGA and enriched PU-IGA with p-refinement, $\triangle h = 0.1$, $\varepsilon = 0.001$

Degree	DOF	NO Enrichment	Enrichment
2	22	1.1843E+16	0.1863
4	42	1.8064	6.0128E-009
6	62	1.1829	5.8175E-014

Table 4: Maximum error of 1D convection-diffusion problem obtained by standard IGA and enriched PU-IGA with h-refinement, $p = 6$, $\varepsilon = 0.001$

$\triangle$h	DOF	NO Enrichment	Enrichment
1	8	4.6265	0.6912
0.5	14	5.9244	0.3538
0.1	62	1.1829	5.8175E-014

the boundary layer function $\hat{\varphi}_0$ for enrichment.

$$\hat{\varphi}_0 = (1 - e^{-x/\epsilon})\psi(x),$$

where $\psi(x)$ is a PU function defined by (29).

We compare the numerical results of standard IGA and enriched PU-IGA for the one-dimensional convection-diffusion problem. In Table 3, we use enriched p-refinement of IGA and standard IGA. Enriched PU-IGA has almost true solution when the degree of basis functions is six, while standard IGA does not yield any reasonable solution. In Table 4, we use enriched h-refinement of PU-IGA and obtain similar results to that of p-refinement of PU-IGA. In Figure 8, standard IGA produces oscillation, and it propagates beyond boundary layer in the direction of a convective term, while enriched PU-IGA captures rapid transition in the boundary layer.

Singularly Perturbed Convection-Diffusion Equation in a Circle

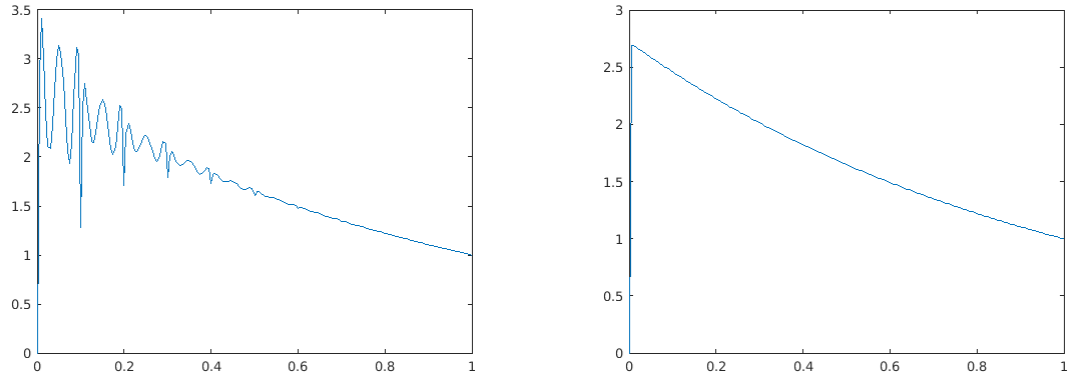

Figure 8: Numerical solution of 1D convection-diffusion problem obtained by standard IGA (left) and enriched PU-IGA(right), $\varepsilon = 10^{-3}, N = 62, M = 1, \triangle h = 0.1$, h-refinement

We approximate the following exact solution u of (22):

$$u(x,y) = \begin{cases} (1-x^2)^2(-y+\sqrt{1-x^2} + \dfrac{\epsilon+\sqrt{1-x^2}}{(1-x^2)^{3/2}}), & \text{in } \Omega \\ 0 \quad \text{on } \partial\Omega. \end{cases}$$

[15] shows that the corresponding f turns out to be $f = (1-x^2)^2 + \mathcal{O}(\varepsilon)$. With the derived boundary layer function and basis functions, we construct an approximation space for enriched PU-IGA in the previous section and now present numerical results by the approximation space.

Relative error in percent in the l-norm $\|\cdot\|_l$ is defined by

$$\|err\|_{l,rel}(\%) = \frac{\|u_{ex} - u^h\|_l}{\|u_{ex}\|_l} \times 100.$$

Numerical results of the enriched PU-IGA, using the approximation space $\mathcal{V}$, defined by (43), are shown in Figures 9 and 10 and Table 5, in which we observe the following:

1. The proposed enriched PU-IGA yields better results with lower degrees of free-

Table 5: Relative error in percent for 2D convection-diffusion problem on a circle when $\varepsilon = 10^{-4}$. The results in the third column are relative errors in percent by enriched FEM reported in [15].

enriched PU-IGA		PU-IGA adapt msh		Hong et al.[15]		IGA with radical msh	
dof	$\|err\|_{L^2,rel}(\%)$	dof	$\|err\|_{L^2,rel}(\%)$	dof	$\|err\|_{L^2,rel}(\%)$	dof	$\|err\|_{L^2,rel}(\%)$
1352	69.56	1332	70.01	1516	5.77	400	4.067
2004	3.480	1980	3.516	2347	5.01	1024	1.031
2784	0.074	2756	0.113	4130	4.43	1936	0.929
3692	0.038	3660	0.041	9217	3.39	3136	0.929

dom than those of the enriched FEM of [15], as shown in Table 5. We compare the results with those in Table 1 of [15].

2. The authors in [15] used piecewise linear basis functions for enriched FEM, while we use high degree of B-spline basis functions constructed through the p-refinement or the k-refinement . Thus, enriched PU-IGA requires more quadrature points than those of the enriched FEM of [15] for numerical integration. Since no internal knots are repeated in the k-refinement of IGA, the support of a B-spline function of degree p covers $p+1$ (non-void) knot spans for extreme cases. Hence, the integral region of a B-spline function of degree p should be divided into $p+1$ intervals for accurate integrations since B-splines are piecewise polynomial. Therefore, operation counts of enriched PU-IGA with higher degree of B-spline basis functions might be more than those of FEM in [15].

   For the results in Table 5, we use the p-refinement of IGA in which internal knots are repeated $p-1$ times and hence supports of corresponding B-splines consist of two knot spans. For a comparison of operation counts between PU-FEM and PU-IGA, suppose each piecewise linear basis function consists of four

2-dimensional shape functions in FEM. We use B-splines of degrees $p = 10$ and $q = 10$ in the framework of the p-refinement of IGA. Then we may use one Gauss point per shape function in FEM, whereas we use six Gauss points per B-spline function of degree 10 on each knot span. Thus, we have the following:

- The number of function evaluations is $9217 \times 1 \times 4 = 36,868$ (dof $\times$ Gauss points $\times$ number of shape function) in FEM, whereas the number of function evaluations is $3692 \times 36 \times 4 = 531,648$ (dof $\times$ Gauss points $\times$ number of knot span) in the proposed method. Here, 9217 and 3692, respectively, are degrees of freedom shown at the last row of Table 5. Since the polynomials of degree 10 have more terms than linear polynomials, the proposed method requires much more function evaluations than enriched FEM for numerical integrations. Since both enriched IGA and enriched FEM use a similar boundary layer function for enrichment, extra Gauss points used for evaluations of enrichment functions and PU functions are not counted.

By the same reasons, if we assume that the bandwidths k of IGA and FEM are similar, then we have the following.

- The Cholesky factorization costs $9217(k^2 + 3k)$ flops for the enriched PU-FEM and $3692(k^2 + 3k)$ flops for the enriched PU-IGA, respectively. That is, the enriched PU-FEM requires more flops for the factorization than those of the proposed method.
- Since we use higher degree of B-splines and the bandwidth is bigger than

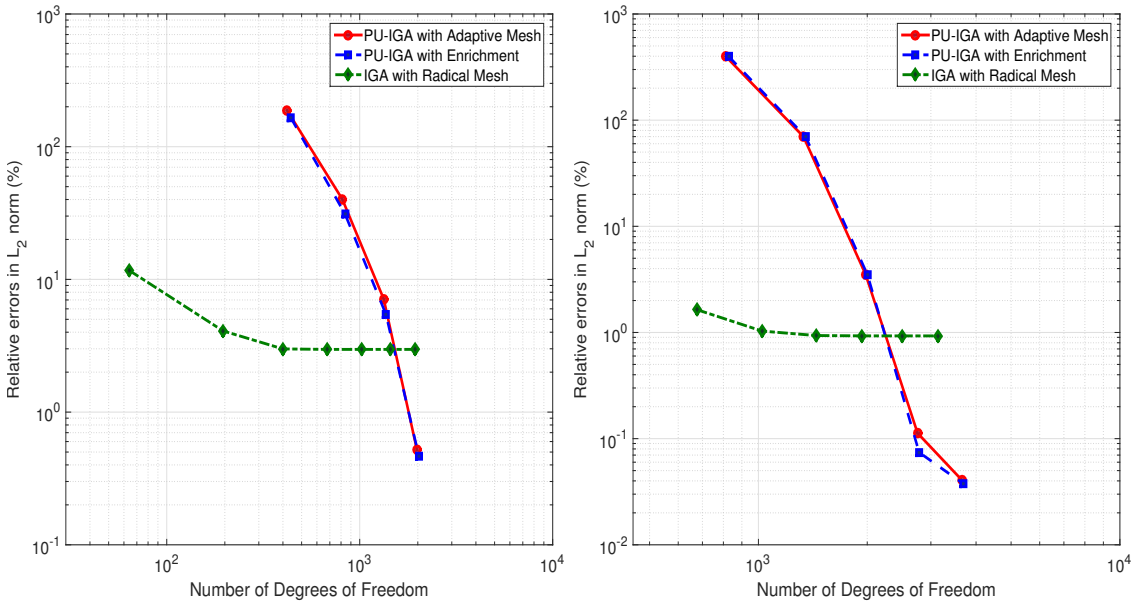

Figure 9: Relative error plot of 2D convection-diffusion problem, relative errors in percent when $\varepsilon = 10^{-3}, a - \delta = 0.05, b = 0.5, \delta = 0.01$ (Left), relative errors in percent when $\varepsilon = 10^{-4}, a - \delta = 0.005, b = 0.5, \delta = 0.001$ (Right)

that of FEM generally, even though degree of freedom is much smaller, we cannot guarantee smaller flops for the factorization overall.

Refer to [45] for detailed discussion for the bandwidths of IGA and FEM.

3. In both cases of $\varepsilon = 10^{-3}$ and $\varepsilon = 10^{-4}$, PU-IGA yields numerical solutions with relative error 0.00038, which is as small as ε. Since we compare numerical solutions with the true solution that satisfies the stiff convection-diffusion equation only upto ε, it has no meaning to pursue more accurate solutions than those in the column "enriched PU-IGA" and " PU-IGA adaptive" of Table 5.

4. PU-IGA with adaptive k-refinement and enriched PU-IGA are compared as follows:

   - We use B-splines of high order ($6 \leq p \leq 12$) as basis functions for both

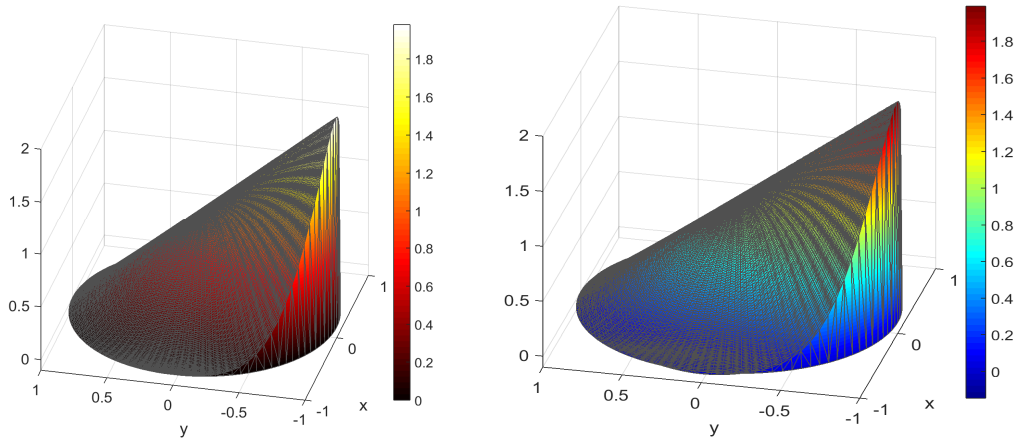

Figure 10: Numerical solution of 2D singularly perturbed convection-diffusion problem obtained by enriched PU-IGA when $\varepsilon = 10^{-3}$(Left) and $\varepsilon = 10^{-5}$(Right).

approaches. As shown in Table 5, the enriched PU-IGA yields accurate solution at low cost (dof = 2784).

- For PU-IGA with adaptive mesh shown in Figure 9, we choose Ω_3^* to be almost as small as the boundary layer zone and insert knots adaptively for the k-refinement of the radial direction basis functions, $\widetilde{M}_l^C(\eta), 1 \leq l \leq q+1$. In other words, using the PU function Ψ_3 with small supports, basis functions of high degree are constructed inside the boundary layer zone. Relative errors in the last row of the column " PU-IGA Adapt msh" of Table 5 show that PU-IGA with adaptive mesh is as good as enriched PU-IGA with boundary layer function. The goal we achieve in this dissertation is to avoid fine mesh around boundary layer; however, we can note that partition of unity with flat-top makes enrichment simple as well as refinement.

5. Figure 10 shows that enriched PU-IGA captures the boundary layer behavior, and there is no oscillation around boundary layer for both $\varepsilon = 10^{-3}$ and $\varepsilon = 10^{-4}$.

Singularly Perturbed Convection-Diffustion Equation in a Square

To present the effectiveness of the proposed enriched PU-IGA, we compare the performance of enriched PU-IGA with other numerical methods. For simplicity, we test enriched PU-IGA to a singularly perturbed convection-diffusion problem on a square with mild boundary layer effect.

Consider a singularly perturbed convection-diffusion problem with an exponential layer at the outflow boundary and two characteristic layers given by

$$\begin{cases} -\varepsilon \Delta u - b u_x + cu = f \quad \text{in } \Omega = (0,1)^2, \\ \\ u = 0 \quad \text{on } \partial\Omega, \end{cases} \tag{46}$$

where $b = 2 - x$, $c = 3/2$, $\varepsilon = 10^{-2}$, and f is calculated from the following solution of (46)

$$u(x,y) = \left(\cos \frac{\pi x}{2} - \frac{e^{-x/\varepsilon} - e^{-1/\varepsilon}}{1 - e^{-1/\varepsilon}} \right) \frac{(1 - e^{-y/\sqrt{\varepsilon}})(1 - e^{-(1-y)/\sqrt{\varepsilon}})}{1 - e^{-1/\sqrt{\varepsilon}}}.$$

The function has an exponential boundary layer at $x = 0$, two characteristic boundary layers at $y = 0$ and $y = 1$, respectively.

To find the inner approximation u_i, we introduce a boundary-layer coordinate given as

$$\bar{x} = \frac{x}{\varepsilon^{\alpha}}$$

Using this boundary-layer coordinate, (46) transforms to

$$-\varepsilon^{1-2\alpha}\frac{\partial^2 u}{\partial \bar{x}^2} - \varepsilon\frac{\partial^2 u}{\partial y^2} - 2\varepsilon^{-\alpha}\frac{\partial u}{\partial \bar{x}} + \bar{x}\frac{\partial u}{\partial \bar{x}} + 2/3u(\varepsilon^{\alpha}\bar{x}, y) = f(\varepsilon^{\alpha}\bar{x}, y).$$

The leading terms are

$$-\varepsilon^{1-2\alpha}\frac{\partial^2 u}{\partial \bar{x}^2}, \qquad -2\varepsilon^{-\alpha}\frac{\partial u}{\partial \bar{x}}.$$

By the dominant balancing, $\alpha = 1$. With this we have the following problem to solve:

$$-\frac{\partial^2 u}{\partial \bar{x}^2} - 2\frac{\partial u}{\partial \bar{x}} = 0$$

with the boundary condition $u(0, y) = 0$. The general solution of this problem is

$$u_i(x, y) = C(1 - \exp(-\frac{2x}{\varepsilon}))$$

where C is a constant that we could find by matching condition. We modify the inner approximation u_i and obtain the boundary layer function ϕ_0 for enrichment:

$$\varphi_0(x) = 1 - \exp(-\frac{2x}{\varepsilon}).$$

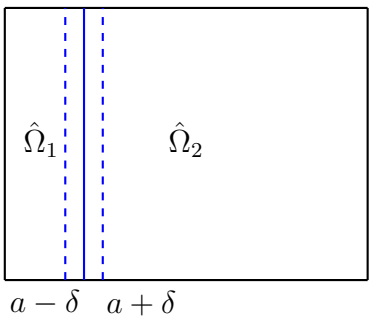

Figure 11: Supports of PU for 2D convection-diffusion problem on a square, $\hat{\Omega}_1 = [0, a] \times [0, 1], \hat{\Omega}_2 = [a, 1] \times [0, 1]$, where $a = 0.1$ and $\delta = 0.05$. The supports of PU functions with flat-top, Ψ_1 and Ψ_2, are $\hat{\Omega}_1^* = [0, a + \delta] \times [0, 1] = \text{supp}(\Psi_1)$, and $\hat{\Omega}_2^* = [a - \delta, 1] \times [0, 1] = \text{supp}(\Psi_2)$

In this problem, the parameter and physical domains are both $[0,1] \times [0,1]$, and the geometric mapping G is an identity mapping. For the results shown in Table 6 and Figure 12, we use the following parameters and PU-functions:

We divide the reference domain, $\hat{\Omega} = [0,1] \times [0,1]$ into two subdomains shown in the Figure 11:

$$\hat{\Omega}_1 = [0,a] \times [0,1], \quad \hat{\Omega}_2 = [a,1] \times [0,1], \text{ where } a = 0.1.$$

Two PU-function with flat-top are defined by

$$\hat{\Psi}_1(\xi,\eta) = \psi^{(\delta,1)}_{[0,a]}(\xi) \times \eta \quad \text{and} \quad \hat{\Psi}_2(\xi,\eta) = \psi^{(\delta,1)}_{[a,1]}(\xi) \times \eta,$$

where $\delta = 0.05$, $\psi^{(\delta,1)}_{[0,a]}$ and $\psi^{(\delta,1)}_{[a,1]}$ are defined by (7). Then, the supports of $\hat{\Psi}_1$ and $\hat{\Psi}_2$, respectively, are $[0, a+\delta] \times [0,1]$ and $[a-\delta, 1] \times [0,1]$. The refinements, B-splines, and an enrichment function used to get the results shown in Figure 12 are as follows:

1. For the result of *" PU-IGA "*, we use two different sets of basis functions in the ξ-direction:

   (i) the scaled B-splines $\hat{N}^{[0,a+\delta]}_{k,p+1}(\xi) \cdot \psi^{(\delta,1)}_{[0,a]}(\xi), k = 1, \ldots, n_1$ that are B-spline functions corresponding to an open knot vector on $[0, a+\delta]$, scaled by the PU function $\psi^{(\delta,1)}_{[0,a]}(\xi)$.

   (ii) the scaled B-splines $\hat{N}^{[a-\delta,1]}_{l,p+1}(\xi) \cdot \psi^{(\delta,1)}_{[a,1]}(\xi), l = 1, \ldots, n_2$, that are another set of B-splines corresponding to an open knot vector on $[a-\delta, 1]$, scaled by the PU function $\psi^{(\delta,1)}_{[a,1]}(\xi)$.

2. For the result of *" Enriched PU-IGA "* of Table 6 and Fig. 12, we use the

following basis functions:

(i) By the boundary layer analysis, we get the enrichment function $\phi_0(\xi) = 1 - e^{-2\xi/\varepsilon}$. On the boundary layer zone $[0, a+\delta] \times [0, 1]$, we use the enrichment functions $H_j(\xi, \eta)$ defined by

$$H_j(\xi, \eta) = \left(\phi_0(\xi) \cdot \psi^{(\delta,1)}_{[0,a]}(\xi)\right) \times M_j(\eta), \quad 0 \le j \le p,$$

as well as

$$\left(\hat{N}^{[0,a+\delta]}_{k,p+1}(\xi) \cdot \psi^{(\delta,1)}_{[0,a]}(\xi)\right) \times M_j(\eta), \quad 2 \le k \le n_1, \quad 0 \le j \le p,$$

where $M_j(\eta), j = 0, 1, \ldots, p,$ are Bézier functions of degree p.

Because of the enrichment function $\phi_0(\xi)$, it is not necessary to use B-splines corresponding to a fine mesh on the boundary layer zone.

(ii) On $[a - \delta, 1]$, we construct B-splines by the k-refinement of IGA in the ξ-direction.

$$\left(\hat{N}^{[a-\delta,1]}_{k,p+1}(\xi) \cdot \psi^{(\delta,1)}_{[a-\delta,1]}(\xi)\right) \times M_j(\eta), \quad 1 \le k \le n_1, \quad 0 \le j \le p,$$

3. For the result of *"IGA with radical mesh refinement"*, we use B-splines obtained by the k-refinement with inserting n_ξ knots determined by

$$r_i = \left(\frac{i}{n_\xi + 1}\right)^{1/3}, \ i = 1, \ldots, n_\xi,$$

where the number of knots, n_ξ, is increased as the p-degree is elevated.

4. For the result of *" IGA "*, we use the k-refinement of IGA in both ξ- and

Table 6: Relative errors in L^2-norm in percent of 2D convection-diffusion problem on a square obtained by IGA, PU-IGA, enriched PU-IGA, and IGA with radical mesh refinement when $\varepsilon = 10^{-2}$

IGA		PU-IGA		Enrich PU-IGA		IGA with Rad msh	
dof(p-deg)	$\|err\|_{L^2,r}(\%)$	dof	$\|err\|_{L^2,r}(\%)$	dof(p-deg)	$\|err\|_{L^2,r}(\%)$	dof	$\|err\|_{L^2,r}(\%)$
121(6)	8.98E-0	119	2.32E-2	65(4)	4.39E-1	121	1.13E-0
225(8)	1.52E-0	180	1.02E-2	107(6)	7.47E-2	225	9.93E-2
361(10)	1.35E-1	275	1.38E-3	195 (8)	3.81E-3	361	5.07E-3
529(12)	7.84E-3	364	3.10E-4	309 (10)	1.80E-4	529	3.60E-4
729(14)	3.12E-3	495	3.08E-5	449 (12)	7.59E-6	729	9.50E-5
		612	2.08E-6	615 (14)	6.14E-7		

η-directions.

Even though the boundary layer effect is not very strong (since $\varepsilon = 10^{-2}$), we observe the following from the results shown in Table 6 and Figure 12:

1. Enriched PU-IGA is superior over any other methods (including streamline diffusion techniques).

2. To get the *streamline diffusion* method, we multiply the equation (46) by the test function $v + \delta V_\beta$, where $v \in H_0^1(\Omega)$, we get

$$-\epsilon\delta(\triangle u, v_\beta) + \epsilon(\nabla u, \nabla v) + (\beta\nabla u, v) = 0$$

where $\beta = (-1, 0)$, $\delta = Ch$ if $\epsilon < h$ with $C > 0$ sufficiently small.

We now formulate the following streamline diffusion method for (46): Find $u^h \in V_h$ such that

$$\epsilon(\nabla u^h, \nabla v) - \epsilon\delta(\triangle u^h, v_\beta) + (u^h_\beta, v + \delta v_\beta) = 0 \quad \forall v \in V_h$$

where $v_\beta = \beta \cdot \nabla v$

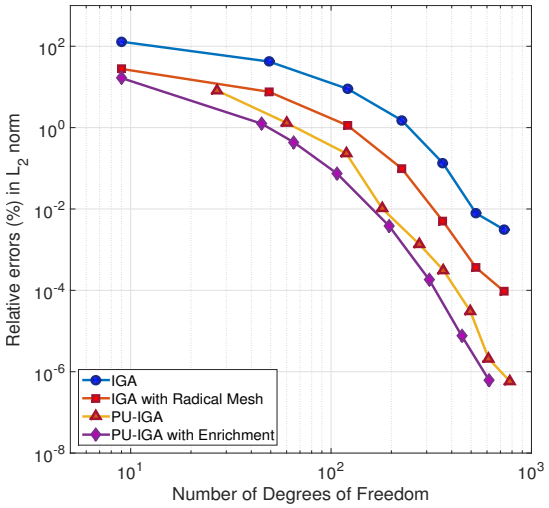

Figure 12: Relative errors in L^2-norm in percent for 2D convection-diffusion problem on a square obtained by IGA, PU-IGA, enriched PU-IGA, and IGA with radical mesh.

3. One can use only one patch with sufficiently large number of knot insertions in the k-refinement of IGA to get similar results to enriched PU-IGA. However, in such case, the degrees of freedom become much lager.

4. When ε gets smaller, one should consider the boundary layer in y direction also for this problem. Without considering the boundary layer in y direction, we may not able to get an accurate solution.

4.7 Singulary Perturbed Convection-Diffusion Equation in an Ellipse

We consider the same convection-diffusion problem on an ellipse.

$$\begin{cases} -\varepsilon \triangle u - u_y = f(x,y) & \text{in } \Omega \\ u = 0 & \text{on } \partial\Omega \end{cases} \tag{47}$$

where $0 < \varepsilon \ll 1$, Ω is an ellipse centered at $(0,0)$ and one radius along the x-axis is $2r$ and the other along the y-axis is r. The function f is as smooth as needed.

The geometry mapping $G : \hat{\Omega} \longrightarrow \Omega$ is defined by

$$G(\xi, \eta) = (x(\xi, \eta), y(\xi, \eta) = (2(1-\eta)\cos 2\pi\xi, (1-\eta)\sin 2\pi\xi)$$

where $\eta = 1 - r, r$ is the distance to the origin along the y-axis and $2\pi\xi$ is the polar angle from the origin of the ellipse. We define the reference domain $\hat{\Omega} = [0,1] \times [0,1]$ and divide the domain into two patches, $\hat{\Omega}_1 = [0,1] \times [0, b+\delta]$ and $\hat{\Omega}_2 = [0,1] \times [b-\delta, 1]$. To find the boundary layer approximation u_i, we pullback the problem (47) to the reference domain. Using the stretched variable, $\bar{\eta} = \dfrac{\eta}{\varepsilon^{\alpha}}$. we obtain the transformed equation of (47).

$$\begin{aligned}
&\frac{3\varepsilon}{4\pi(1-\varepsilon^{\alpha}\bar{\eta}}\sin 2\pi\xi\cos 2\pi\xi\frac{\partial\hat{u}}{\partial\xi} - \frac{\varepsilon}{4\pi^2(1-\varepsilon^{\alpha}\bar{\eta}^2}(\frac{1}{4}\sin^2 2\pi\xi + \cos^2 2\pi\xi)\frac{\partial^2\hat{u}}{\partial\xi^2} \\
&+\frac{\varepsilon^{1-\alpha}}{1-\varepsilon^{\alpha}\bar{\eta}}(\frac{1}{4}\sin^2 2\pi\xi + \cos^2 2\pi\xi)\frac{\partial\hat{u}}{\partial\bar{\eta}} + \frac{\varepsilon^{1-\alpha}}{2\pi(1-\varepsilon^{\alpha}\bar{\eta})}\sin 2\pi\xi\cos 2\pi\xi\frac{\partial^2\hat{u}}{\partial\bar{\eta}\partial\xi} \\
&-\varepsilon^{1-2\alpha}(\frac{1}{4}\sin^2 2\pi\xi + \cos^2 2\pi\xi)\frac{\partial^2\hat{u}}{\partial\bar{\eta}^2} - \frac{1}{2\pi(1-\varepsilon^{\alpha}\bar{\eta})}\cos 2\pi\xi\frac{\partial\hat{u}}{\partial\xi} + \varepsilon^{-\alpha}\sin 2\pi\xi\frac{\partial\hat{u}}{\partial\bar{\eta}} = f(G(\xi,\eta))
\end{aligned}$$

Dominating terms are

$$-\varepsilon^{1-2\alpha}(\frac{1}{4}\sin^2 2\pi\xi + \cos^2 2\pi\xi)\frac{\partial^2\hat{u}}{\partial\bar{\eta}^2}, \qquad \varepsilon^{-\alpha}\sin 2\pi\xi\frac{\partial\hat{u}}{\partial\bar{\eta}}.$$

Therefore, a consistent scaling is possible if we select $\alpha = 1$. Because we are interested only in the leading-order approximation, we obtain

$$-(\frac{1}{4}\sin^2 2\pi\xi + \cos^2 2\pi\xi)\frac{\partial^2\hat{u}}{\partial\bar{\eta}^2} + \sin 2\pi\xi\frac{\partial\hat{u}}{\partial\bar{\eta}} = 0$$

The general solution is

$$u_i = C_1 + C_2\exp(\frac{\sin 2\pi\xi}{1/4\cos^2 2\pi\xi + \sin^2 2\pi\xi)}\bar{\eta}), \quad 1/2 < \xi < 1$$

Because the boundary layer is located near $\eta = 0$, we apply the boundary condition $\hat{u} = 0$ at $\eta = 0$, and so

$$u_i = C_1(1 - \exp(\frac{\sin 2\pi\xi}{1/4\cos^2 2\pi\xi + \sin^2 2\pi\xi} \cdot \frac{\eta}{\varepsilon}), \quad 1/2 < \xi < 1$$

We modify the boundary layer approximation to get our boundary layer function ϕ_0 for enrichment, plugging $\xi = 3/2$ in for the numerical simulation:

$$\varphi_0 = 1 - \exp(-\frac{\eta}{\varepsilon}).$$

Applying the proposed enriched PU-IGA similarly as the circular case of the previous section, we believe to have an accurate numerical solution of the singularly perturbed problem in an ellipse.

CHAPTER 5: SINGULARLY PERTURBED PARABOLIC EQUATION IN A CIRCLE

5.1 Introduction

We consider the two-dimensional singularly perturbed heat equation of the form

$$\begin{cases} \dfrac{\partial u}{\partial t} - \varepsilon \triangle u = f, \quad \text{in } \Omega \times (0,T) \\ u(x,y,t) = 0, \quad \text{on } \partial\Omega \times (0,T) \\ u(x,y,0) = u_0(x,y), \quad \text{on } \Omega \end{cases} \tag{48}$$

where $0 < \varepsilon \ll 1$ is the heat conductivity and Ω is the unit circle centered at (0, 0). The functions f and u_0 are assumed to be sufficiently regular. We also assume the compatibility condition

$$u_0 = 0 \quad \text{on } \partial\Omega.$$

Most of the numerical methods used to solve singularly perturbed parabolic problems are based on the finite difference methods with fine mesh on the rectangular domain, [43], [44], [46] and [47]. For time-dependent problems, mesh refinement is costly since we need to solve the linear system at every time step. In [17], instead of using fine mesh refinement on the boundary layer zone, the author use the conventional FEM enriched with boundary layer correctors. In this dissertation, we use B-spline basis functions enriched with boundary layer approximation developed by the boundary layer analysis. We can avoid the costly mesh refinements by enriching the approxi-

mation space on the circular domain. We believe this enriched PU-IGA should also be applicable to many other types of time-dependent singularly perturbed problems such as reaction-diffusion equations.

5.2 Discretization

The semi-discrete analogue of (48) will be based on the variational formulation: Find $u(t) \in V$, $t \in I$ such that

$$\begin{cases} (\dot{u}(t), v) + a(u(t), v) = (f(t), v) \quad \text{for all} \quad v \in \mathcal{V}, \ \ t \in I, \\ \\ u(0) = u^0. \end{cases} \tag{49}$$

Now, let $\mathcal{V}_h$ be a finite-dimensional subspace of $\mathcal{V}$ with basis $\{\underbrace{\varphi_1, \varphi_2, ..., \varphi_N}_{B-spline}, \underbrace{\varphi_{N+1}, ..., \varphi_{N+M}}_{enrichment}\}$. We find the following *semi-discrete* analogue of (49): Find $u_h(t) \in \mathcal{V}_h$, $t \in I$, such that

$$\begin{cases} (\dot{u}_h(t), v) + a(u_n(t), v) = (f(t), v) \quad \forall v \in \mathcal{V}_h, \ \ t \in I, \\ \\ (u_h(0), v) = (u^0, v) \quad \in \mathcal{V}_h. \end{cases} \tag{50}$$

For a full discretization, we apply the unconditionally stable *backward Euler* method to the semi-discrete problem (50). Now, we seek approximations $u_n^h \in \mathcal{V}_h$ of $u(., t_n), n = 0, ..., N$, satisfying

$$\begin{cases} (\dfrac{u_h^n - u_h^{n-1}}{k_n}, v) + a(u_h^n, v) = (f(t_n), v) \quad \forall v \in \mathcal{V}_h, n = 1, 2, , .., N, \\ \\ (u_h^0, v) = (u^0, v) \quad \forall v \in \mathcal{V}_h. \end{cases} \tag{51}$$

The classcial time-discretization method, the backward Euler method, satisfies the stability condition, which is stable regardless of the size of the time steps k_n; namely,

this method is *unconditionally stable*.

5.3 Boundary Layer Analysis

The unperturbed problem of (48), namely when $\varepsilon \longrightarrow 0$, is

$$\begin{cases} \dfrac{\partial u}{\partial t} = f, \quad \text{in } \Omega \times (0,T) \\ \\ u(x,y,0) = u_0(x,y) \quad \text{on } \Omega. \end{cases} \tag{52}$$

We find the explicit solution

$$u_{outer}(x,y,t) = u_0(x,y) + \int_0^t f(x,y,s)ds.$$

Define a geometric mapping $G : [0,1] \times [0,1] \longrightarrow \Omega$ by

$$G(x,y) = ((1-\eta)\cos 2\pi\xi, (1-\eta)\sin 2\pi\xi).$$

To investigate the boundary layer in the circular domain, we pull back the (48) to the reference domain by the geometry mapping, G. Using the change of variables, we obtain

$$\frac{\partial u}{\partial x} = -\frac{\sin 2\pi\xi}{2\pi(1-\eta)}\frac{\partial \hat{u}}{\partial \xi} - \cos 2\pi\xi \frac{\partial \hat{u}}{\partial \eta}, \qquad \frac{\partial u}{\partial y} = -\frac{\cos 2\pi\xi}{2\pi(1-\eta)}\frac{\partial \hat{u}}{\partial \xi} - \sin 2\pi\xi \frac{\partial \hat{u}}{\partial \eta}.$$

$$\triangle u = \frac{\partial^2 u}{\partial x^2} + \frac{\partial^2 u}{\partial y^2} = \frac{\partial^2 \hat{u}}{\partial \eta^2} - \frac{1}{1-\eta}\frac{\partial \hat{u}}{\partial \eta} + \frac{1}{(1-\eta)^2}\frac{\partial^2 \hat{u}}{\partial \xi^2}.$$

The equation (48) becomes

$$\frac{\partial u}{\partial t} - \varepsilon \triangle u = \frac{\partial \hat{u}}{\partial t} - \varepsilon \frac{\partial^2 \hat{u}}{\partial \eta^2} - \frac{\varepsilon}{4\pi^2(1-\eta)^2}\frac{\partial^2 \hat{u}}{\partial \xi^2} + \frac{\varepsilon}{1-\eta}\frac{\partial \hat{u}}{\partial \eta} = f(G(\xi,\eta)).$$

We look for the expansion of u at fist order:

$$u \simeq u_{outer} + u_{inner}$$

where u_{outer} is the solution of (52), and u_{inner} is the first order boundary layer approximation. Setting $f = 0$ in (48), we introduce the stretched variable to find the boundary layer approximation.

$$\bar{\eta} = \frac{\eta}{\varepsilon^{\alpha}}$$

The parabolic problem (48) is transformed to

$$\frac{\partial \hat{u}}{\partial t} - \varepsilon^{1-2\alpha}\frac{\partial^2 \hat{u}}{\partial \bar{\eta}^2} - \frac{\varepsilon}{4\pi^2(1-\varepsilon^{\alpha}\bar{\eta})^2}\frac{\partial^2 \hat{u}}{\partial \xi^2} + \frac{\varepsilon^{1-\alpha}}{1-\varepsilon^{\alpha}\bar{\eta}}\frac{\partial \hat{u}}{\partial \bar{\eta}} = 0.$$

The coefficients of the terms in the differential equation are

$$1, \quad \varepsilon^{1-2\alpha}, \quad \varepsilon, \quad \varepsilon^{1-\alpha}$$

To determine α, we estimate these magnitudes by dominant balancing. The dominating terms are

$$\frac{\partial \hat{u}}{\partial t} - \varepsilon^{1-2\alpha}\frac{\partial^2 \hat{u}}{\partial \bar{\eta}^2} = 0.$$

A consistent scaling is possible if we select $\alpha = 1/2$. We obtain the equations for boundary layer approximation:

$$\begin{cases} \dfrac{\partial u}{\partial t} - \dfrac{\partial^2 u}{\partial \bar{\eta}^2} = 0, \quad \text{in } \Omega \times (0,T) \\ u(0,t) = -u_{outer} \quad \text{at } \bar{\eta} = 0 \\ u(x,0) = 0 \\ u \longrightarrow 0, \text{ as } \bar{\eta} \longrightarrow \infty \end{cases} \tag{53}$$

We refer to [17] for the details. The solution of (53) is

$$u_{inner} = -\int_0^t I(\eta, t-s) \frac{\partial u_{outer}}{\partial t}(\xi, 0, s) ds,$$

where

$$\begin{aligned} I(x,t) &= \operatorname{erfc}(\frac{x}{\sqrt{2\varepsilon t}}), \\ \operatorname{erfc}(z) &= 1 - \operatorname{erf}(z) = \sqrt{\frac{2}{\pi}} \int_z^\infty \exp(-\frac{y^2}{2}) dy, \\ \operatorname{erf}(z) &= \sqrt{\frac{2}{\pi}} \int_0^z \exp(-\frac{y^2}{2}) dy. \end{aligned}$$

We refer to [4] for the details.

5.4 1D Numerical Results

We present the numerical result of a one-dimensional singularly perturbed parabolic problem using the standard IGA and enriched PU-IGA.

We do not use the boundary layer approximation directly since the term $I(\eta, t-s)$ is not convenient for the integration. Instead, we modify the boundary layer

approximation and obtain a boundary layer function ϕ_0 for enrichment:

$$\begin{aligned} u_{inner} &\sim \int_0^t I(\eta, t-s)ds, \qquad f \text{ is bounded} \\ &= \int_0^t 1 - \frac{1}{\sqrt{\pi\varepsilon t}}\exp(-\frac{\eta^2}{4\varepsilon t})ds \\ &\sim 1 - \frac{1}{\sqrt{\pi\varepsilon t}}\exp(-\frac{\eta^2}{4\varepsilon t}), \qquad t \text{ is bounded} \\ &\equiv \phi_0(\eta, t). \end{aligned}$$

Consider the singularly perturbed problem:

$$\begin{cases} u_t - \varepsilon u_{xx} = f(x,t), \quad \text{on } (0,1)\times(0,T) \\ u(0,t) = u(1,t) = 0, \quad t \in (0,T) \\ u(x,0) = u^0(x), \quad x \in (0,1). \end{cases} \tag{54}$$

We choose the exact solution u as

$$u = t(1 - \exp(-\frac{x}{\sqrt{\varepsilon}})\cos(\frac{x}{\sqrt{\varepsilon}}))(1 - \cos(\frac{1-x}{\sqrt{\varepsilon}})\exp(-\frac{1-x}{\sqrt{\varepsilon}})).$$

Hence, f is computed from (54). We have two boundary layers at the end points of the interval $(0,1)$. Similarly, we could derive the boundary layer function at $x = 1$. Since ϕ_0 depends on time, we need to calculate different boundary layer functions for each time step. To improve computational efficiency, we introduce the modified time-independent boundary layer elements ϕ_0 and ϕ_1 such that

$$\begin{cases} \phi_0(x) &= 1 - \exp(-\frac{x^2}{4\varepsilon})\psi_1(x), \\ \phi_1(x) &= 1 - \exp(-\frac{(1-x)^2}{4\varepsilon})\psi_3(x), \end{cases} \tag{55}$$

where PU functions ψ_1 and ψ_3 are used to avoid the singularity of ϕ at $x = 0$ and

$x = 1$:

$$\psi_1(\eta) = \begin{cases} 0, & \text{if } \eta \in [a+\delta, 1] \\ \phi^R_{g_2}(\dfrac{\eta-(a-\delta)}{2\delta}, & \text{if } \eta \in [a-\delta, a+\delta] \\ 1, & \text{if } \eta \in [0, a-\delta] \end{cases}$$

$$\psi_3(\eta) = \begin{cases} 0, & \text{if } \eta \in [0, b-\delta] \\ \phi^L_{g_2}(\dfrac{\eta-(b+\delta)}{2\delta}, & \text{if } \eta \in [b-\delta, b+\delta] \\ 1, & \text{if } \eta \in [b+\delta, 1] \end{cases}$$

where

$$\begin{cases} \phi^R_{g_2}(x) = (1-x)^2(1+2x) \\ \phi^L_{g_2}(x) = (1+x)^2(1-2x). \end{cases}$$

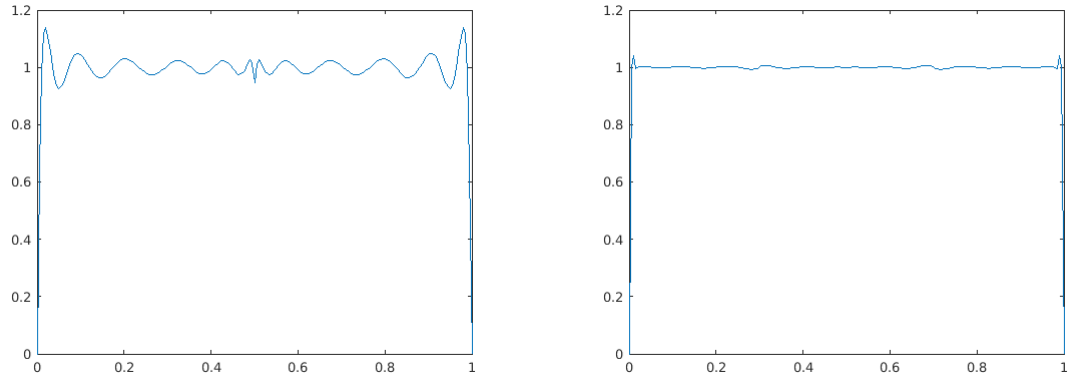

Figure 13: Numerical solution of 1D singularly perturbed parabolic problem obtained by standard IGA(left) and enriched PU-IGA (right), $\varepsilon = 10^{-5}, N = 25, M = 2$, $\triangle h = 0.5$, h-refinement

We present numerical results of (54) using the standard IGA and enriched PU-IGA, which is enriched by the boundary layer function. In Figures 13 and 14, we observe

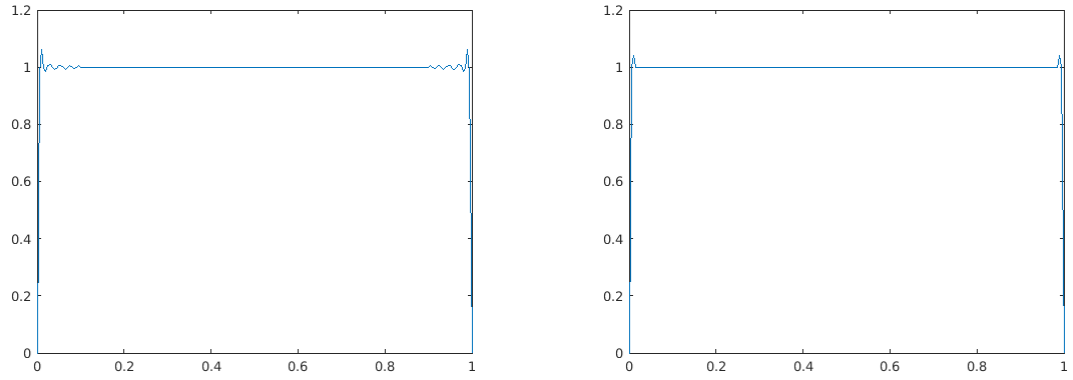

Figure 14: Numerical solution of 1D singularly perturbed parabolic problem obtained by standard IGA(left) and enriched PU-IGA (right) with smaller h, $\varepsilon = 10^{-5}, N = 121, M = 2$, $\triangle h = 0.1$, h-refinement

Table 7: Maximum errors of 1D parabolic problem obtained by standard IGA and enriched PU-IGA , h-refinement, $p = 12$

$\triangle$h	DOF	IGA	Enriched PU-IGA
1	13	0.6084	2.0256E-002
0.5	25	0.3545	6.8586E-003
0.1	121	2.0443E-002	6.4348E-013

that standard IGA produces oscillations near the boundary; however, enriched PU-IGA captures the sharp transition near the boundary. From Table 7, we observe that the errors of enriched PU-IGA is significantly smaller than those of standard IGA. We believe that we can obtain an accurate numerical solution for two-dimensional parabolic problems on a circle with developed enrichment functions.

5.5 Error Estimates for Fully Discrete Approximations

We obtain an error estimate for the backward Euler scheme with $\mathcal{V}_h$ piecewise linear finite space from [20].

Theorem 5. Let U^n be the numerical solution of (51) and u be the solution of (48)

Table 8: Maximum error and space convergence rate of 1D parabolic problem, h-refinement in space direction, with $p = 1$, $\triangle k = 0.001$

$\triangle$h	DOF	Error	Convergence Rate
1	2	0.8671	0.56577648602290742
0.5	3	0.5858	1.2734234229268424
0.1	11	7.5459E-002	1.9739747308538562
0.05	21	1.9208E-002	1.9825994760155063
0.01	101	7.9015E-004	1.9609085209372052
0.005	201	2.0296E-004	

for $n = 1, ..., N$. Then, there is a constant C such that

$$\max_{t\in I} \|u(t) - U(t)\| \leq C(\max_{n\leq N} k_n \|\dot{u}\|_{\infty,I_n} + \max_{t\in I} h^2 \|u(t)\|_{H^2(\Omega)}). \tag{56}$$

Here, the first term bounds the time discretization error, and the second term bounds the space discretization error. Note that this error estimation is for linear finite element space. We present numerical results of one-dimensional parabolic problem (54) using linear IGA to show that the convergence rates from the numerical test support Theorem 5. For a numerical test for the error estimate, we consider (54) with the true solution:

$$u = \exp(-xt)\big(1 - \exp(-\frac{x}{\sqrt{\varepsilon}})\cos(\frac{x}{\sqrt{\varepsilon}})\big)\big(1 - \cos(\frac{1-x}{\sqrt{\varepsilon}})\exp(-\frac{1-x}{\sqrt{\varepsilon}})\big).$$

We use boundary layer functions (55) developed in the last section. We calculate the convergence rate for h and k, by

$$\frac{\log \dfrac{e_{i+1}}{e_i}}{\log \dfrac{t_{i+1}}{t_i}}$$

where e_i is error at the time level t_i. Tables 8 and 9 show that the convergence rate for space h is about two, and the convergence rate for time t is about one, which support Theorem 5. We generally use higher degrees of B-spline basis functions for

Table 9: Maximum error and convergence rate obtained by IGA, h-refinement in space direction, with $p = 1$, $\triangle h = 0.01$

$\triangle$k	DOF	Error	Convergence rate
1	101	0.15387	0.84659173615218630
0.5	101	8.5569E-002	0.93983918732470273
0.1	101	1.8853E-002	0.97872058935658002
0.05	101	9.5670E-003	0.98369693616531739
0.01	101	1.9642E-003	0.96873175100314268
0.005	101	1.0036E-003	

IGA, and we will pursue to prove error estimates for a higher order approximation space in later work.

CHAPTER 6: FOURTH ORDER DIFFERENTIAL EQUATIONS CONTAINING SINGULARITIES

6.1 Introduction

We consider the fourth order equations with clamped boundary condition on a cracked disk.

$$\begin{cases} \triangle^2 u = f \quad \text{in } \Omega \\ u(1,\theta) = \dfrac{\partial u}{\partial n}(1,\theta) = 0 \quad \text{on } \partial\Omega \\ u(r,0) = u(r,2\pi) = 0 \\ \dfrac{\partial u}{\partial y}(r,0) = \dfrac{\partial u}{\partial y}(r,2\pi) = 0 \end{cases}$$

where Ω is the cracked unit disc centered at (0, 0).

The Galerkin method for fourth order differential equations requires at least C^1-continuous basis functions, which is a challenging task for the classical FEM. In Isogeometric Analysis in which NURBS basis functions are used for design as well as analysis, one can construct the basis functions with any regularity easily.

However, the standard IGA is not able to yield reasonable solutions to the fourth-order equations containing singularities. Hence, the B-spline functions are enriched by singular functions that resemble the singularities of the fourth-order equation on the cracked domain.

But, such enrichment methods as GFEM or X-FEM usually encounter large condition numbers of stiffness matrix and integrals of singular functions. We propose

a mapping method to overcome these limitations of the enriched Galerkin method in which enrichment functions are externally added to approximation spaces. In the frame of FEM, a mapping method for the elasticity equations on cracked domain, was introduced in [29]. Also, in the frame of IGA, a mapping method for second order PDEs with singularities was introduced in [35]. We generalize the proposed mapping method introduced in [35] and apply it to fourth-order equations containing singularities.

Enriched PU-IGA, which is developed to handle the singularly perturbed problems in previous chapters, is extended to solve the fourth-order equation with singularities. In singularly perturbed problems, we approximate the boundary layer functions on the reference domain and then push-forward them to the physical domain to construct enrichment basis functions. Now, we consider fourth order PDEs with domain singularities whose asymptotic behaviors are known. First, we apply enriched PU-IGA in which we add singular functions into the approximation space directly. Secondly, we propose a new approach in which we construct a singular geometric mapping from the reference domain onto the physical domain that generates singular basis functions on the physical domain, referred to as PU-IGA with Mapping Method.

Enriched PU-IGA with external enrichment functions gives an accurate numerical solution but yields large condition numbers and has singular integrals. However, PU-IGA with Mapping Method does not have large condition numbers nor integrals of singular functions because the singular basis functions are generated through a particular geometric mapping without introducing external enrichment functions.

6.2 Condition Number and 1D Model Problem

The condition number $\kappa(A)$ of A is defined by

$$\kappa(A) = \frac{\lambda_{max}}{\lambda_{min}}$$

where $\lambda_{max} = \max\lambda_j, \lambda_{min} = \min\lambda_j,\ \lambda_j, j = 1, \ldots, M$ are positive eigenvalues of A. For a problem of order four such as the biharmonic problem, one has $\kappa(A) = \mathcal{O}(h^{-4})$. These estimates hold if the finite element mesh is quasi-uniform, i.e, all elements have roughly the same size, and if the usual minimum angle assumption is valid [20]. We can see that the condition number of a fourth-order equation is higher than that of a second-order equation. Furthermore, an enriched Galerkin method has a much higher condition number than that of a Galerkin method without enrichment. Thus, we expect to have a higher condition number of the fourth-order equation with enriched PU-IGA.

Consider the following one-dimensional model problem with clamped boundary conditions:

$$\begin{cases} u^{(4)}(x) = f(x) \quad \text{in } (a,b) \\ u(a) = u'(a) = 0 \\ u(b) = u'(b) = 0 \end{cases} \tag{57}$$

Let $\mathcal{V} = \{w \in H^2(a,b) : w, w' \in H_0^1(a,b)\}$. Multiplying the equation by an arbitrary function $v \in \mathcal{V}$ and using integration by part along with clamped boundary condition, we have

$$\int_a^b u^{(4)} v dx = \int_a^b u^{(2)} v^{(2)} dx = \int_a^b f v dx \quad \forall v \in \mathcal{V}.$$

Thus the variational equation is

$$\mathcal{B}(u,v) \equiv \int_a^b u^{(2)} v^{(2)} dx = \int_a^b f v dx \equiv \mathcal{F}(v), \quad \forall v \in \mathcal{V}.$$

We construct an example of a fourth-order equation containing singularity of the type x^α. To determine how strong the intensity of singularity α is allowed, we prove the following lemma.

Lemma 6. Suppose $v \in H_0^2(a,b), \quad 0 \le a < b$. Then,

$$(1) \quad |v(x)| < Cx^{1.5}$$

$$(2) \quad |\int_a^b x^{\alpha-4} v(x) dx| < \infty \qquad \text{if } \alpha > 1.5.$$

Proof. (1) Since $v(x) \in H_0^2(a,b)$, $v'(x) \in H_0^1(a,b)$, then $|v'(x)| < Cx^{0.5}$, $C \in \mathbb{R}$ by Theorem 7.17 in [8]. Hence we have

$$|v(x)| = |\int_a^x v'(t) dt| \le C \int_0^x t^{0.5} dt \le Cx^{1.5}.$$

(2) $$\Big|\int_a^b x^{\alpha-4} v(x) dx\Big| < C \int_0^b x^{\alpha-4} x^{1.5} dx \quad \text{to be integrable,}$$

$\alpha - 4 + 1.5 > -1$. Therefore, $\alpha > 1.5$.

□

6.3 Enriched PU-IGA

For simplicity, we assume that the physical domain is the same as the reference domain. Therefore, B-spline functions $\hat{N}_{i,p+1}(\xi)$ and their push-forwards $N_{i,p+1}(x)$ onto the physical domain are same. Consider a fourth-order equation containing

singularities ξ^{α} and $\xi^{\alpha/2+1}$ with $1.5 < \alpha < 2$ (due to Lemma 6).

I. Partition of the physical domain

We divide the physical domain into singular, $\Omega_{sing} = [0, 0.4]$ and regular zones, $\Omega_{reg} = [0.3, 1]$.

II. Construct C^1-continuous B-spline functions

We present PU-IGA with the p-refinement as well as with the k-refinement of IGA. Consider the following two open knot vectors that correspond to the p-refinement and the k-refinement, respectively:

$$\Xi^p = \Big\{ \underbrace{0,..,0}_{p+1}, \underbrace{0.1,..,0.1}_{p-1}, \underbrace{0.2,..,0.2}_{p-1}, .., \underbrace{0.8,..,0.8}_{p-1}, \underbrace{0.9,..,0.9}_{p-1}, \underbrace{1,..,1}_{p+1}, \Big\} \tag{58}$$

$$\Xi^k = \Big\{ \underbrace{0,\ldots,0}_{p+1}, \quad 0.1, \quad 0.2, \quad \ldots \quad 0.8, \quad 0.9, \quad \underbrace{1,\ldots,1}_{p+1} \Big\}. \tag{59}$$

Then we have C^1-continuous B-spline functions according to (58) and C^{p-1}-continuous B-spline functions according to (59). The corresponding approximation spaces for the p-refinement and the k-refinement, respectively, are as follows:

$$\mathcal{V}^p = \{N_{k,p+1}(x) \mid k = 1, \ldots, 10p - 8\}, \tag{60}$$

$$\mathcal{V}^k = \{N_{k,p+1}(x) \mid k = 1, \ldots, p + 10\}. \tag{61}$$

III. Boundary Conditions

To satisfy the clamped boundary conditions at both ends with the B-spline functions (60) and (61), we consider the following two approaches.

- **Discarded** The first two and the last two B-spline functions from (60) and (61)

are discarded.

$$\begin{aligned} \mathcal{V}_I^p &= \Big\{ N_i(\xi) : 3 \le i \le 10p - 10 \Big\}, \\ \mathcal{V}_I^k &= \Big\{ N_i(\xi) : 3 \le i \le p + 8 \Big\}. \end{aligned}$$

- **Modified** The first two and the last two B-spline functions from (60) and (61) are modified by PU functions with flat-top as follows:

$${}^pN_i^*(\xi) = \begin{cases} N_i(\xi) \times \psi^R(\xi + 0.02), & \text{if } i = 1, 2, \\ N_i(\xi) \times \psi^L(\xi - 0.45), & \text{if } i = 10p - 9, 10p - 8 \end{cases}$$

$${}^kN_i^*(\xi) = \begin{cases} N_i(\xi) \times \psi^R(\xi + 0.02), & \text{if } i = 1, 2, \\ N_i(\xi) \times \psi^L(\xi - 0.45), & \text{if } i = p + 9, p + 10 \end{cases}$$

Now modified $\mathcal{C}^1$-continuous B-spline approximation functions for the p-refinement and the k-refinement, respectively, are as follows:

$$\begin{aligned} \mathcal{V}_{\text{II}}^p &= \mathcal{V}_I^p \cup \{ {}^pN_1^*, {}^pN_2^*, {}^pN_{10p-8}^*, {}^pN_{10p-9}^* \} \\ \mathcal{V}_{\text{II}}^k &= \mathcal{V}_I^k \cup \{ {}^kN_1^*, {}^kN_2^*, {}^kN_{p+9}^*, {}^kN_{p+10}^* \} \end{aligned} \tag{62}$$

where

$$\psi^R(\xi) = \begin{cases} 0 & \text{if } \xi \le 0.02 \\ N_5^{pu}(\xi) + N_6^{pu}(\xi) & \text{if } 0.02 \le \xi \le 0.06 \\ 1 & \text{if } 0.06 \le \xi \end{cases}$$

$$\psi^L(\xi) = \begin{cases} 1 & \text{if } \xi \leq 0.5 \\ N_7^{pu}(\xi) + N_8^{pu}(\xi) & \text{if } 0.5 \leq \xi \leq 0.55 \\ 0 & \text{if } 0.55 \leq \xi \end{cases}$$

and N_j^{pu} is B-spline function corresponding to the knot vector:

$$\Xi^{pu} = \Big\{ \underbrace{0,..,0}_{4}, \underbrace{0.02,0.02}_{2}, \underbrace{0.06,0.06}_{2}, \underbrace{0.5,0.5}_{2}, \underbrace{0.55,0.55}_{2}, \underbrace{0.8,0.8}_{2}, \underbrace{1,..,1}_{4} \Big\}$$

IV. Approximation Space

Two singular enrichment functions, ξ^α and $\xi^{\alpha/2+1}$, are added to the basis functions listed above. We define a modified and enriched C^1-continuous approximation space as union of scaled enrichment functions and family of basis functions in (62).

Enriched p-refinement of PU-IGA

Construct two PU functions with flat-top ψ_2 and ψ_2^* by the B-spline functions generated by the knot vector Ξ^p defined by (58). Notice that the two PU functions change as the p-degree varies. We divide the domain into two patches, which are the supports of these two PU functions. The local approximation functions on the two patches are the same set of B-splines generated by Ξ^p. Additionally, two enrichment functions are added to the family of B-splines.

The two PU functions ψ_2 and ψ_2^* are constructed by:

$$\psi_2(\xi) = \sum_{j=1}^{3p-1} N_j^p(\xi) = \begin{cases} 1 & \text{if } 0 \leq \xi \leq 0.3, \\ N_{3p-2}^p(\xi) + N_{3p-1}^p(\xi) & \text{if } 0.3 \leq \xi \leq 0.4, \\ 0 & \text{if } 0.4 \leq \xi \end{cases}$$

$$\psi_2^*(\xi) = 1 - \psi_2(\xi)$$

Enrichment functions N_i^s are scaled by PU function ψ_2 :

$$N_i^s(\xi) = \begin{cases} \xi^\alpha \times \psi_2(\xi), & \text{if } i = 1, \\ \xi^{\alpha/2+1} \times \psi_2(\xi), & \text{if } i = 2. \end{cases}$$

Now define a modified and enriched $\mathcal{C}^1$-continuous approximation space as follows:

$$\begin{aligned} \mathcal{V}_{\text{rich}}^p &= \{N_1^s, N_2^s\} \ \cup \ \{\psi_2(\xi)N_k(\xi) : 1 \le k \le 4p-2, \ \ N_k(\xi) \in \mathcal{V}_{\text{II}}^p\} \\ &\cup \ \{\psi_2^*(\xi)N_k(\xi) : 3p-2 \le k \le 10p-8, \ \ N_k(\xi) \in \mathcal{V}_{\text{II}}^p\}. \end{aligned} \tag{63}$$

Note that the number of basis functions used in this approach is

$$\text{card}(\mathcal{V}_{\text{rich}}^p) = 11p - 5.$$

This approach gives accurate solution but, yields large matrix condition numbers. Hence, in order to reduce condition numbers, next consider another approach that reduces a number of B-spline basis functions in the singular zone, the support of ψ_2. Moreover, since the maximum error occurs over the common non flat-top zone $[0.3, 0.4]$ of two PU functions ψ_2 and ψ_2^*, we choose PU functions that have a smaller non flat-top zone $[0.35, 0.4]$.

Reduced, enriched p-refinement of IGA

Consider

$$\Xi^p = \Big\{ \underbrace{0,\ldots,0}_{p+1}, \underbrace{0.1,..,0.1}_{p-1}, \underbrace{0.2,..,0.2}_{p-1}, \underbrace{0.3+\delta^*,..,0.3+\delta^*}_{p-1}, \underbrace{0.4,..,0.4}_{p-1}, \ldots, \underbrace{0.9,..,0.9}_{p-1}, \underbrace{1,..,1}_{p+1} \Big\},$$

with $\delta^* = 0.05$. We define a PU function as follows:

$$\tilde{\psi}_2(\xi) = \begin{cases} 1 & \text{if } 0 \le \xi \le 0.3 + \delta^*, \\ N_{3p-2}(\xi) + N_{3p-1}(\xi) & \text{if } 0.3 + \delta^* \le \xi \le 0.4, \\ 0 & \text{if } 0.4 \le \xi, \end{cases}$$

Enrichment functions $N_i^s(\xi)$ are scaled by PU function $\tilde{\psi}_2$:

$$N_i^s(\xi) = \begin{cases} \xi^\alpha \times \tilde{\psi}_2(\xi), & \text{if } i = 1, \\ \xi^{\alpha/2+1} \times \tilde{\psi}_2(\xi), & \text{if } i = 2, \\ \xi^2 \times \tilde{\psi}_2(\xi), & \text{if } i = 3. \end{cases}$$

The corresponding approximation space is as follows:

$$\mathcal{W}^p_{\text{rich2}} \;=\; \{N_1^s, N_2^s, N_3^s\} \cup \{N_k(\xi) : 3p \le k \le 10p - 8, N_k(\xi) \in \mathcal{V}^p_{II}\}.$$

Let us note the following:

1. $\text{card}(\mathcal{W}^p_{\text{rich2}}) = 7p - 4 \ll \text{card}(\mathcal{V}^p_{\text{rich}}) = 11p - 5$.

2. $1 = \sum_{k=1}^{10p-8} N_k(\xi) = \sum_{i=1}^{3p-1} N_i(\xi) + \sum_{k=3p}^{10p-8} N_k(\xi) = \tilde{\psi}_2(\xi) + \sum_{k=3p}^{10p-8} N_k(\xi)$ on $[0, 1]$.

3. Numerical results, presented in Table 10, show that condition numbers are reduced by half, but accuracy is also decreased by more than two orders of magnitude.

Enriched k-refinement of IGA

Since the B-spline functions generated by the knot vector Ξ^k are highly regular, we consider two $\mathcal{C}^2$-continuous PU functions defined as follows:

$$\begin{aligned}\psi_3(\xi) &= \begin{cases} 1 & \text{if } 0 \le \xi \le 0.3, \\ (4-10x)^3(600x^2-330x+46) & \text{if } 0.3 \le \xi \le 0.4, \\ 0 & \text{if } 0.4 \le \xi, \end{cases} \\ \psi_3^*(\xi) &= 1-\psi_3(\xi).\end{aligned}$$

Two enrichment functions are scaled by a PU function with flat-top, ψ_3.

$$N_j^s(\xi) = \begin{cases} \xi^\alpha \times \psi_3(\xi), & \text{if } j=3 \\ \xi^{\alpha/2+1} \times \psi_3(\xi), & \text{if } j=4 \end{cases}$$

A modified and enriched approximation space is as follows:

$$\begin{aligned}\mathcal{V}_{\text{rich}}^k &= \{N_3^s, N_4^s\} \cup \{\psi_3(\xi)N_i(\xi) : 1 \le i \le p+4,\ N_i(\xi) \in \mathcal{V}_{\text{II}}^k\} \\ &\cup \{\psi_3^*(\xi)N_i(\xi) : 4 \le i \le p+10,\ N_i(\xi) \in \mathcal{V}_{\text{II}}^k\} \end{aligned} \tag{64}$$

Note that:

1. $\text{card}(\mathcal{V}_{\text{rich}}^k) = 2p+13 \ll card(\mathcal{V}_{\text{rich}}^p) = 11p-5$

2. Numerical results, presented in Tables 10 and 11, show that the condition numbers are about one half of the enriched p-refinement of IGA because the degree of freedom is significantly smaller.

Both enriched p-refinement and k-refinement of IGA yield accurate solutions. However, their condition numbers are still large. Furthermore, since enrichment functions

and their derivatives are singular, this method fails to give reasonable solutions without special treatment for accurate integrals.

V. Substitution method to deal with singular integrals

We use a special substitution method to treat singular integrals.

1. Let $T(x) = x^\beta$ be a substitution function, whose exponent β is determined by the strongest singular term.

$$\int_{[a,b]} ((\xi^\alpha)'')^2 d\xi = C \int_{[a,b]} \xi^{2(\alpha-2)} d\xi = C \int_{T^{-1}([a,b])} x^{2(\alpha-2)\beta} x^{\beta-1} dx$$

Choose β for this to be a regular integral:

$$2(\alpha-2)\beta + \beta - 1 \geq 0, \quad \text{that is} \quad \beta \geq \frac{1}{2\alpha - 3}.$$

2. Since $\alpha = 1.6$, we select a substitution function $T : [0, 0.4^{1/5}] \longrightarrow [0, 0.4]$ defined by $\xi = T(x) = x^5$. Then this substitution function converts a singular to a regular integral. For example,

$$\int_0^{0.3} [(\xi^{1.6})'']d\xi = \int_0^{0.3^{1/5}} 0.96(T(x)^{-0.4})5x^4 dx = \int_0^{0.3^{1/5}} 4.8x^2 dx$$

3. **The p-refinement of PU-IGA** For $N_j, N_i^s \in \mathcal{V}_{rich}^p$ of (63), we compute the bilinear form by the substitution method as follows:

$$\begin{aligned} \mathcal{B}(N_i^s, N_j) &= \sum_{k=0}^{3} \int_{a_k}^{a_{k+1}} N_j^{(2)}(T(x))(N_i^s)^{(2)}(T(x))5x^4 dx \\ \mathcal{F}(N_i^s) &= \sum_{k=0}^{3} \int_{a_k}^{a_{k+1}} f(T(x))(N_i^s(T(x))5x^4 dx \\ \text{where} \qquad a_i &= T^{-1}(x_i), \quad x_i = 0.1, 0.2, 0.3, 0.4. \end{aligned}$$

4. **The k-refinement of PU-IGA** For $N_j, N_i^s \in \mathcal{V}_{rich}^k$ of (64), we compute the bilinear form by the substitution method as follows:

$$\begin{aligned} \mathcal{B}(N_i^s, N_j) &= \sum_{k=0}^{3} \int_{a_k}^{a_{k+1}} N_j^{(2)}(T(x))(N_i^s)^{(2)}(T(x))5x^4 dx \\ \mathcal{F}(N_i^s) &= \sum_{k=0}^{3} \int_{a_k}^{a_{k+1}} f(T(x))(N_i^s(T(x))5x^4 dx \\ \text{where} \qquad a_i &= T^{-1}(x_i), \quad x_i = 0.1, 0.2, 0.3, 0.4. \end{aligned}$$

6.4 Enriched PU-IGA with Mapping Method

In this section, we propose a mapping method that reduces the matrix condition number and does not have singular integrals caused by adding external enrichment functions to the approximation spaces. The proposed mapping method generates singular functions through a mapping from the reference domain onto the singular zone. Then, the condition number is as small as that of IGA with no enrichment. Moreover, singular integrals do not appear in computation of stiffness matrices.

Consider a fourth order equation whose true solution is

$$u(x) = x^{1.6} - 2x^{1.8} + x^2,$$

which is singular at the left end of the physical domain $\Omega = [0, 1]$. Note that the physical domain is the same as the reference domain.

I. Partition of the physical domain and construction of Mappings

We divide the domain into singular $\Omega_{sing} = [0, 0.5]$ and regular zones $\Omega_{reg} = [0.4, 1]$.

Next, we define two mappings to construct singular basis functions on a singular

zone and regular basis functions on a regular zone, respectively,

$$F : \hat{\Omega} = [0,1] \longrightarrow \Omega_{sing}, \qquad G : \hat{\Omega} = [0,1] \longrightarrow \Omega_{reg},$$

defined by

$$x = F(\xi) = 0.5 \cdot \xi^5, \qquad x = G(\xi) = 0.6\xi + 0.4. \tag{65}$$

Then we have

$$G^{-1}(x) \;=\; \frac{x - 0.4}{0.6}, \quad G^{-1}([0.4, 0.5]) = [0, 1/6], \quad F^{-1}([0.4, 0.5]) = [0.8^{0.2}, 1].$$

The selection of F and G depend on the strength of singularity. More specifically, the mappings (65) correspond to the intensity of singularity $\alpha = 1.6$. The inverse mapping $\xi = F^{-1}(x)$ brings

$$\xi^8, \xi^9, \xi^{10}, \xi^{15}, \xi^{20}, \ldots \xi^{5k}$$

in the reference domain to

$$(2x)^{1.6}, (2x)^{1.8}, (2x)^2, (2x)^3, (2x)^4, \ldots, (2x)^k$$

in the physical domain. These functions satisfy the clamped boundary conditions at $x = 0$.

Note that push-forwards $\xi^k, k \leq 7$, through F mapping, are not acceptable basis functions in the physical domain.

$$\xi^k \circ F^{-1}(x) = (2x)^{k/5} < (2x)^{7/5} = (2x)^{1.4}.$$

This cannot be a basis function on the physical domain since its second derivative is

not integrable by Lemma 6.

II. $\mathcal{C}^1$-continuous PU functions with flat-top on the physical domain

Note that we can construct PU on the reference domain for enriched PU-IGA. However, for the Mapping Method, we need to construct PU on the physical domain since we have a singular geometry mapping to a singular zone and a regular geometry mapping to a regular zone, respectively, through which push-forwards of PU on the reference domain can no longer be PU on the physical domain.

Let us define two PU functions on the physical domain as follows:

$$\begin{aligned}
\psi_4(x) &= \begin{cases} 1 & \text{if } 0 \le x \le 0.4 \\ (5-10x)^2(20x-7) & \text{if } 0.4 \le x \le 0.5 \\ 0 & \text{if } 0.5 \le x \le 1 \end{cases} \qquad (66) \\
&= \begin{cases} 1 & \text{if } x \in [0, 0.4] \\ N_{5,4}(x) + N_{6,4}(x) & \text{if } x \in [0.4, 0.5] \\ 0 & \text{if } x \in [0.5, 1] \end{cases} \\
\psi_4^*(x) &= 1 - \psi_4(x) \qquad (67)
\end{aligned}$$

Pull-backs of these PU functions are

$$\hat{\psi}_4(\xi) = \psi_4 \circ F, \quad \hat{\psi}_4^*(\xi) = \psi_4^* \circ G.$$

Here, $N_{k,4}(x),\ 1 \le k \le 14$ are the B-spline functions corresponding to the following knot vector

$$\{\underbrace{0\ldots0}_{4}, \underbrace{0.2, 0.2}_{2}, \underbrace{0.4, 0.4}_{2}, \underbrace{0.5, 0.5}_{2}, \underbrace{0.6, 0.6}_{2}, \underbrace{0.8, 0.8}_{2}, \underbrace{1\cdots1}_{4}\}.$$

Note that

$$\psi_4(x) + \psi_4^*(x) = 1, \quad \forall x \in \Omega, \quad \text{but} \quad \hat{\psi}_4(\xi) + \hat{\psi}_4^*(\xi) \neq 1, \quad \forall \xi \in \hat{\Omega}.$$

Pull-back of PU functions through different mappings are not PU functions on the reference domain.

The physical and the reference domains are partitioned as follows:

$$\begin{aligned} \Omega &= [0, 0.4] \cup [0.4, 0.5] \cup [0.5, 1], \\ \hat{\Omega}_F &= [0, 0.8^{0.2}] \cup [0.8^{0.2}, 1], \quad \hat{\Omega}_G = [0, 1/6] \cup [1/6, 1]. \end{aligned}$$

Non flat-top zones of $\hat{\psi}_4$ and $\hat{\psi}_4^*$ are $[0.8^{0.2}, 1]$ and $[0, 1/6]$, respectively.

III. Basis functions on the reference domain

We construct monomials for the singular zone and B-splines for the regular zone, respectively.

$$\hat{\mathcal{V}}_F = \hat{\psi}_4(\xi) \times \{\hat{M}_1 = \xi^8, \hat{M}_2 = \xi^9, \hat{M}_{1+k} = \xi^{5k}, k = 2, 3, 4\} \tag{68}$$

$$\hat{\mathcal{V}}_G^p = \hat{\psi}_4^*(\xi) \times \{\hat{N}_{k,p+1}(\xi) : k = 1, \ldots, 2p-1\}, \tag{69}$$

where $\hat{\psi}_4$ and $\hat{\psi}_4^*$ are defined by (66) and (67), and $\hat{N}_{k,p+1}(\xi)$ are B-spline functions corresponding to the following knot vector:

$$\Xi = \{\underbrace{0 \cdots 0}_{p+1}, \ \underbrace{1/p+1}_{1}, \ \underbrace{2/p+1}_{1}, \cdots, \underbrace{p/p+1}_{1}, \ \underbrace{1 \cdots 1}_{p+1}\}.$$

For the singular zone, the push-forwards of these monomial basis functions (68) through F mapping resemble the singularities. For the regular zone, the last two B-spline functions in $\hat{\mathcal{V}}_G^p$ were discarded to satisfy the clamped boundary conditions.

Then, we have the number of basis functions as follows:

$$\mathrm{card}(\hat{\mathcal{V}}_F \cup \hat{\mathcal{V}}_G^p) = 2p + 4.$$

IV. Bilinear Form and load vector

We have the following two lemmas for calculation of bilinear forms and load vectors. Their proofs are straightforward.

Lemma 7. If $\hat{u}(\xi) = (u \circ F)(\xi)$, then

$$\begin{aligned} u_{xx} \circ F &= \hat{u}_{\xi\xi}\Big((\frac{dF}{d\xi})^{-1}\Big)^2 + \hat{u}_{\xi}\Big((\frac{dF}{d\xi})^{-1}\Big)_{\xi}(\frac{dF}{d\xi})^{-1} \\ &= (\hat{u}_{\xi\xi})(16\xi^{-8}) + (\hat{u}_{\xi})((-16)\xi^{-5})(4\xi^{-4}) \\ &= 0.16\Big(\hat{u}_{\xi\xi}\xi^{-8} - 4\hat{u}_{\xi}\xi^{-9}\Big). \end{aligned} \tag{70}$$

Lemma 8. If $\hat{w}(\xi) = (w \circ G)(\xi)$, then

$$\begin{aligned} w_{xx} \circ G &= \hat{w}_{\xi\xi}\Big((\frac{dG}{d\xi})^{-1}\Big)^2 + \hat{w}_{\xi}\Big((\frac{dG}{d\xi})^{-1}\Big)_{\xi}(\frac{dG}{d\xi})^{-1} \\ &= \hat{w}_{\xi\xi}(\frac{1}{0.36}). \end{aligned} \tag{71}$$

Bilinear forms are one of the following three cases.

1. Bilinear form for two basis functions in $\mathcal{V}_F$

Suppose $u = \hat{u} \circ F^{-1}, v = \hat{v} \circ F^{-1}$, where $\hat{u} = \hat{\psi}_4(\xi) \cdot \hat{M}_k$ and $\hat{v} = \hat{\psi}_4(\xi) \cdot \hat{M}_l$ are in $\hat{\mathcal{V}}_F$. By Lemma 7 , we have

$$\begin{aligned} \mathcal{B}(u,v) &= \int_0^{0.5} u_{xx}v_{xx}dx = \int_0^1 (u_{xx} \circ F)(v_{xx} \circ F)|J(F)|d\xi \\ &= \Big(\int_0^{0.8^2} + \int_{0.8^2}^1 \Big)(u_{xx} \circ F)(v_{xx} \circ F)|J(F)|d\xi \\ &= (0.16^2)\Big(\int_0^{0.8^2} + \int_{0.8^2}^1 \Big)\Big(\hat{u}_{\xi\xi}\xi^{-8} - 4\hat{u}_{\xi}\xi^{-9}\Big)\Big(\hat{v}_{\xi\xi}\xi^{-8} - 4\hat{v}_{\xi}\xi^{-9}\Big)|J(F)|d\xi \end{aligned}$$

$$
\begin{aligned}
&= (0.16^2)\int_0^{0.8^2}\Big((\hat{M}_k)_{\xi\xi}\xi^{-8}-4(\hat{M}_k)_{\xi}\xi^{-9}\Big)\Big((\hat{M}_l)_{\xi\xi}\xi^{-8}-4(\hat{M}_l)_{\xi}\xi^{-9}\Big)|J(F)|d\xi\\
&\quad +(0.16^2)\int_{0.8^2}^1\Big((\hat{\psi}_4\cdot\hat{M}_k)_{\xi\xi}\xi^{-8}-4(\hat{\psi}_4\cdot\hat{M}_k)_{\xi}\xi^{-9}\Big)\\
&\qquad \cdot\Big((\hat{\psi}_4\cdot\hat{M}_l)_{\xi\xi}\xi^{-8}-4(\hat{\psi}_4\cdot\hat{M}_l)_{\xi}\xi^{-9}\Big)|J(F)|d\xi\\
\mathcal{F}(v) &= \int_0^{0.5} fv dx=\int_0^1 (f\circ F)(v\circ F)|J(F)|d\xi\\
&= \Big(\int_0^{0.8^2}+\int_{0.8^2}^1\Big)(f\circ F)(v\circ F)|J(F)|d\xi\\
&= \int_0^{0.8^2}(f\circ F)(\hat{M}_l)|J(F)|d\xi+\int_{0.8^2}^1(f\circ F)(\hat{\psi}_4\cdot\hat{M}_l)|J(F)|d\xi
\end{aligned}
$$

where $|J(F)|=2.5\xi^4$ and

$$
\hat{\psi}_4(\xi) = \Big(5-10\cdot F(\xi)\Big)^2\Big(20\cdot F(\xi)-7\Big)=(5-5\xi^5)(10\xi^5-7),\ \text{for } \xi\in[0.8^2,1].
$$

2. Bilinear form for two basis functions in $\hat{\mathcal{V}}_G$

Suppose $u=\hat{u}\circ G^{-1}, v=\hat{v}\circ G^{-1}$, where $\hat{u}=\hat{\psi}_4^*(\xi)\cdot\hat{N}_k(\xi)$ and $\hat{v}=\hat{\psi}_4^*(\xi)\cdot\hat{N}_l(\xi)$ are in $\hat{\mathcal{V}}_G$. By Lemma 8, we have

$$
\begin{aligned}
\mathcal{B}(u,v) &= \int_{0.4}^1 u_{xx}v_{xx}dx=\int_0^1(u_{xx}\circ G)(v_{xx}\circ G)|J(G)|d\xi\\
&= \Big(\int_0^{1/6}+\int_{1/6}^1\Big)(u_{xx}\circ G)(v_{xx}\circ G)|J(G)|d\xi\\
&= (\frac{1}{0.36})^2\int_{1/6}^1(\hat{N}_k)_{\xi\xi}(\hat{N}_l)_{\xi\xi}|J(G)|d\xi+(\frac{1}{0.36})^2\int_0^{1/6}(\hat{\psi}_4^*\hat{N}_k)_{\xi\xi}(\hat{\psi}_4^*\hat{N}_l)_{\xi\xi}|J(G)|d\xi
\end{aligned}
$$

$$
\begin{aligned}
\mathcal{F}(v) &= \int_{0.4}^1 fv dx=\int_0^1(f\circ G)(v\circ G)|J(G)|d\xi\\
&= \Big(\int_0^{1/6}+\int_{1/6}^1\Big)(f\circ G)\cdot(\hat{v})|J(G)|d\xi\\
&= \int_0^{1/6}(f\circ G)\cdot(\hat{\psi}_4^*\hat{N}_l)\cdot|J(G)|d\xi+\int_{1/6}^1(f\circ G)\cdot\hat{N}_l\cdot|J(G)|d\xi
\end{aligned}
$$

where $|J(G)| = 0.6$ and

$$\hat{\psi}_4^* = 1 - \Big(5 - 10 \cdot G(\xi)\Big)^2 \Big(20 \cdot G(\xi) - 7\Big) = 1 - (1-6\xi)^2(12\xi + 1), \quad \text{for } \xi \in [0, 1/6].$$

3. Bilinear form for mixed type: one in $\hat{\mathcal{V}}_F$ and one in $\hat{\mathcal{V}}_G$

Suppose $u = \hat{u} \circ F^{-1}$ and $v = \hat{v} \circ G^{-1}$, where $\hat{u} = \hat{\psi}_4(x)\hat{M}$ and $\hat{v} = \psi_4^*(x)\hat{N}$. The product of two basis functions u and v vanish except for points in $[0.4, 0.5]$. In other words, the supports of u and v intersects only on $[0.4, 0.5]$.

By Lemmas 7 and 8, we have the following:

$$\begin{aligned}
\mathcal{B}(u,v) &= \int_{0.4}^{0.5} u_{xx} v_{xx} dx \\
&= \int_{0.4}^{0.5} \Big((\hat{u} \circ F^{-1})_{xx} (\hat{v} \circ G^{-1})_{xx}\Big) dx \\
&= \int_{0.4}^{0.5} \Big((\hat{u} \circ F^{-1})_{xx} (\hat{v} \circ G^{-1})_{xx}\Big) \circ G \circ G^{-1} dx, \qquad \text{by } G \circ G^{-1} = 1 \\
&= \int_{0.4}^{0.5} \Big((\hat{\psi}_4 \cdot \hat{M} \circ F^{-1})_{xx} \circ G\Big) \cdot \Big((\hat{\psi}_4^* \cdot \hat{N} \circ G^{-1})_{xx} \circ G\Big) \circ G^{-1} dx \\
&= \int_{0.4}^{0.5} \Big((\hat{\psi}_4 \cdot \hat{M} \circ F^{-1})_{xx} \circ G\Big) \cdot \Big(\frac{1}{0.36} (\hat{\psi}_4^* \hat{N})_{\xi\xi}\Big) \circ G^{-1} d\xi \\
&= \int_{F^{-1}(0.4)}^{F^{-1}(0.5)} \Big(((\hat{\psi}_4 \cdot \hat{M}) \circ F^{-1})_{xx} \circ F\Big) \cdot \frac{1}{0.36} \Big((\hat{\psi}_4^* \hat{N})_{\xi\xi} \circ (G^{-1} \circ F)\Big) |J(F)| d\xi \\
&= \int_{0.8^2}^{1} 0.16 \Big((\hat{\psi}_4 \cdot \hat{M})_{\xi\xi} \xi^{-8} - 4(\hat{\psi}_4 \cdot \hat{M})_{\xi} \xi^{-9}\Big) \cdot \\
&\quad \frac{1}{0.36} \Big((\hat{\psi}_4^* \hat{N})_{\xi\xi} \circ (G^{-1} \circ F)\Big) |J(F)| d\xi
\end{aligned}$$

where $(G^{-1} \circ F)(\xi) = \dfrac{5}{6}(\xi^5 - 0.8)$.

Note that it is necessary to divide integrals over $[0.8^2, 1]$ whenever knots are inserted in $[0, 1/6]$ for the knot vector (70).

6.5 Numerical Results

We test enriched PU-IGA and PU-IGA with the Mapping Method to one dimensional fourth order differential equation containing singularities. We also test the standard IGA with modified B-spline functions to a fourth order problem with smooth solution to compare condition numbers of enriched PU-IGA and the standard IGA.

We calculate relative errors in the maximum and the energy norms to measure accuracy.

The energy norm of $u \in H^2(a,b)$ is defined by

$$\left\{\frac{1}{2}\int_a^b u^{(2)}u^{(2)}dx\right\}^{1/2} = \sqrt{\frac{1}{2}\mathcal{B}(u,u)} = \|u\|_{Eng}$$

The relative error in the energy norm is

$$\|u-U\|^2_{Eng,rel} = \left|\frac{\|u\|^2_{Eng} - \|U\|^2_{Eng}}{\|u\|^2_{Eng}}\right|$$

Example 9. **Fourth-order differential equation containing singularities**

Suppose

$$u(x) = \left(x^{\alpha/2} - x\right)^2 = x^\alpha - 2x^{\alpha/2+1} + x^2$$

is the true solution of the model problem (57), satisfying the clamped boundary conditions at both ends of $\Omega = (0,1)$. Then, we have

$$u^{(4)}(x) = (\alpha)(\alpha-1)(\alpha-2)(\alpha-3)x^{\alpha-4} - 2(\alpha/2+1)(\alpha/2)(\alpha/2-1)(\alpha/2-2)x^{\alpha/2-3} = f(x).$$

Suppose we select an intensity of singularity $\alpha = 1.6$, then

$$\|u\|^2_{eng} = 0.304.$$

By Lemma 6, we have

$$|\int_0^1 f(x)v(x)dx| < \infty, \;\; v \in H_0^2(0,1).$$

Table 10: Relative maximum and energy errors of 1D fourth-order equation containing singularities by enrcihed p-refinement of PU-IGA. $\kappa(A)$ denotes the matrix condition number.

Enriched p-refinement PU-IGA				
DEG	DOF	$\|Err\|_{Max}$	$\|Err\|_{Eng}$	$\kappa(A)$
3	28	1.355E-05	9.727E-05	3.4986E+19
4	39	4.963E-08	5.737E-06	1.7504E+17
5	50	3.814E-09	2.750E-06	6.6324E+17
6	61	3.224E-10	3.917E-06	1.0178E+19
7	72	9.160E-11	1.314E-06	1.6273E+19
8	83	1.546E-10	2.949E-05	2.4194E+18
9	94	5.818E-11	4.083E-06	1.0687E+19
10	105	1.018E-09	4.766E-06	9.1598E+18
Reduced, Enriched p-refinement of PU-IGA				
DEG	DOF	$\|Err\|_{Max}$	$\|Err\|_{Eng}$	$\kappa(A)$
3	17	8.509E-02	1.882E-02	4.4658E+09
4	24	5.265E-02	1.212E-02	4.5521E+09
5	31	1.546E-02	5.160E-03	4.5545E+09
6	38	9.254E-04	1.244E-03	4.4294E+09
7	45	3.674E-04	6.800E-04	4.2640E+09
8	52	1.281E-04	5.002E-04	4.1050E+09
9	59	2.626E-05	2.766E-04	3.9573E+09
10	66	4.297E-06	1.306E-04	3.8204E+09

We test enriched PU-IGA - p-refinement, reduced p-refinement, and k-refinement-, and PU-IGA with Mapping Method to the fourth-order equation containing singularities. We observe the following:

1. Table 10 shows that enriched p-refinement of IGA yields highly accurate numerical solutions of the fourth-order equation containing singularities; however, condition numbers are unacceptably large. For the reduced p-refinement of IGA

Table 11: Relative maximum and energy errors of 1D fourth-order PDE containing singularities obtained by enriched k-refinement of PU-IGA. $\kappa(A)$ denotes the matrix condition number.

Enriched k-refinement PU-IGA				
DEG	DOF	$\|Err\|_{Max}$	$\|Err\|_{Eng}$	$\kappa(A)$
3	19	1.504E-05	9.903E-05	1.4983E+10
4	21	2.700E-07	2.197E-06	2.4058E+10
5	23	6.678E-08	1.315E-06	3.6642E+10
6	25	1.037E-08	1.558E-06	5.8168E+11
7	27	1.642E-09	1.738E-06	5.3845E+13
8	29	2.716E-10	1.015E-06	5.6871E+15
9	31	5.867E-11	1.278E-06	6.6014E+17
10	33	2.618E-11	1.126E-06	7.7665E+16

in which degree of freedom is much smaller, the condition numbers become smaller; however, we cannot get as much accuracy as enriched p-refinement of IGA.

2. Condition numbers exceeding E+10 would be problematic. It would be better to use a preconditioner to transform the linear system for more numerical precision.

3. Table 11 shows that enriched k-refinement of IGA is also able to yield highly accurate numerical solutions. However, the condition numbers are still large. The second half of Table 12 shows that the k-refinement of IGA with no enrichment cannot solve singularity problems.

4. The first half of Table 12 shows that the mapping method is able to yield accurate numerical solutions as well as small condition numbers.

5. The matrix condition number $\kappa(A)$ does not depend on the regularity of PU functions. Applying PU-IGA with Mapping Method with degree 10 and degree

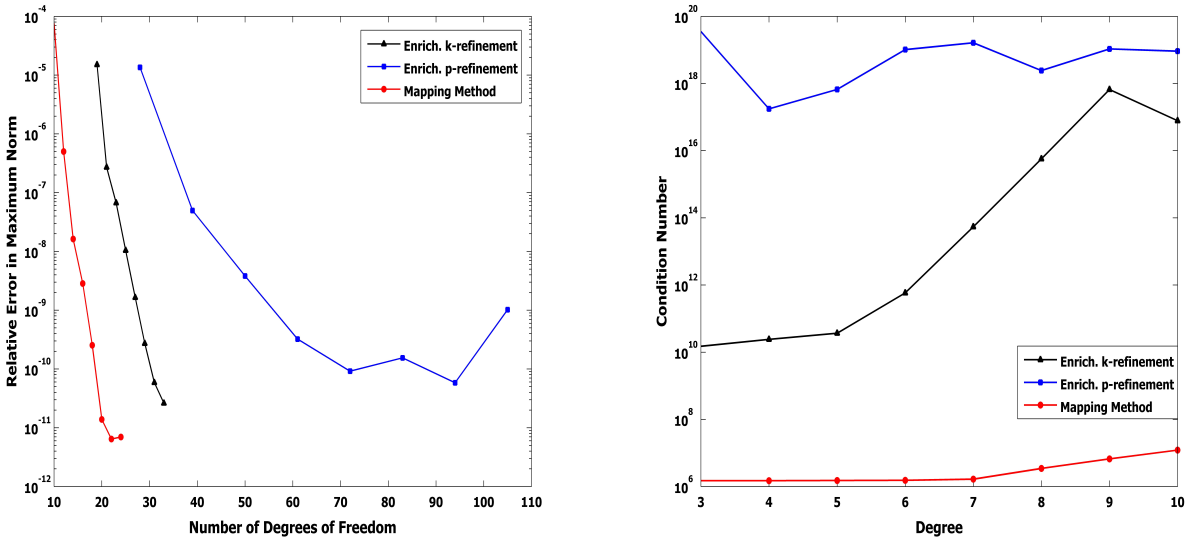

Figure 15: Relative error in maximum norm versus DOF (Left) and condition numbers versus degrees in semi log scale (Right) of 1D fourth-order PDE with singularities

of freedom 24 to the model problem with singularities, we have the following condition numbers for various regularities of PU.

$$\kappa(A) = 1.9814E+8, \quad \text{PU: } C^1\text{-continuous},$$

$$\kappa(A) = 2.1041E+8, \quad \text{PU: } C^2\text{-continuous},$$

$$\kappa(A) = 2.1203E+8, \quad \text{PU: } C^3\text{-continuous},$$

$$\kappa(A) = 7.0361E+8, \quad \text{PU: } C^4\text{-continuous}.$$

6. Figure 15 shows that Mapping Method has better accuracy with smaller degrees of freedom and smaller condition numbers for the same degrees than those of enriched PU-IGA.

To demonstrate the effectiveness of the mapping method, we compute the condition numbers and relative errors obtained by applying the standard IGA to the model

Table 12: Relative maximum and energy errors of 1D fourth-order PDE containing singularities obtained by PU-IGA with mapping method and by k-Refinement of IGA with no enrichment. $\kappa(A)$ denotes the matrix condition number.

PU-IGA with Mapping Method				
DEG	DOF	$\|Err\|_{Max}$	$\|Err\|_{Eng}$	$\kappa(A)$
3	10	7.6014E-05	1.8016E-04	1.4912E+06
4	12	5.0087E-07	3.4060E-06	1.4924E+06
5	14	1.6232E-08	1.1203E-06	1.5133E+06
6	16	2.8455E-09	1.2240E-06	1.5320E+06
7	18	2.5328E-10	8.3857E-07	1.6545E+06
8	20	1.3839E-11	2.5675E-07	3.4523E+06
9	22	6.4221E-12	5.4473E-07	6.6485E+06
10	24	6.9568E-12	1.2311E-07	1.2109E+07
k-refinement of IGA without enrichment				
DEG	DOF	$\|Err\|_{Max}$	$\|Err\|_{Eng}$	$\kappa(A)$
3	13	7.339E-02	0.866E-00	5.4460E+03
4	14	3.144E-02	0.785E-00	7.1718E+03
5	15	2.395E-02	0.717E-00	1.1849E+04
6	16	2.035E-02	0.658E-00	1.9012E+04
7	17	1.679E-02	0.605E-00	2.9001E+04
8	18	1.584E-02	0.557E-00	4.2240E+04
9	19	1.433E-02	0.512E-00	5.9166E+04
10	20	1.339E-02	0.468E-00	8.0227E+04

problem with a smooth true solution.

Example 10. **Fourth-order differential equation with smooth solution**

Suppose

$$u(x) = e^x\Big((1-x)^3x^2\Big)$$

is the true solution of model problem (57) with clamped boundary conditions at both ends of the domain $\Omega = (0,1)$. Then we have

$$\begin{aligned} f(x) &= \Big(e^x((1-x)^3x^2)\Big)^{(4)} = -e^x(x+2)(x^4+15x^3+45x^2-31x-6) \\ u^{(2)}(x) &= e^x(x-1)(x^4+8x^3+7x^2-12x+2) \\ \|u\|^2_{Eng} &= 0.315697892048689. \end{aligned}$$

Relative errors of numerical solutions obtained by IGA using approximation spaces $\mathcal{V}^p_{\rm II}$, constructed by the p-refinement, $\mathcal{V}^k_{\rm II}$, constructed by the k-refinement, and $\mathcal{V}^h_{\rm II}$, constructed by the h-refinement with fixed $p = 5$, respectively, are shown in Table 13. Their condition numbers are shown in Table 14. The approximation spaces $\mathcal{V}^p_{\rm II}$ and $\mathcal{V}^k_{\rm II}$ are defined by (62) and $\mathcal{V}^h_{\rm II}$ is similarly defined.

The numerical results in Table 13 and 14 show that the numerical results by PU-IGA with Mapping Method are as accurate as results by standard IGA to the fourth order equation with smooth true solution. Moreover, the condition numbers are compatible. In other words, the mapping method virtually makes a singularity problem as simple as a regular problem.

Table 13: Relative maximum and energy errors of 1D smooth forth-order equation by IGA. For the h-refinement of IGA, p-degree is fixed to be $p = 5$

k-refinement			p-refinement		h-refinement (deg=5)		
DEG	DOF	$\|Err\|_{Max}$	DOF	$\|Err\|_{Max}$	h-size	DOF	$\|Err\|_{Max}$
3	13	8.440E-04	22	6.768E-04	1/10	42	2.034E-07
4	14	3.230E-05	32	1.253E-05	1/20	82	3.234E-09
5	15	3.056E-06	42	2.034E-07	1/40	162	1.427E-10
6	16	1.303E-07	52	1.816E-09	1/100	402	4.428E-09
7	17	3.886E-09	62	5.881E-11			
8	18	1.793E-10	72	4.208E-11			
9	19	8.994E-11	82	3.120E-11			
10	20	9.149E-11	92	2.824E-11			
k-refinement			p-refinement		h-refinement (deg=5)		
DEG	DOF	$\|Err\|_{Eng}$	DOF	$\|Err\|_{Eng}$	h-size	DOF	$\|Err\|_{Eng}$
3	13	2.734E-02	22	2.559E-02	1/10	42	4.142E-05
4	14	2.447E-03	32	1.511E-03	1/20	82	1.548E-06
5	15	1.674E-04	42	4.142E-05	1/40	162	1.065E-05
6	16	8.836E-06	52	7.680E-07	1/100	402	6.314E-05
7	17	3.684E-07	62	5.955E-07			
8	18	7.956E-08	72	1.302E-06			
9	19	9.744E-08	82	1.336E-06			
10	20	8.795E-08	92	2.880E-06			

Table 14: Condition numbers of 1D smooth fourth-order equation obtained by IGA. $\kappa(A)$ denotes the matrix condition number.

Condition numbers							
	k-refinement		p-refinement		h-refinement(deg=5)		
DEG	DOF	$\kappa(A)$	DOF	$\kappa(A)$	h-size	DOF	$\kappa(A)$
3	13	5.44E+03	22	5.36E+04	1/10	42	1.67E+05
4	14	7.17E+03	32	9.54E+04	1/20	82	1.34E+06
5	15	1.18E+04	42	1.67E+05	1/40	162	1.07E+07
6	16	1.90E+04	52	2.90E+05	1/100	402	1.68E+08
7	17	2.90E+04	62	4.52E+05			
8	18	4.22E+04	72	6.68E+05			
9	19	5.91E+04	82	9.52E+05			
10	20	8.02E+04	92	1.31E+06			

6.6 Two Dimensional Fourth Order Elliptic Equations on a Cracked Disk

We extend the proposed PU-IGA with mapping method to the two-dimensional fourth order equation containing singularities.

It was shown in [10] that the fourth-order equation in a cracked domain with clamped boundary conditions along the crack face has the following asymptotical behaviors.

Theorem 11. [10] If $f \in P_2^k(\Omega)$, i.e. $r^{-k+|\alpha|}D^\alpha f \in L_2(\Omega)$, $|\alpha| \le k$, then the solution of $\Delta^2 u = f$ in cracked domain $\Omega = \{(r,\theta)|0 \le \theta \le 2\pi, r > 0\}$ is locally of the following formula:

$$u(r,\theta) = \sum_{1\le m<k+5/2} r^{m+1/2}\Big(\lambda_m s_m^1 + \nu_m s_m^2\Big) + u_{reg}(r,\theta) \tag{72}$$

$$\begin{aligned} \text{where} \quad s_m^1 &= \sin(m+1/2)\theta - \frac{2m+1}{2m-3}\sin(m-3/2)\theta, \\ s_m^2 &= \cos(m+1/2)\theta - \cos(m-3/2)\theta, \quad u_{reg} \in P_2^{k+4}(\Omega), \end{aligned}$$

where λ_m, ν_m are constants.

We construct a test problem with the highest singular term from the asymptotic solution in the Theorem.

Example 12. Consider the fourth-order equation, $\Delta^2 u = f$, in the cracked unit circular domain Ω with clamped boundary conditions whose solution is

$$u(r,\theta) = (1-r)^2 r^{1.5}\Big(\sin(1.5\theta) - 3\sin(0.5\theta) + \cos(1.5\theta) - \cos(0.5\theta)\Big).$$

Then $u(1,\theta) = \dfrac{\partial u}{\partial n}(1,\theta) = 0,$

$$u(r,0) = u(r,2\pi) = 0, \quad \frac{\partial u}{\partial y}(r,0) = \frac{\partial u}{\partial y}(r,2\pi) = 0.$$

$$f(r,\theta) = \Delta^2 u = -r^{-3/2}\Big(24r\cos(\theta/2) - 16\sqrt{2}\sin(3\theta/2+\pi/4) + 72r\sin(\theta/2)\Big),$$

$$\text{Energy} = \frac{1}{2}\iint_{\Omega} \Delta u \Delta u = 16.755160678572160.$$

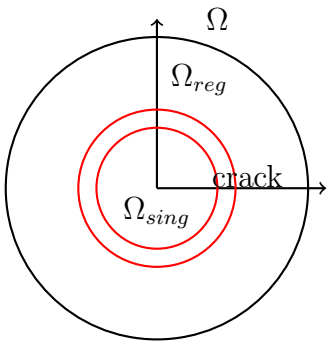

Figure 16: Two patches on cracked disk, $\Omega = \Omega_{sing} \cup \Omega_{reg}$.

PU-IGA with Mapping Method

I. Partition of the physical domain

We divide the physical domain into two subdomains, $\Omega_{sing} = \{(x,y)|0 \le x^2+y^2 \le 0.5^2\}$ and $\Omega_{reg} = \{(x,y) : 0.4^2 \le x^2+y^2 \le 1\}$.

II. Mappings

We construct one geometric mapping onto Ω_{reg}, denoted by G-mapping, and a singular mapping, denoted by F-mapping that generates singular functions to resemble the singularities.

[G-mapping] Define a geometric mapping $G : \hat{\Omega} = [0,1]\times[0,1] \longrightarrow \Omega_{reg}$ by

$$G(\xi,\eta) = (0.4+0.6\eta)\Big(\cos 2\pi(1-\xi), \sin 2\pi(1-\xi)\Big), \tag{73}$$

where Ω_{reg} has a crack along the positive x-axis. Then we have

$$G^{-1}(x,y) \;=\; (\xi(x,y),\eta(x,y))$$

$$\text{where}\quad \xi(x,y) \;=\; \begin{cases} \dfrac{1}{2\pi}\cos^{-1}(\dfrac{x}{r}) & \text{if } y<0 \\ 1-\frac{1}{2\pi}\cos^{-1}(\frac{x}{r}) & \text{if } 0\le y \end{cases}, \qquad \eta(x,y)=\frac{(r-0.4)}{0.6}$$

$$r \;=\; \sqrt{x^2+y^2}, \qquad |J(G)| = 1.2\pi\Big(0.4+0.6\eta\Big).$$

[F-mapping] To generate singular basis functions, we define a singular mapping $F:\hat{\Omega}=[0,1]\times[0,1]\longrightarrow\Omega_{sing}$ by

$$F(\xi,\eta) \;=\; 0.5\eta^2\Big(\cos 2\pi(1-\xi),\sin 2\pi(1-\xi)\Big).$$

$$\text{Then}\quad F^{-1}(x,y) \;=\; (\xi(x,y),\eta(x,y)).$$

$$\text{where}\quad \xi(x,y) \;=\; \begin{cases} \dfrac{1}{2\pi}\cos^{-1}(\dfrac{x}{r}) & \text{if } y<0 \\ 1-\frac{1}{2\pi}\cos^{-1}(\frac{x}{r}) & \text{if } 0\le y \end{cases}, \qquad \eta(x,y)=\frac{r^{1/2}}{\sqrt{0.5}},$$

$$J(F) \;=\; \begin{bmatrix} \pi\eta^2\sin 2\pi(1-\xi), & -\pi\eta^2\cos 2\pi(1-\xi) \\ \eta\cos 2\pi(1-\xi), & \eta\sin 2\pi(1-\xi) \end{bmatrix}, \quad |J(F)|=\pi\eta^3.$$

III. C^1-continuous PU functions with flat-top on the physical domain

We construct PU functions on the physical domain as follows:

$$\psi_R(r,\theta)=\begin{cases} 1 & \text{if } 0\le r\le 0.4 \\ \Big(5-10r\Big)^2\Big(20r-7\Big) & \text{if } 0.4\le r\le 0.5 \\ 0 & \text{if } 0.5\le r\le 1 \end{cases} \tag{74}$$

$$\psi_L(r,\theta) = 1 - \psi_R(r,\theta). \tag{75}$$

Pullbacks of PUs by the F- and G-mappings, respectively, are

$$\begin{aligned}
\hat{\psi}_R(\xi,\eta) &= \psi_R \circ F \\
&= \begin{cases} 1 & \text{if } 0 \le \eta \le \sqrt{0.8} \\ \left(5 - 5\eta^2\right)^2 \left(10\eta^2 - 7\right) & \text{if } \sqrt{0.8} \le \eta \le 1 \\ 0 & \text{if } 1 \le \eta \end{cases}
\end{aligned} \tag{76}$$

$$\begin{aligned}
\hat{\psi}_L(\xi,\eta) &= \psi_L \circ G \\
&= \begin{cases} 0 & \text{if } \eta \le 0 \\ 1 - \left(6\eta - 1\right)^2 \left(1 + 12\eta\right) & \text{if } 0 \le \eta \le 1/6 \\ 1 & \text{if } 1/6 \le \eta. \end{cases}
\end{aligned}$$

Note that

1. ψ_R defined by (74) on the two-dimensional physical domain is similar to ψ_4 defined by (66) on the one-dimensional physical domain.

2. The choice of non flat-top zones for PU functions ψ_R and ψ_L is flexible. For a non flat-top zone, one can choose any $[a, b]$ with $0.2 \le a < b \le 0.5$ instead of $[0.4, 0.5]$.

3. Since we construct PU on the physical domain, the pull backs of PU by different mappings cannot be PU on the reference domain. That is,

   $\psi_L(r,\theta) + \psi_R(r,\theta) = 1$ for all $(r,\theta) \in \Omega$, but $\hat{\psi}_L(\xi,\eta) + \hat{\psi}_R(\xi,\eta) \neq 1$. for all $(\xi,\eta) \in \hat{\Omega}$.

IV. Construction of $\mathcal{C}^1$-continuous basis functions

In the following, we construct basis functions on the singular Ω_{sing} and on the regular zones Ω_{reg}, respectively.

Basis functions on Ω_{sing}

We assume $p \geq 3$ and $q^* \geq 4$. $\hat{N}_{k,p+1}(\xi), k = 1, 2, \ldots, p+10$, are $\mathcal{C}^{p-1}$-continuous B-splines of degree p, corresponding to a uniformly spaced open knot vector:

$$S_\xi = \{\underbrace{0 \ldots 0}_{p+1}, \underbrace{\frac{1}{p+1}}_{1}, \underbrace{\frac{2}{p+1}}_{1}, \ldots, \underbrace{\frac{p-1}{p+1}}_{1}, \underbrace{\frac{p}{p+1}}_{1}, \underbrace{1 \cdots 1}_{p+1}\}. \tag{77}$$

We modify these B-splines to satisfy the clamped boundary conditions. Like the one dimensional cases, it can be done by either modifying the first two and the last two B-splines or discarding these four functions. In the construction of an approximation space, we removed the first two and the last two B-spline functions among $\hat{N}_{i,p+1}(\xi), 1 \leq i \leq p+10$, so that the clamped boundary conditions are satisfied at both ends. We define basis functions on the reference domain for the F-mapping, which are tensor products of the modified B-splines and monomials as follows:

$$\hat{\mathcal{V}}_F = \{\hat{N}_{i,p+1}(\xi)(\eta\sqrt{0.5})^l : i = 3, \ldots, p+8; l = 2, 3, 4, 5, 6, 7, 8, \ldots, q^*\},$$

where $q^* \geq 2k+5$, k determined by (72), which depends on the regularity of the source function f.

Then the set $\hat{\mathcal{V}}_F \circ F^{-1}$ generates the crack singularity as well as the complete polynomials of degree $[q^*/2]$ in the radial direction:

$$r, r^{1.5}, r^2, r^{2.5}, r^3, r^{3.5}, \ldots, r^{q^*/2}, \tag{78}$$

where $r^2 = x^2 + y^2$.

We construct basis functions defined on Ω_{sing}, which push-forwards of $\hat{\mathcal{V}}_F$ through F are scaled by ψ_R as follows:

$$\begin{aligned}\mathcal{V}_F &= (\hat{\mathcal{V}}_F \circ F^{-1}) \cdot \psi_R \\ &= \Big\{ \Big(\hat{N}_{i,p+1}(\xi) \cdot (\eta\sqrt{0.5})^l \cdot \hat{\psi}_R(\xi,\eta) \Big) \circ F^{-1} : \\ &\qquad\qquad i = 3, \ldots, p+8; l = 2, 3, 4, 6, 7, \ldots, q^* \Big\}, \end{aligned} \tag{79}$$

where $\hat{\psi}_R$ is defined by (76). The degree of freedom of $\mathcal{V}_F$ is

$$\text{card}(\mathcal{V}_F) = (2p-3)(6+q^*-3).$$

Basis functions on Ω_{reg}

Suppose for $q \geq 3$, $\hat{M}_{k,q+1}(\eta), k = 1, 2, \ldots, 2q+1$, are $\mathcal{C}^{q-1}$-continuous B-splines corresponding to an open knot vector

$$S_\eta = \{\underbrace{0 \ldots 0}_{q+1}, \underbrace{\frac{1}{q+1}}_{1}, \underbrace{\frac{2}{q+1}}_{1}, \ldots, \underbrace{\frac{q-1}{q+1}}_{1}, \underbrace{\frac{q}{q+1}}_{1}, \underbrace{1 \cdots 1}_{q+1}\}. \tag{80}$$

Define basis functions on the reference domain for the G-mapping as follows:

$$\hat{\mathcal{V}}_G = \{\hat{N}_{i,p+1}(\xi) \cdot \hat{M}_{j,q+1}(\eta) : i = 3, \ldots, 2p-1; j = 1, \cdots, 2q-1\}.$$

Now, using the PU function ψ_L, we construct basis functions defined on Ω_{reg} as follows:

$$\begin{aligned}\mathcal{V}_G &= (\hat{\mathcal{V}}_G \circ G^{-1}) \cdot \psi_L \\ &= \Big\{ \Big(\hat{N}_{i,p+1}(\xi) \cdot \hat{M}_{j,q+1}(\eta) \cdot \hat{\psi}_L(\xi,\eta) \Big) \circ G^{-1} : 3 \leq i \leq 2p-1; 1 \leq j \leq 2q-1 \Big\} \end{aligned} \tag{81}$$

The degree of freedom of $\mathcal{V}_G$ is

$$\text{card}(\mathcal{V}_G) = (2p-3)(2q-1).$$

[IV] Approximation Space on Ω

Note the following features of basis functions on the physical subdomains Ω_{sing} and Ω_{reg}.

1. The first two and the last two among $\hat{N}_{i,p+1}, 1 \leq i \leq 2p+1$ were discarded in the ξ-direction to satisfy the cramped boundary condition along the crack.

2. The last two among $\hat{M}_{j,q+1}, 1 \leq i \leq 2q+1$ were removed in the η-direction to satisfy the cramped boundary condition on the boundary.

Our approximation space to handle the fourth-order partial differential equation on a cracked circular domain Ω is the union of the families of basis functions for singular and regular zones:

$$\mathcal{V}_\Omega = \mathcal{V}_G \cup \mathcal{V}_F. \tag{82}$$

We observe the following:

1. The number of the degree of freedom is

$$\begin{aligned} \text{card}(\mathcal{V}_\Omega) &= \text{card}(\mathcal{V}_F) + \text{card}(\mathcal{V}_G) \\ &= (2p-3)\Big(6 + q^* - 3) + (2q-1)\Big) \end{aligned}$$

2. The intersections of basis functions in $\mathcal{V}_F$ and those in $\mathcal{V}_G$ occur only in the

annular region

$$\Omega_{sing} \cap \Omega_{reg} = \{(r, \theta) : 0 < \theta < 2\pi, \quad 0.4 \leq r \leq 0.5\}.$$

V. Bilinear Form on the reference domain

Pullbacks of the Laplacian need to be calculated for the stiffness matrix when Laplacian on the physical domain is pulled back to the reference domain.

Let $\Phi : \hat{\Omega} \longrightarrow \Omega$ be a mapping from the parameter space to the physical space defined by

$$\Phi(\xi, \eta) = (x(\xi, \eta), y(\xi, \eta)),$$

and let

$$\hat{u} = u \circ \Phi, \quad \nabla_x = (\partial_x, \partial_y)^T, \quad \nabla_\xi = (\partial_\xi, \partial_\eta)^T,$$

where u is a differentiable function defined on Ω. Then, we have

$$(\nabla_x u) \circ \Phi = J(\Phi)^{-1} \nabla_\xi \hat{u} \quad \text{or} \tag{83}$$

$$\begin{bmatrix} u_x \circ \Phi \\ u_y \circ \Phi \end{bmatrix} = \frac{1}{|J(\Phi)|} \begin{bmatrix} y_\eta & -y_\xi \\ -x_\eta & x_\xi \end{bmatrix} \begin{bmatrix} \hat{u}_\xi \\ \hat{u}_\eta \end{bmatrix} = \begin{bmatrix} J_{11}^{-1} & J_{12}^{-1} \\ J_{21}^{-1} & J_{22}^{-1} \end{bmatrix} \begin{bmatrix} \hat{u}_\xi \\ \hat{u}_\eta \end{bmatrix}.$$

Using (83), we have

$$\begin{aligned} (\nabla_x u_x) \circ \Phi &= J(\Phi)^{-1} \nabla_\xi (u_x \circ \Phi) \\ &= J(\Phi)^{-1} \nabla_\xi (J_{11}^{-1} \hat{u}_\xi + J_{12}^{-1} \hat{u}_\eta) \end{aligned} \tag{84}$$

$$\begin{bmatrix} u_{xx} \circ \Phi \\ u_{xy} \circ \Phi \end{bmatrix} = J(\Phi)^{-1} \begin{bmatrix} (J_{11}^{-1}\hat{u}_\xi + J_{12}^{-1}\hat{u}_\eta)_\xi \\ (J_{11}^{-1}\hat{u}_\xi + J_{12}^{-1}\hat{u}_\eta)_\eta \end{bmatrix}$$

Similarly, we have

$$\begin{aligned} (\nabla_x u_y) \circ \Phi &= J(\Phi)^{-1}\nabla_\xi (u_y \circ \Phi) \\ &= J(\Phi)^{-1}\nabla_\xi (J_{21}^{-1}\hat{u}_\xi + J_{22}^{-1}\hat{u}_\eta) \end{aligned} \tag{85}$$

$$\begin{bmatrix} u_{yx} \circ \Phi \\ u_{yy} \circ \Phi \end{bmatrix} = J(\Phi)^{-1} \begin{bmatrix} (J_{21}^{-1}\hat{u}_\xi + J_{22}^{-1}\hat{u}_\eta)_\xi \\ (J_{21}^{-1}\hat{u}_\xi + J_{22}^{-1}\hat{u}_\eta)_\eta \end{bmatrix}$$

Let $\varphi(x,y) = \hat{\varphi} \circ \Phi^{-1}(x,y)$. Then

$$\begin{aligned} (\partial_{xx}\varphi) \circ \Phi &= J_{11}^{-1}\frac{\partial}{\partial\xi}(J_{11}^{-1}\frac{\partial}{\partial\xi}\hat{\varphi} + J_{12}^{-1}\frac{\partial}{\partial\eta}\hat{\varphi}) + J_{12}^{-1}\frac{\partial}{\partial\eta}(J_{11}^{-1}\frac{\partial}{\partial\xi}\hat{\varphi} + J_{12}^{-1}\frac{\partial}{\partial\eta}\hat{\varphi}) \\ (\partial_{yy}\varphi) \circ \Phi &= J_{21}^{-1}\frac{\partial}{\partial\xi}(J_{21}^{-1}\frac{\partial}{\partial\xi}\hat{\varphi} + J_{22}^{-1}\frac{\partial}{\partial\eta}\hat{\varphi}) + J_{22}^{-1}\frac{\partial}{\partial\eta}(J_{21}^{-1}\frac{\partial}{\partial\xi}\hat{\varphi} + J_{22}^{-1}\frac{\partial}{\partial\eta}\hat{\varphi}) \\ (\partial_{xy}\varphi) \circ \Phi &= J_{21}^{-1}\frac{\partial}{\partial\xi}(J_{11}^{-1}\frac{\partial}{\partial\xi}\hat{\varphi} + J_{12}^{-1}\frac{\partial}{\partial\eta}\hat{\varphi}) + J_{22}^{-1}\frac{\partial}{\partial\eta}(J_{11}^{-1}\frac{\partial}{\partial\xi}\hat{\varphi} + J_{12}^{-1}\frac{\partial}{\partial\eta}\hat{\varphi}) \\ (\partial_{yx}\varphi) \circ \Phi &= J_{11}^{-1}\frac{\partial}{\partial\xi}(J_{21}^{-1}\frac{\partial}{\partial\xi}\hat{\varphi} + J_{22}^{-1}\frac{\partial}{\partial\eta}\hat{\varphi}) + J_{12}^{-1}\frac{\partial}{\partial\eta}(J_{21}^{-1}\frac{\partial}{\partial\xi}\hat{\varphi} + J_{22}^{-1}\frac{\partial}{\partial\eta}\hat{\varphi}) \end{aligned} \tag{86}$$

For $u, v \in \mathcal{V}_\Omega$, we can calculate the bilinear form $\mathcal{B}(u,v)$ and the linear functional $\mathcal{F}(v)$ in a similar manner as those in one-dimensional cases. Let $\triangle_x = \dfrac{\partial^2}{\partial x^2} + \dfrac{\partial^2}{\partial y^2}$

Case 1: For $u, v \in \mathcal{V}_F$, we have

$$\begin{aligned}
\mathcal{B}(u,v) &= \int\int_{\Omega_{sing}} (\Delta_x u)(\Delta_x v) dxdy \\
&= \int_0^1 \int_0^1 (\Delta_x u \circ F) \cdot (\Delta_x v \circ F) |J(F)| d\xi d\eta \\
&= \Big(\int_0^1 \int_0^{F^{-1}(0.4)} + \int_0^1 \int_{F^{-1}(0.4)}^1 \Big) (\Delta_x u \circ F) \cdot (\Delta_x v \circ F) |J(F)| d\xi d\eta \\
\mathcal{F}(v) &= \int\int_{\Omega_{sing}} f v dx = \int_0^1 \int_0^1 (f \circ F)(v \circ F) |J(F)| d\xi d\eta \\
&= \Big(\int_0^1 \int_0^{F^{-1}(0.4)} + \int_0^1 \int_{F^{-1}(0.4)}^1 \Big) (f \circ F) \cdot \hat{v} \cdot |J(F)| d\xi d\eta.
\end{aligned}$$

Case 2: For $u, v \in \mathcal{V}_G$, we have

$$\begin{aligned}
\mathcal{B}(u,v) &= \int\int_{\Omega_{reg}} (\Delta_x u)(\Delta_x v) dxdy \\
&= \int_0^1 \int_0^1 (\Delta_x u \circ G) \cdot (\Delta_x v \circ G) |J(G)| d\xi d\eta \\
&= \Big(\int_0^1 \int_0^{G^{-1}(0.5)} + \int_0^1 \int_{G^{-1}(0.5)}^1 \Big) (\Delta_x u \circ G) \cdot (\Delta_x v \circ G) |J(G)| d\xi d\eta
\end{aligned}$$

$$\begin{aligned}
\mathcal{F}(v) &= \int\int_{\Omega_{reg}} f v dx = \int_0^1 \int_0^1 (f \circ G)(v \circ G) |J(G)| d\xi d\eta \\
&= \Big(\int_0^1 \int_0^{G^{-1}(0.5)} + \int_0^1 \int_{G^{-1}(0.5)}^1 \Big) (f \circ G) \cdot \hat{v} \cdot |J(G)| d\xi d\eta.
\end{aligned}$$

Case 3: For $u \in \mathcal{V}_F$ and $v \in \mathcal{V}_G$

This calculation of the bilinear form is similar to that of the one-dimensional counterpart shown in the previous section. The two basis functions u and v intersect only

on annulus, $\Omega_{sing} \cap \Omega_{reg}$.

$$\begin{aligned}
\mathcal{B}(u,v) &= \int\int_{\Omega_{sing}\cap\Omega_{reg}} (\Delta_x u)(\Delta_x v)dxdy \\
&= \int\int_{\Omega_{sing}\cap\Omega_{reg}} \Delta_x(\hat{u}\circ F^{-1})\Delta_x(\hat{v}\circ G^{-1})\circ G\circ G^{-1}dxdy \\
&= \int\int_{\Omega_{sing}\cap\Omega_{reg}} \Big(\Delta_x(\hat{u}\circ F^{-1})\circ G\cdot\Delta_x(\hat{v}\circ G^{-1})\circ G\Big)\circ G^{-1}dxdy \\
&= \int_0^1\int_{F^{-1}(0.4)}^1 \Big((\Delta_x(\hat{u}\circ F^{-1})\circ G\cdot\Delta_x(\hat{v}\circ G^{-1})\circ G\Big)\circ(G^{-1}\circ F)|J(F)|d\xi d\eta \\
&= \int_0^1\int_{F^{-1}(0.4)}^1 \Big(\Delta_x(\hat{u}\circ F^{-1})\circ F\Big)\cdot\Big(\Delta_x(\hat{v}\circ G^{-1})\circ G\Big)\circ(G^{-1}\circ F)|J(F)|d\xi d\eta,
\end{aligned}$$

where

$$(G^{-1}\circ F)(\xi,\eta) = (\xi, \quad \frac{0.5\eta^2 - 0.4}{0.6}).$$

Table 15: Relative maximum error for 2D fourth-order PDE on a cracked disk obtained by PU-IGA with mapping method. $\kappa(A)$ stands for the condition numbers of stiffness matrices

PU-IGA with Mapping Method				
DEG	DOF	$\|Err\|_{Max}$	$\|Err\|_{Eng}$	$\kappa(A)$
3	24	5.3597E-02	1.3072E-01	2.1058E+06
4	50	6.6570E-03	2.8878E-02	4.0600E+06
5	84	6.3363E-04	4.6050E-03	1.9574E+07
6	126	4.4320E-05	5.6291E-04	1.0146E+08
7	176	3.4687E-06	7.1296E-05	4.6353E+08
8	234	2.1079E-07	9.1481E-05	2.0954E+09
9	300	1.3017E-08	9.1610E-05	8.6866E+09
10	374	6.1083E-10	9.1632E-05	3.5862E+10

VI. Numerical Results

Applying the described two dimensional PU-IGA with Mapping Method to Example 12, we list the numerical results in Table 15. We observe the following:

1. We have fairly accurate solutions as well as small condition numbers with the

mapping method.

2. Since the solution $u(r,\theta)$ contains singular terms $r^{1.5}, r^{2.5}, and r^{3.5}$, we must choose $q^* \geq 7$ in the construction of the approximation space $\mathcal{V}_F$. Otherwise, we do not have enough singular functions.

3. An approximation space can be enriched by adding the singular functions directly, $\left(r^{1.5}, r^{2.5}, r^{2.5}\right) \times \left(\sin(1.5\theta) - 3\sin(0.5\theta) + \cos(1.5\theta) - \cos(0.5\theta)\right)$ to obtain a similar spectral accuracy, shown in Table 15. However, this directly enriched IGA in the physical space will face integrations of singular functions as well as large matrix condition numbers, which we observed in the one dimensional counterpart.

4. Since this example does not have a regular part in the solution, the G-mapping is not necessary. However, if a domain has n corners and/or cracks, we have to construct n singular mappings $F_i : \hat{\Omega} \longrightarrow \Omega_i, i = 1, \cdots, n$ and a regular mapping $G : \hat{\Omega} \longrightarrow \Omega \setminus \cup_{i=1}^{n} \Omega_i$ to apply the Mapping Method.

5. Figure 17 shows numerical solutions obtained by IGA with Mapping Method and by the standard IGA without Mapping Method. These two approximate solutions are compared with the true solution in the figure.

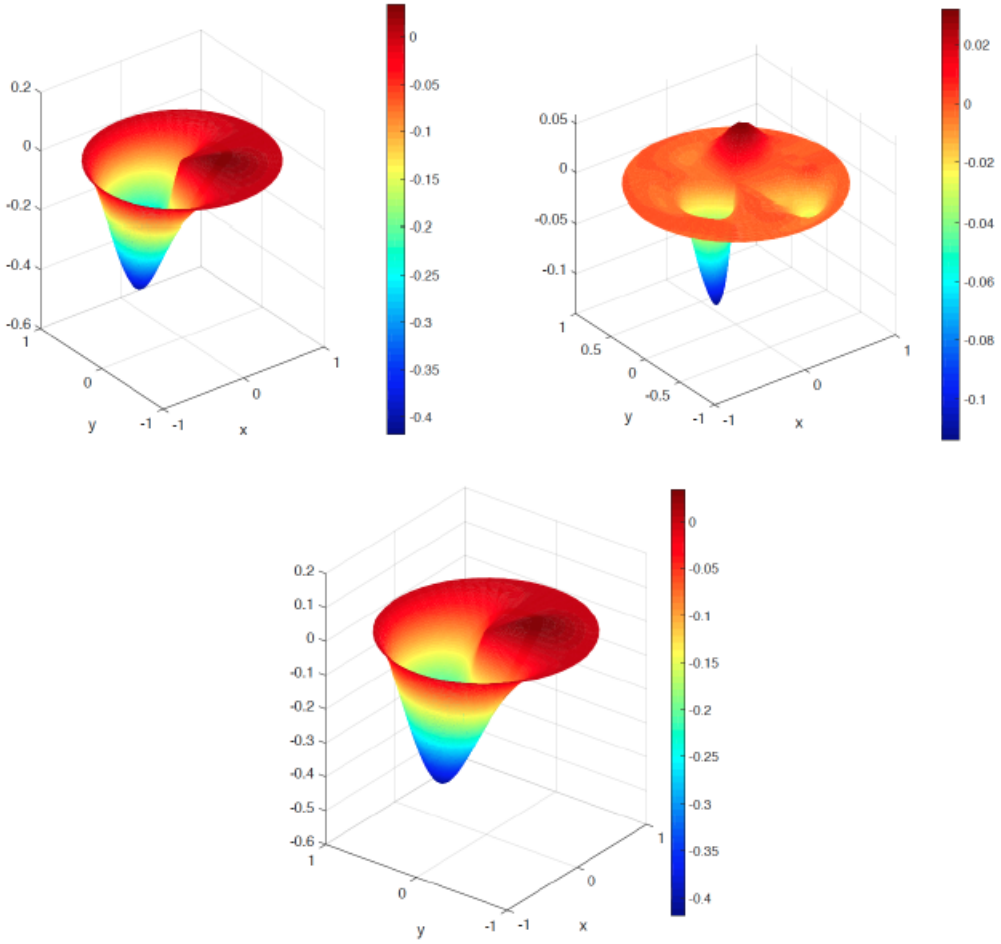

Figure 17: Numerical solution of 2D fourth-order PDE on a cracked disk by PU-IGA with mapping method(Left) and by standard IGA(Right), true Solution(Down center), when B-spline basis functions of degree $p = 5$ are used.

CHAPTER 7: CONCLUSION AND FUTURE DIRECTIONS

We show that enriched PU-IGA yields accurate numerical solutions of convection-diffusion equations with small convection coefficients and parabolic equations with small thermal conductivities. One of the goals of this research is to get non oscillatory numerical solutions using B-spline basis functions, enriched with boundary layer functions, to avoid extensive mesh refinement in a curved domain.

In order to make local refinement and implementation of enrichment functions simple in the framework of IGA, we introduce partition of unity isogeometric analysis (PU-IGA). We adopt the partition of unity with flat-top to keep the enrichment functions on the singular zone only. We implement PU functions in the reference domain whose supports divide the reference domain into several rectangular patches. When the enrichment functions and B-spline basis functions are pulled back by a geometric mapping, the supports of pull-backs become rectangles in the reference domain. Thus the integrals for stiffness matrices and load vectors become easier and more accurate than the cases in which PU functions are implemented in physical domains.

We test the proposed method to boundary layer problems in a disk and a square domain. Comparing enriched PU-IGA to all other methods, we conclude that enriched PU-IGA is superior over other existing numerical methods whenever the boundary layer behavior of the given problem is known.

This enriched PU-IGA is also extended to solve the fourth-order equations with singularities and has accurate numerical solutions; however, we encounter high condition numbers and singular integrals. Thus, we introduce PU-IGA with Mapping Method to overcome these limitations and tested the proposed method to the fourth order equation containing singularities on a cracked disk. The numerical results show that the Mapping Method gives accurate solutions as well as small matrix condition numbers. The proposed Mapping Method can be extended to handle various types of singularities, such as corners and/or cracks of non convex physical domain.

REFERENCES

[1] Babuška I. , Banerjee U., Osborn J.E., *Survey of meshless and generalized finite element methods:A unified approach,* Acta Numerica, Cambridge Press (2003) 1-125.

[2] Bazilevs Y., Beirao Da Veiga L., Cottrell J. A., Hughes T. J. R., Sangalli G., *Isogeometric analysis: Approximation, stability and error estimates for h-refined meshes*, Mathematical Models and Methods in Applied Sciences **16** (2006), 1031–1090.

[3] Bujanda, B., Clavero, C., Gracia, J.L., Jorge, J.C.: A high order uniformly convergent alternating direction scheme for time dependent reaction-diffusion singularly perturbed problems.. Numer. Math. 107(1), 1-25(2007)

[4] Cannon, J.R: The one-dimensional heat equation

[5] Clavero, C., Gracia, J.L.: A high order HODIE finite difference scheme for 1D parabolic singularly perturbed reaction-diffusion problems. Appl.Math. Comput. 218(9), 5067-5080(2012)

[6] Cockburn B, Shu CW. The local discontinuous Galerkin method for timedependent convectiondiffusion systems. SIAM J Numer Anal 1998;35: 244063.

[7] Cottrell J. A., Hughes T. J. R. and Bazilevs Y., *Isogeometric analysis: Toward integration of CAD and FEM*, Wiley, 2009.

[8] Gilbarg, D, Trudinger, N.;Elliptic partial differential equations of second order;Berlin ; New York : Springer-Verlag, [1977]

[9] Griebel M., Schweitzer M.A.:*A particle-Partition of Unity Methods Part VII: Adaptivity,* Meshfree Methods for partial Differential Equations III, Lect. Notes in Compu. Science and Engr. 57, Springer 2007

[10] Grisvard, P. Elliptic Problems in Nonsmooth domains, SIAM, 2011

[11] Han W., Meng X.:*Error analysis of reproducing kernel particle method*, Comput. Meth. Appl. Mech. Engrg. 190 (2001) 6157-6181.

[12] Han, W. and Meng, X. :*On a Meshfree method for singular problems*, CMES(Tech Science Press), 3 (2002) 65-76.

[13] Jung C.Y, Temam, R. : Convection-diffusion equations in a circle: The compatible case, Journal de mathematiques pures et appliquees, v96 n1 (2011): 88-10

[14] Jung C.-Y.; Temam R. :Singular perturbations and boundary layer theory for convection-diffusion equations in a circle: the generic noncompatible case, SIAM Journal on Mathematical Analysis, v44 n6 (2012 12 31): 4274-4296

[15] Hong Y., Jung C., Temam R. : *On Numerical approximation of stiff convection-diffusion equations in a circle,* Numer. math. 127(2) (2014) 292-313.

[16] Hong Y., Jung C. , Temam R.: *Singular perturbation of time dependent convection-diffusion equations in a circle,* Nonlinear Analysis, 119 (2015) 127-148.

[17] Hong, Y.: Numerical Approximation of the Singularly Perturbed Heat Equation in a Circle, Springer Science+Business Media New York 2014

[18] Hughes T. J. R., Cottrell J. A., and Bazilevs Y., *Isogeometric analysis: CAD, finite elements, NURBS, exact geometry and mesh refinement*, Comput. Methods Appl. Mech. Engrg. **194** (2005), 4135–4195.

[19] Jeong J.W., *Implementation of reproducing polynomial particle(RPP) shape functions in meshless particle methods for two dimensional elliptic partial differential equations*, PhD dissertation, University of North Carolina at Charlotte, 2008.

[20] Johnson, Claes: Numerical solution of partial differential equations by the finite element method;Cambridge [England] ; New York : Cambridge University Press(1987)

[21] Kopteva, N., Savescu, S.B.: Pointwise error estimates for a singularly perturbed time-dependent semilinear reaction-diffusion problem. IMA J. Number. Anal. 31(2), 616-639(2011)

[22] De Luycker E., Benson D. J., Belytschko T., Bazilevs Y. and Hsu M. C., *X-FEM in isogeometric analysis for linear fracture mechanics*, International Journal for Numerical Methethod in Engrg **87** (2011), 541–565.

[23] Lions, J.L.: Perturbations Singulieres dans les Problemses aux Limites et en Controle Optimal. In Lecutre Notes in Math., vol. 323, Springer, Berlin(1973) (in French)

[24] Li S., Liu W. K. : Meshfree Particle Methods, Springer-Verlag 2004.

[25] Liu W. K., Han W., Lu H., Li S., Cao J.: *Reproducing Kernel Element Method: Part I. Theoretical formulation,* Comput. Methods Appl. Mech. Engrg., Vol. 193 (2004) 933-951.

[26] Linss, T., Madden, N. : Analysis of an alternating direction method applied to singularly perturbed reaction-diffusion problems.. Int. J. Number. Anal. Model. 7(3), 507-519(2010)

[27] J David Logan: Applied Mathematics, New York, NY John Wiley & Sons, 2013

[28] Melenk J. M., Babuška I. :*The partition of unity finite element method:Theory and application* , Comput. Methods Appl. Mech. Engr. 139 (1996) 239-314.

[29] Oh H.-S., Babuska: The method of auxiliary mapping for the finite element solutions of elasticity problems containing singularities; Journal of Computational Physics, v121 n2 (1995): 193-212

[30] Oh H.-S., Kim J. G., Hong W.T. *The Piecewise Polynomial Partition of Unity Shape Functions for the Generalized Finite Element Methods,* Comput. Methods Appl. Mech. Engrg. 197 (2008) 3702-3711

[31] Oh H.-S., Kim J.G., Jeong J.W. :*The Closed Form Reproducing Polynomial Particle Shape Functions for Meshfree Particle Methods*, Comput. Methods Appl. Mech. Engrg. 196 (2007) 3435-3461

[32] Oh H.-S., Kim J. G., Jeong J.W. , *The smooth piecewise polynomial particle shape functions corresponding to patch-wise non-uniformly spaced particles for meshfree particles methods,* Comput Mech 40 (2007) 569-594

[33] Oh H.-S., Jeong J.W. , Hong, W.T. *The generalized product partition of unity for the meshes methods,* J Comput Phyics 229 (2010) 100-1620

[34] Oh H.-S. , Jeong J.W. , Kim J. G., *The Reproducing Singularity Particle Shape function for problems containing singularities,* Comput Mech 41 (2007) 135-157

[35] Jeong J. W., Oh H.-S. , Kang S., Kim H., *Mapping Techniques in Isogeometric Analysis for elliptic boundary value problems containing singularities,* Comput. Methods Appl. Mech. Engrg. 254 (2013) 334-352.

[36] Oh H.-S., Kim H., Jeong J. W. *Enriched isogeometric analysis of elliptic boundary value problems in domains with crackes and/or corners,* Int. J. Numer. Meth. Engrg 97 (2014) 149-180.

[37] Oleinik, O.A., Samokhin, V.N.: Mathematical models in boundary layer theory. In: Applied mathematics and mathematical computation. Chapman and Hall, Boca Raton(1999)

[38] O'Malley, R.E.: Singularly perturbed linear two-point boundary value problems. SIAM Rev. 50(3), 459-482(2008)

[39] Ciarlet P. G., *Basic error estimates for elliptic problems*, Handbook of Numerical Analysis, Vol. II, North-Holland, 1991.

[40] Hughes T. J. R., *The finite element method: linear static and dynamic finite element analysis*, Dover, 2000.

[41] Rogers D. F., *An introduction to NURBS*, Academic Press, 2001.

[42] Piegl L. and Tiller W., *The NURBS Book,* 2nd ed, Springer, 1997.

[43] Roos, ,H., Styness, M., Tobiska, L.: Robust Numerical Methods for Singularly Perturbed Differential Equations, Volume 24 of Springer Series in Computational Mathematics, 2nd edition. Springer, Berlin(2008). Convection-diffusion-reaction and flow problems

[44] Roos, H., Uzelac, Z.: The SDFEM for a convection-diffusion problem with two small parameters. Comput. Methods Appl. Math. 3(3), 443-458(2003). (electronic) Dedicated to John J. H. Miller on the occasion of his 65th birthday

[45] Schillinger D., Evans J.A., Reali A., Scott M.A., Hughs T.J.R. : *Isogeometric Collocation: Cost Comparison with Galerkin methods and Extension to Adaptive Hierarchical NURBS Discretization,* Comput. Methods Appl. Mech. Engrg., V. 267 (2013) 170-232.

[46] Stynes, M.: Steady-state convection-diffusion problems. Acta Number. 14. 445-508 (2005)

[47] Stynes, M., Tobiska, L.: The SDFEM for a convection-diffusion problem with a bounary layer: optimal error analysis and enhancement of accuracy. SIAM J. Numer. Anal. 41(5), 1620-1642(2003) (electronic)

[48] Szabo B., Babuska I., Finite Element Analysis, John Wiley, 1991.

[49] Temme N.M.: *Analytical methods for an elliptic singular perturbation problems in a circle,* J. of Computational and applied Math. 207 (2007) 301-322

[50] Vishik, M.I., Lyusternik, L.A.: Regular degeneration and boundary layer for linear differential equations with small parameter. Uspekhi Mat. Nauk. 12, 3-122(1957)

[51] Viscor, M., Stynes, M. : A robust finite difference method for a singularly perturbed degenerate parabolic problem II. IMA J. NUmer. Anal. 33(2), 460-480(2013)